Josef Rabanser, BSc

Numerical Studies on the Behaviour of Timber Pile Foundations

MASTER'S THESIS

to achieve the university degree of

Diplom-Ingenieur

Master's degree programme: Civil Engineering Sciences, Geotechnics and Hydraulics

submitted to

Graz University of Technology

Supervisor

Ass.Prof. Dipl.-Ing. Dr.techn. Franz Tschuchnigg

Institute of Soil Mechanics, Foundation Engineering
and Computational Geotechnics

Dipl.-Ing. Simon Oberhollenzer, BSc

Graz, September 2018

Abstract

For many centuries timber pile foundations were a common method for achieving a deep foundation in subsoil conditions with low bearing capacity. Progression throughout the industrial revolution enabled new materials such as concrete or iron to replace the usage of timber due to better technological qualities. Recently it is been considered to re-introduce timber as construction material of deep foundations, as wood is an environmentally friendly and sustainable material.

The aim of this thesis is to gain a better understanding of the bearing behaviour of these foundations. For this purpose numerical analyses by means of 2D axisymmetric models and 3D models were performed. The studies include validations on the impact due to different tip shapes and due to different tapered pile shafts. The main part is comprised of an investigation on the alteration in terms of pile group configurations. Furthermore the behaviour of timber pile foundations, obtained by different simplified methods is compared with a method capturing the overall behaviour of such foundations.

Based on the conducted research it can be summarised, that there is a high potential for pile groups exhibiting a narrow arrangement of piles. Below the pile tips an arching effect occurs which results in an increase of base resistance.

Kurzfassung

Über viele Jahrhunderte hinweg waren Holzpfahlgründungen eine gängige Methode für die Herstellung von Tiefgründungen bei Untergrundverhältnissen mit geringer Tragfähigkeit. Der Fortschritt der industriellen Revolution ermöglichte es neuen Materialien wie Beton oder Eisen die Verwendung von Holz aufgrund höherer technologischer Eigenschaften zu verdrängen. Aufgrund der Umweltfreundlichkeit und Nachhaltigkeit von Holz bestehen neuerdings Überlegungen, Holz als Pfahlmaterial wieder einzusetzen.

Ziel dieser Arbeit ist es, das Tragverhalten von Holzpfahlgr˘ndungen besser zu verstehen. Zu diesem Zweck wurden numerische Analysen mittels 2D-axisymmetrischen Modellen und 3D-Modellen durchgeführt. Die Studien umfassen Beurteilungen hinsichtlich des Einflusses unterschiedlicher Spitzenformen und unterschiedlicher konischer Pfahlschäfte. Der Hauptteil beinhaltet Untersuchungen von Pfahlgruppen mit variierenden Abmessungen. Des Weiteren werden unterschiedliche Methoden zur Berechnung des Tragverhaltens einer Pfahlgruppe verglichen.

Basierend auf den durchgeführten Untersuchungen kann resümiert werden, dass ein hohes Potential für Pfahlgruppen mit einer engen Anordnung von Pfählen besteht. In solchen Gründungen tritt unter den Pfahlspitzen ein Gewölbeeffekt auf, der zu einer Erhöhung des Spitzenwiderstandes führt.

Acknowledgement

I am deeply grateful to all my teaching supervisors which brought me to love geotechnical engineering and who keenly shared their knowledge. Especially to the head of the institute, Univ.-Prof. Dipl.-Ing. Dr.techn. Roman Marte and to my supervisors Franz and Simon for the excellent guidance during the execution of this thesis.

Furthermore I would like to thank my family who enabled me a thorough education and encouraged me when needed. Not forgetting all my friends who supported me in words and deeds day and night. These guys made my life in Graz a pleasant experience.

Finally I want to give thanks to the coincidental event to which I have to owe this exceptionally interesting topic which combines old handcraft, potential practical application and profound theory.

Statutory declaration

I declare that I have authored this thesis independently, that I have not used other than the declared sources / resources, and that I have explicitly marked all material which has been quoted either literally or by content from the used sources.

Graz, September 2018

. . . . . .

Signature

Contents

Nomenclature

A	area	m^2
c'	(effective) cohesion	kPa
D	pile diameter	m
E	young's modulus	MPa
E_{oed}^{ref}	tangent stiffness for primary oedometer loading	MPa
E_{ur}^{ref}	unloading / reloading stiffness from drained triaxial test	MPa
E_{50}^{ref}	secant stiffness in standard drained triaxial test	MPa
$F_{z,norm}$	normalised applied load in vertical direction	kN/m^2
$F_{z,tot}$	total applied load in vertical direction	kN
G_0^{ref}	reference shear modulus at very small strains	MPa
$k_x,\ k_y,\ k_z$	permeability coefficient	m/day
K_0^{nc}	coefficient of the lateral earth pressure for a normally consolidated stress state	$-$
L	pile length	m
m	power for stress-level dependency of stiffness	$-$
OCR	isotropic over consolidation ratio	$-$
p_{ref}	reference stress for stiffness	kPa
R_{base}	base resistance	kN
R_{base}^*	proportion of base resistance	$-$
R_{inter}	interface reduction factor	$-$
ROT	ratio of taper	cm/m

R_{shaft}	shaft resistance	kN
R^*_{shaft}	proportion of shaft resistance	$-$
R_{soil}	resistance transferred directly to the subsoil	kN
R^*_{soil}	proportion of soil resistance	$-$
Sp	pile spacing	m

α	angle of the pile tip	$\circ$
γ_{sat}	saturated unit weight	kN/m^3
γ_{unsat}	unsaturated unit weight	kN/m^3
$\gamma_{0.7}$	threshold shear strain at wich $G_s * 0.722G_0$	$-$
η_g	efficiency of a pile group	$-$
ν	poisson's ratio	$-$
ν_{ur}	poisson's ratio for unloading-reloading	$-$
τ_{mob}	mobilised shear stress	kN/m^2
τ_{rel}	relative shear stress	$-$
φ'	(effective) angle of internal friction	$\circ$
ψ'	(effective) angle of dilatancy	$\circ$

1 Introduction

In ancient days centres of trade often developed close to water which could be used for transporting goods. At these regions the subsoil is frequently composed out of fine grained material exhibiting a low bearing capacity. Initially buildings where made by light weight materials such as wood. Over time the size of buildings expanded and stone was also used as building material. Higher building loads combined with a relatively low bearing capacity of the subsoil demanded the development of deep foundations. For many centuries timber was used as pile material. By the invention of iron and concrete these materials replaced the function of timber.

Before then, architects had gathered experience for many centuries and various historical buildings founded on timber piles still exist after hundreds of years. This circumstance indicates the high quality and reliability of their work. Since nowadays sustainability plays an important role this opens opportunities to reinvigorate a traditional construction method.

In the field of geotechnical engineering there is no system that can be compared to pile groups with a very small spacing. Moreover, so far no research was conducted. To be able to assess the behaviour of such a foundation the load transferring mechanism has to be understood in its entirety.

The present theses starts with an overview of the development of deep foundations over the time. Next, some empirically and analytically approaches to come up with a bearing capacity of pile foundations are shown. Thereby, the focus is on the one hand laid on single piles and on the other hand on pile groups. Timber as pile material has high qualities but also disadvantages which are pointed out additionally.

The main part of the theses contains numerical studies. For this purpose commercial finite element codes, namely PLAXIS 2D (PLAXIS [2018a]) and PLAXIS 3D (PLAXIS [2017]) were used. Preliminary analyses were performed by means of 2D axisymmetric models. Different tip shapes and tapered shaft shapes were examined. Further on several piles out of an infinite group exhibiting diverse configurations were investigated. In a next step 3D computations were carried out. Initially equality of 2D and 3D computations was validated. Than an assessment of simplification as a monolithic block was performed. And finally various pile group configurations were modelled and investigated.

2 General part

2.1 Historical pile foundations

2.1.1 Introduction

Credit for the concept of piles are given to a tribe in Switzerland about 6 000 years ago. At that time homes were built on platforms supported on timber piles for protection against wildlife. Around 1 600 B.C. the Romans built a timber bridge across the Tiber river in Rome which lasted over 1 000 years. Furthermore they used timber to support some of their roads and aqueducts (Dean M. [2006]). According to Vitruvs writings timber pile foundations were common building practice in the first century B.C. The first evident pile foundation was found at the Ubier Monument in Cologne in the first century A.D. (Borrmann [1992]).

2.1.2 Classical timber pile foundation

At the beginning of deep foundations pile driving was carried out by pure manpower and fairly simple machines with a restricted energy content. Therefore these foundations exhibit small pile dimensions. Due to the development of stronger machines, longer piles were used. Based on the tightly spaced pile arrangement, classical timber pile foundations do not show a typical layout as which is nowadays understood as deep foundation (Borrmann [1992]).
The development of primary pile foundations can be divided into three construction types (Borrmann [1992]; Kempfert and Gebreselassie [2006]):

- **Floating timber pile foundation**
  This type depicts the first kind of pile foundation and was in use until the end of the 18^{th} century. It is the scheme which was applied most frequently. As it is shown in figure 2.1, wooden piles initially with a length of mainly $1 - 2\ m$ and a diameter of $10 - 15\ cm$ were driven vertically in the subsoil. From the 15^{th} century on lengths of $3 - 6\ m$ were used. The pile spacing was from tightly packed up to a clear distance of $\sim 30\ cm$. Concerning the pattern, the pile distribution was regular as well as arbitrary and rarely exceeded the extent of the masonry. The pile tips were tapered and usually charred.

- **Combined sleeper-floating timber pile foundation**
  The combined sleeper-floating timber pile foundation can be seen as an advancement of the floating timber pile foundation and is depicted in figure 2.2. Nevertheless both systems were used at the same time. This type was established in the 9^{th} century. The difference to the previous construction is a layer with longitudinally placed timbers between vertical piles and masonry. This horizontal layer enhances the load distribution to the piles and hence prevents fracturing of the masonry due to differential settlements.

- **Combined timbered floating pile-sleeper foundation**
  Like the previous described combined sleeper-floating timber pile foundation this construction type was again an advancement of the state of the art and was established in the 13^{th} century. Instead of just placing longitudinal timbers on top of the piles, this type has a timbered grid which prevents piles from horizontal movement. It superseded the combined sleeper-floating timber pile foundation but was in use parallel to the floating timber pile foundation. In figure 2.3 a draft of this type is shown.

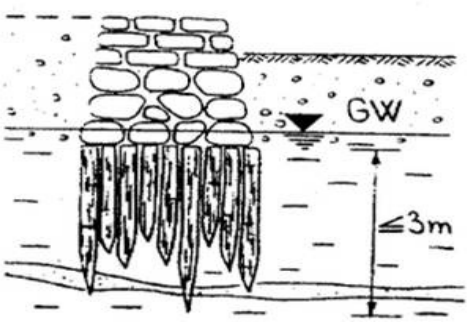

Figure 2.1: *Floating timber pile foundation; (Kempfert and Gebreselassie [2006])*

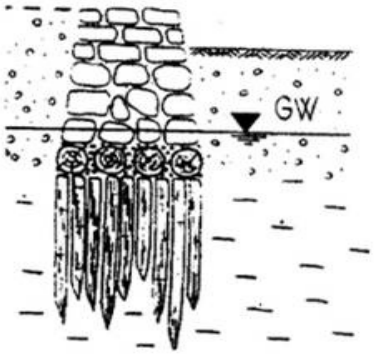

Figure 2.2: *Combined sleeper-floating timber pile foundation; (Kempfert and Gebreselassie [2006])*

The reaction to different subsoil conditions was not carried out by applying different construction types, but rather by a different spacing. Furthermore, it can be said that there was no differentiation regarding building loads and the response to higher loads was not carried out by using longer piles. From time to time a distinction in purpose of the above masonry lead to the application of different schemes. For example, the enclosing walls of a fortress were built on a combined timbered floating pile-sleeper foundation whereas the walls seated inside were resting on a floating timber pile foundation. All wooden construction parts were placed below the ground water table to obtain a preferably high durability. Pile foundations at that time were common building practice and not just a workaround. This fact emphasises the big amount of high quality crafted examples (Borrmann [1992]).

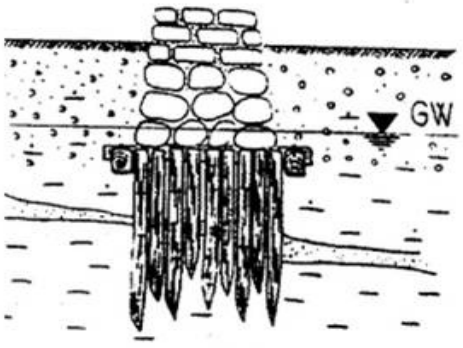

Figure 2.3: *Combined timbered floating pile-sleeper foundation; (Kempfert and Gebreselassie [2006])*

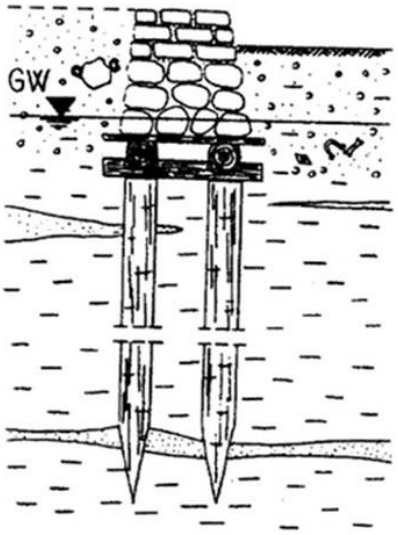

Figure 2.4: *First pile foundations featuring nowadays sense; (Kempfert and Gebreselassie [2006])*

According to written traditions authored by architects from the 15^{th} to 19^{th} century, rules of thumb were used for the design of foundations. Furthermore they suggested to determine the ground water level by means of wells and extract soil samples with a spike which had a scoop shaped barb at its end. Piles were driven as long until they did not penetrate any further after a certain amount of blows (Borrmann [1992]).

2.1.3 First pile foundations featuring nowadays sense

Due to larger buildings which required foundations with a higher capacity, a new construction type was established in the 17^{th} century. By that time, piles had lengths up to $25\ m$ and were arranged in a wider spacing as previously. First similarities to nowadays pile foundations can be seen. A schematic depiction is shown in figure 2.4. If possible piles were driven down to a bearable strata to avoid a floating foundation. From the 19^{th} century on this was the most common scheme.

The pile design was based on earliest empirical approaches which already included the shaft and tip area. Consolidation was already a well known phenomena and architects recommended to interrupt the construction after completing the foundation, moreover they emphasised a uniform brick laying. Load tests were carried out by applying a $1/3$ heavier surcharge as the expected building load. Following a catastrophe in Berlin around 1700 more than one expert were called in for projects to reduce the risk of costy constructions (Borrmann [1992]; Kothe E. [1996]).

2.2 Pile foundations nowadays

2.2.1 Introduction

Based on the invention and higher availability of new materials as e.g. concrete or iron and modern steam operated pile driving machines a revolution concerning pile foundations took place. This offered the opportunity to use more durable materials and to exceed previous dimensions of foundations. In the middle of the 19^{th} century timber piling craft was almost superseded by newer methods (Borrmann [1992]).
Nowadays an enormous spectrum of piles exists. The present thesis tempts to focus upon micro piles carried out as displacement piles. In the following some features concerning single piles and the interaction of piles are presented.

2.2.2 Single piles

A pile depicts the element which transfers loads from the superstructure to the subsoil. The magnitude of transferable load is firstly restricted by the structural capacity of the pile and secondly by the interaction between pile and adjacent soil. Latter can be subdivided into the resistance developed along the shaft ($R_{shaft} =$ shaft resistance) and the resistance which is provided at the toe of the pile ($R_{base} =$ base resistance).

To mobilise resistance of a pile relative displacements between pile and surrounding soil have to take place. For the mobilisation of the ultimate shaft resistance only relatively small displacements are required. With ongoing displacements the shaft resistance usually stagnates. On the contrary, base resistance increases with increasing displacements.

Depending on soil conditions, the load separation between base and shaft resistance and the distribution of the shaft resistance depicts various characteristics. In figure 2.5 some typical load distribution profiles are delineated. (a) shows an end bearing pile where the entire load is transferred via the pile tip. (b) is an ordinary example of a pile situated in a cohesive soil featuring a uniform shaft resistance, whereas (c) depicts an example in a cohesionless soil with an over depth increasing shaft resistance (Collin J.G. [2015]).

For the estimation of the bearing capacity of piles, most commonly simplified analytical approaches are applied to model the complex interaction between pile and surrounding soil. Hereinafter a few applicable techniques are listed in table 2.1. For a description and a step by step application it is referred to Collin J.G. [2015].

Table 2.1: *Design methods (Collin J.G. [2015])*

design method	cohesionless soil	cohesive soil
Meyerhof	yes	no
Nordlund	yes	no
α Method	no	yes
Effective Stress	yes	yes
Nottingham & Schmertmann	yes	yes

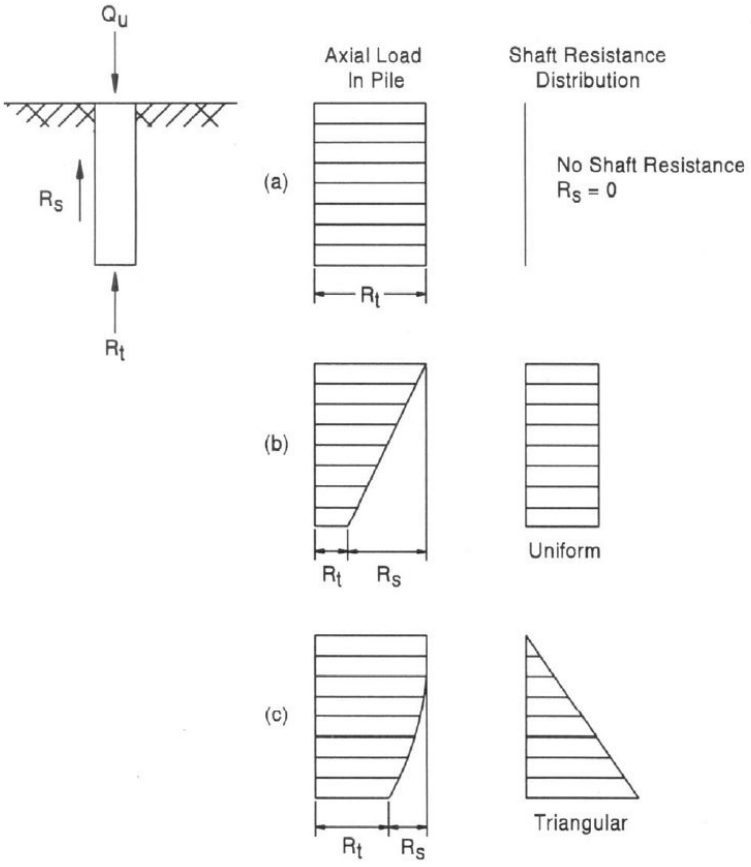

Figure 2.5: *Typical load-transfer profiles; (Collin J.G. [2015])*

2.2.3 Pile groups

For the design of a pile group two criteria have to be satisfied. Firstly the bearing capacity of the designed foundation requires an adequate factor of safety. Besides that, settlements have to be in a tolerable magnitude. In a pile group each individual pile may be influenced by adjacent piles when the spacing is tight enough. Due to this interaction the capacity of an individual pile out of a group can be greater and smaller, respectively (in comparison to a single pile). This is expressed by the efficiency of a pile group η_g which is defined as the ratio of the actual capacity of the group to the summation of the single pile capacities. Several methods for computing the efficiency coefficient were developed. Two of them are presented below (Collin J.G. [2015]; Coyle H.M. and Sulaiman I.H. [1970] Sayed M. and Bakeer M. [1992]).

- **Converse-Labarre Method (Bolin 1941)**

$$\eta_g = 1 - \frac{arctan\left(\frac{d}{s}\right)}{90\circ}\left[\frac{(n-1)*m+(m-1)*n}{m*n}\right] \tag{2.1}$$

  Where $d =$ pile diameter; $s =$ centre to centre spacing; $n =$ number of piles in a row; $m =$ number of piles in a row.

- **Poulos and Davis (1980)**

$$\frac{1}{\eta_g^2} = 1 + \frac{(m*n)^2 * Q_0^2}{Q_B^2} \tag{2.2}$$

  Where Q_B and Q_0 are the ultimate load capacities of the block of piles and that of a single pile, respectively.

The efficiency can also be estimated by a rule of thumb as shown in figure 2.6. In cohesionless soil $\eta_g > 1.0$ can be expected. However, for a conservative design of driven piles $\eta_g = 1.0$ should be applied. For cohesive soils in general $\eta_g \leq 1.0$. A pile spacing of $s \geq 8 * d$ leads to $\eta_g = 1.0$, whereas $s = 3 * d$ results in $\eta_g = 0.7$. Based on the excess pore water pressure generation due to pile driving the efficiency can temporarily go down to $\eta_g = 0.4$ (Sayed M. and Bakeer M. [1992]).

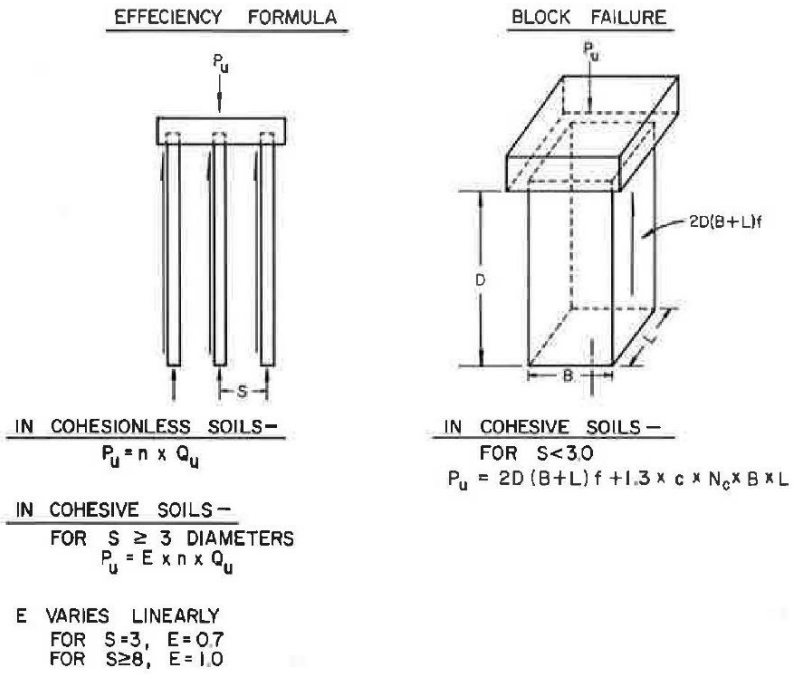

Figure 2.6: *Bearing capacity of pile groups; (Coyle H.M. and Sulaiman I.H. [1970])*

For pile groups in cohesive soils with a spacing $s < 3 * d$ the soil and piles within a pile group may move together, thus block failure has to be considered as shown in eq. 2.3 (Coyle H.M. and Sulaiman I.H. [1970]).

- **Terzaghi and Peck (1967)**

$$P_u = 2 * D * (B + L) * f + 1.3 * c * N_c * B * L \tag{2.3}$$

Where:

D	=	embedded length of piles
B	=	width of group
L	=	length of group
f	=	average friction resistance around the group
c	=	cohesion below the group
N_c	=	bearing capacity factor

To compute settlements of a pile group in cohesive soils, Collin J.G. [2015] suggests to model an equivalent deep seated footing as shown in figure 2.7. For a normally consolidated soil $\left(\sigma'_p = \sigma'_{vo}\right)$ classical consolidation theory can be applied and settlements determined by eq. 2.4.

$$S_c = \frac{C_c}{1 + e_0} * H_0 * log_{10} \frac{\sigma'_{vf}}{\sigma'_{vo}} \tag{2.4}$$

Where:

C_c	=	compression index
e_0	=	initial void ratio
H_0	=	layer thickness
σ'_{vo}	=	initial effective stress at the centre of a layer
σ'_{vf}	=	final effective stress at the centre of a layer

The final effective vertical stress is the summation of initial effective stress and additional vertical stress due to the foundation. For a layered soil the total settlements are obtained by the sum of each individual layer (Collin J.G. [2015]).

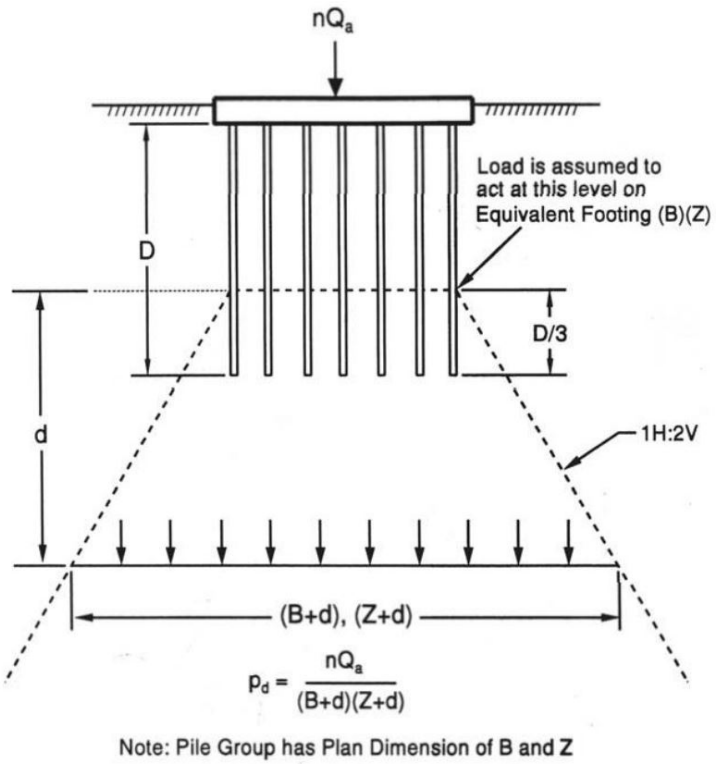

Figure 2.7: *Equivalent deep seated footing; (Collin J.G. [2015])*

2.2.4 Installation effect

The installation of timber piles is carried out by driving or jacking respectively. This procedure requires a displacement of the affected soil which leads to a disturbance of the surrounding soil. Two different characteristics of disturbance can be distinguished:

- **Cohesionless soils**
  In cohesionless soils the disturbed zone around the pile has a lateral distance of $3 - 5.5$ times the pile diameter and $3 - 5$ times below the pile tip, moreover settlements in the immediate proximity of the pile head occur (figure 2.8). This effect can on the one hand lead to an increase of relative density in loose cohesionless soil and hence an increase of bearing capacity. On the other hand in dense cohesionless soils pile driving may decrease the density. Due to the dilation of the dense soil into a lower relative density negative pore pressure is generated which leads to a temporary increase of effective stresses and thus shear resistance. As the negative pore pressure dissipates, shear strength and pile capacity decrease again (Collin J.G. [2015]).

- **Cohesive soils**
  For cohesive soils, pile driving exhibits features different to what was previously described. This is demonstrated in figure 2.9. The disturbed zone around the pile, both laterally and below the pile tip is approximately one pile diameter for soft, normally consolidated clays. At the surface a heave happens. The driving procedure generates a high excess pore water pressure, which conducts a decrease in shear strength. Dissipation of the excess pore water pressure results in an increase of shear strength and pile capacity over time. This phenomena can also be observed for fine grained cohesionless soil (Collin J.G. [2015]).

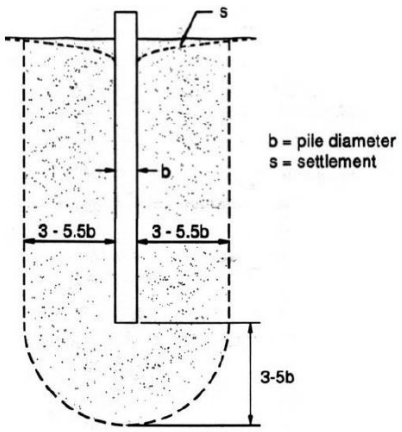

Figure 2.8: *Disturbed zone in cohesionless soils; (Collin J.G. [2015])*

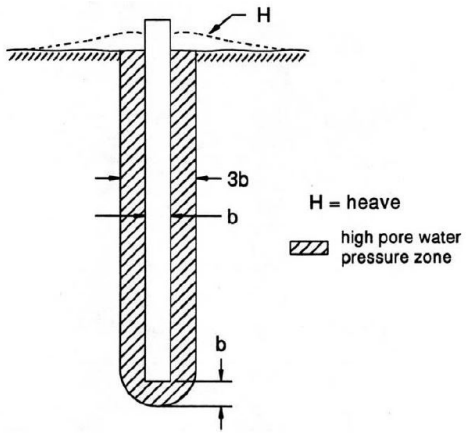

Figure 2.9: *Disturbed zone in cohesive soils; (Collin J.G. [2015])*

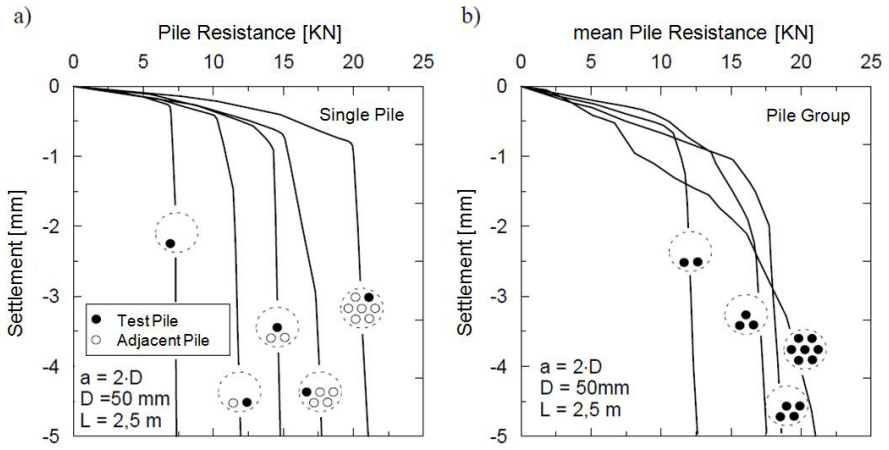

Figure 2.10: *Pile load tests: (a) single piles, (b) pile groups; (Rudolf M. [2005])*

As already mentioned in section 2.2.3, the interaction of individual piles defines the bearing behaviour of the entire pile group. Cambefort H. [1953] carried out pile load tests on single piles while constructing a pile group. The test field was composed out of 0.5 m topsoil on top of a 1.0 m thick layer of clay. Below the clay a 1.0 m thick layer of fine grained sand was encountered which was underlain by gravel. As can be seen from figure 2.10 (a) a notable increase of pile resistance happened the more adjacent piles were executed.

In addition to the pile load tests on single piles, group tests were carried out. As shown in from figure 2.10 (b), the characteristics of the load versus settlement behaviour changes significantly by the amount of tested piles. For pile groups composed out of a small amount of piles an initially stiff behaviour changes to a more or less brittle failure. Whereas larger pile groups show at the beginning more settlements and a ductile deformation pattern. Finally a higher resistance can be provided.

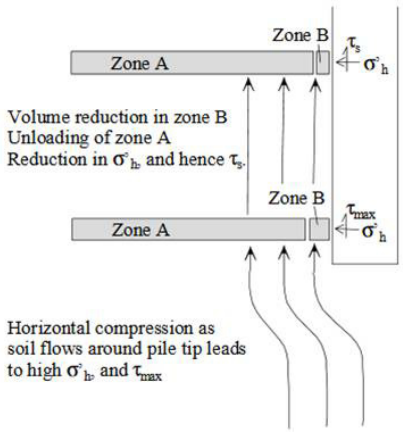

Figure 2.11: *Mechanism of friction degradation; (White R.T. and Bolton M.D. [2002])*

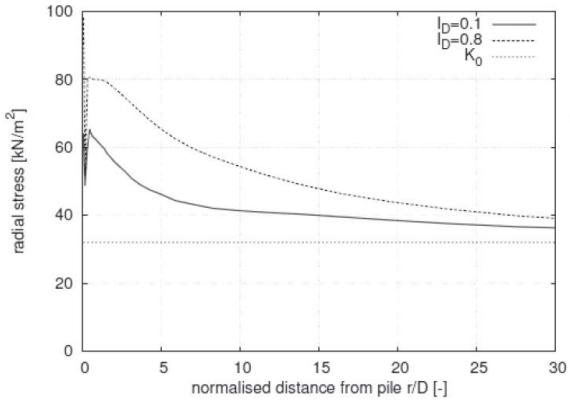

Figure 2.12: *Radial stress distribution after pile jacking in a loose and dense sand; (Mahutka K.P. et al. [2006])*

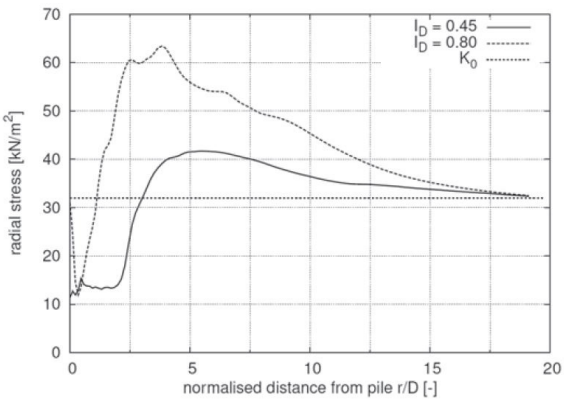

Figure 2.13: *Radial stress distribution after pile driving in a loose and dense sand; (Mahutka K.P. et al. [2006])*

An adverse phenomena of pile driving in cohesionless soils is friction degradation. During the pile installation process the soil is subjected to a zone of high stress close to the pile tip as shown in figure 2.11 as zone A, hence it is heavily overconsolidated. The physical basis of friction degradation is the gradual densification of soil adjacent to the pile shaft under cyclic shearing during installation (zone B in figure 2.11). This process is enhanced by the migration of crushed particles into uncrushed material. Since the far field soil acts like a spring with a stiffness resulting from the overconsolidated soil, unloading in respect to normal stress acting on the pile shaft takes place (Randolph M. [2003]) . According to Dejog J.T. and Frost J.D. [2002] it can be assumed, that the cyclic stress reversal is the main point causing compressive volumetric strains. Based on this fact friction degradation has to be very low for continuously jacked piles. This was confirmed by means of numerical analysis carried out by Mahutka K.P. et al. [2006]. A conclusion of their research was, that for jacked piles the soil was only slightly densified or acted almost dilatant respectively, which resulted in high radial stresses around the pile. On the contrary, for dynamic installation methods the densification was much larger which lead to lower radial stresses. The radial stress distribution versus distance to the pile in case of pile jacking and pile driving respectively is shown in figure 2.12 and figure 2.13.

2.3 Timber as pile material

2.3.1 Introduction

Timber as a basic building material has a long tradition. On account of the industrial revolution timber was partly superseded by other materials as concrete or steel. In the last decade timber as building material had a comeback due to its environmentally friendly and sustainable properties (Schickhofer G. [2006]). Hence it is definitely worth to reconsider the application of wood as pile material.
In the following some advantages and drawbacks of timber piles are highlighted:

advantages	**disadvantages**
• low cost	• decay of wood
• renewable resource	• difficult to connect
• easy to handle	• stiffness and strength loss due to increasing wood moisture
• easy to drive	
• low weight	
• tapered shape provides higher resistance in granular soil than uniform piles	

2.3.2 Durability of wood

The durability of wooden piles is mainly influenced by the resistance acting against bacterial and fungal attack. Construction parts which are constantly placed below the water table show a much higher durability due to their air tight conservation. For spruce lifetimes of approximately 100 years can be assumed. The weakest point is posed by parts which are exposed to the fluctuation of the water table. At the transition area decay is very fast and a durability shorter than 10 years can be the result. In practice different methods of impregnation are used to decelerate decomposition (Smettan K. [2003]). Reconsidering the lifespan of nowadays superstructure the question about the reasonability of applying expensive preservation measures arises. Under suitable site conditions a well conceived design should be sufficient.

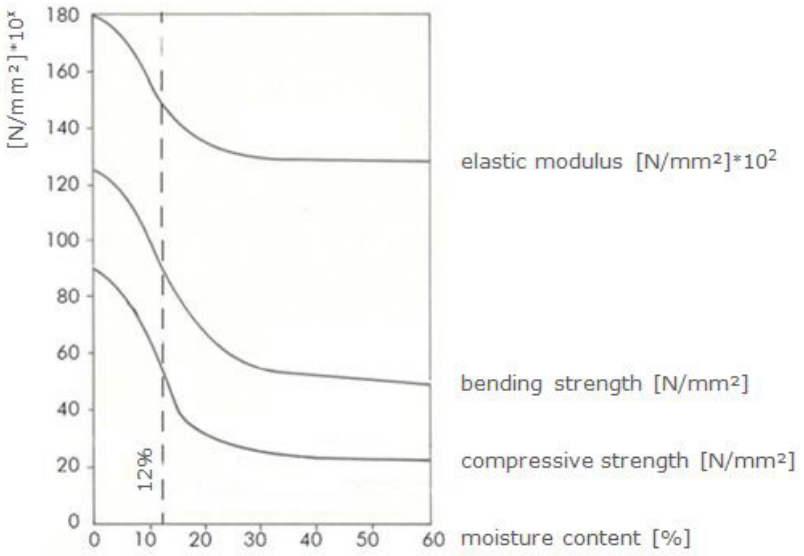

Figure 2.14: *Decrease of properties due to rising moisture content; (Niemz P. [1993], edited)*

2.3.3 Strength and stiffness of wood dependent on the moisture content

The moisture content of wood has an major effect upon stiffness and strength properties. In the hygroscopic range (below full saturation of the fibres which is approximately at $28-32\,\%$) with increasing moisture content a decrease in stiffness and strength properties happens. This can be explained by a relaxation of the fabric through swelling due to the water absorption. After full saturation of the fibres stiffness and strength properties reach more or less a constant value. This feature is demonstrated in figure 2.14 (Niemz P. [1993]).

2.3.4 Transportability of water in wood

A main field of application for timber pile foundations are cohesive soils as subsoil conditions. As mentioned before, high excess pore water pressures evolve due to the pile installation which as a further consequence induces a temporarily decrease of bearing capacity. A possibility to shorten the time of the bearing capacity reduction could be an acceleration of consolidation. This can be performed by applying vertical drains and hence reducing the length of the drainage path. Alternatively to vertical drains the concept of permeable piles can be pursued. Latter impact was evaluated by Ni P. et al. [2017] by means of numerical analyses. For that reason the installation process of a steel pipe pile featuring a diameter of $0.6\ m$ and an embedded length of $18\ m$ was modelled to confect proper initial boundary conditions. The concept of the permeable pile was executed by perforating the steel pipe with drainage holes. Illustrating the results as a chart of average degree of consolidation versus time. In figure 2.15 the positive effect of additional drainage possibilities is revealed. As can be seen, there is a high effectiveness of permeable piles, since it requires less time to reach a specific degree of consolidation.

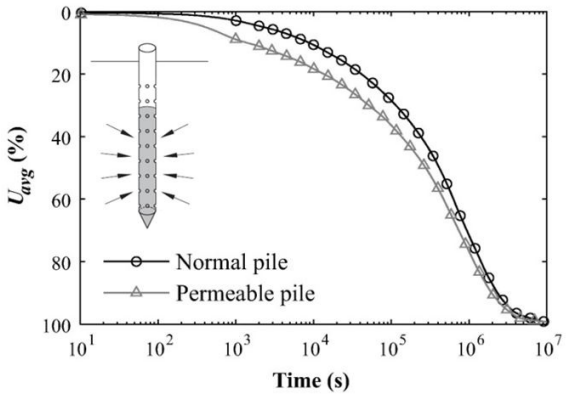

Figure 2.15: *Performance of permeable piles; (Ni P. et al. [2017], edited)*

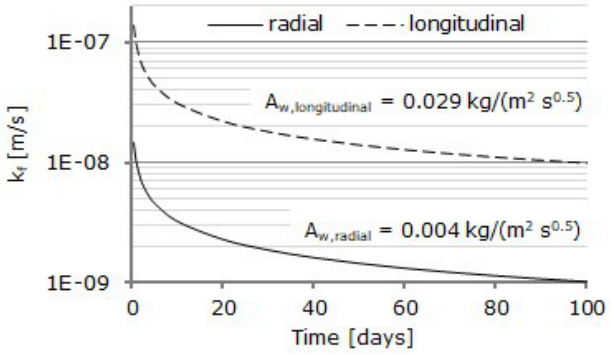

Figure 2.16: *Water absorption coefficient converted to a permeability*

Based on this study a fundamental idea arose to use the water absorption ability of wood to provide a drainage effect. The ability to absorb water is different on radial, tangential and longitudinal direction due to the high anisotropy of wood. Tests to figure out the ability are carried out on cubical small specimens individually for all three directions. As a results of this test the water adsorption coefficient A_w expressed in $[kg/m^2 s^{0.5}]$ is determined (Niemz P. et al. [2010]). In a further step the water absorption coefficient was converted to a permeability which is changing over time as demonstrated in figure 2.16. It can be deduced that the permeability of wood is in general very low and no drainage effect can be achieved. The above conclusion has to be treated with caution since trials were carried out using small specimen, moreover according to Niemz P. [2018] (personal contact) the fabric of wood is composed out of non permeable elements and thus capillary rise is restricted to approximately $20\ cm$ above the pile head. Nevertheless, absorption to the point of saturation can be taken into account.

2.3.5 Swelling of wood

A variation of moisture content in the hygroscopic range of wood leads to a volume change. For an increasing moisture content swelling takes place. Swelling and shrinkage occurs in a different extent for all three main directions of wood. The degree of swelling α is expressed by the elongation due to a moisture change in proportion to the kiln-dry length of the specimen. Among normal conditions dry wood has a moisture content of approximately $12\,\%$ (Niemz P. [2011]). Deduced from the decisive curve (α_{rad}) shown in figure 2.17 a maximum swelling in radial direction of approximately $2\,\%$ can appear. In further consequence a gradual radial volume increase after installation of the pile can lead to higher normal stresses acting on the shaft. Hence an increase of bearing capacity can be expected.

Again this thought has to be treated with caution. The water absorption and swelling process has to be seen as a combination. Whether this consideration has any favorable impact should be validated by model tests.

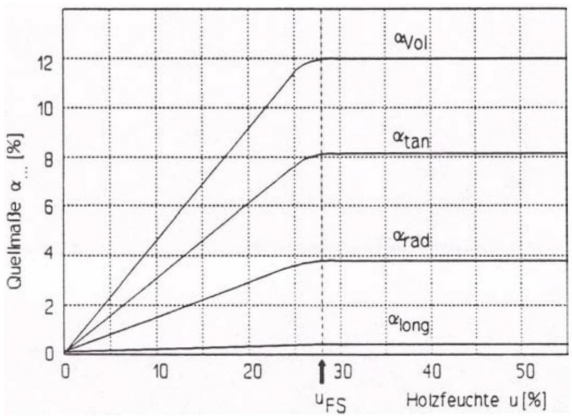

Figure 2.17: *Swelling of wood; (Ressel J. [1992])*

3 Introduction to the numerical studies

3.1 General

In consideration of the previous chapter, timber pile foundations exhibit an economical and environmentally friendly solution which was in wide use up to the last century. There is no apparent reason for prohibiting a comeback of timber pile foundations. To gain a better understanding, this thesis contains numerical studies on the bearing behaviour of this foundation type. Therefore numerical comparative analyses were performed. For conducting the computations, the finite element codes PLAXIS 2D Version 2017 (PLAXIS [2018a]) and PLAXIS 3D Version 2017.01 (PLAXIS [2017]) respectively were used. Post processing was carried out with the aid of MS Excel.

To carry out the comparative analysis, the main variations were done in terms of pile group setup. In table 3.1 the combination of variable dimensions is displayed. Supplementary to the investigation of various dimensions, an evaluation of the impact due to different tip shapes and shaft shapes was carried out. Furthermore two load distributing layers, exhibiting a different stiffness were examined. It has to be noted that installation effects were not considered.

Table 3.1: *Pile group setup*

stiffness	**diameter**	**length**	**spacing**
concrete	12.5 cm	2.5 m	0.5 m
		4.0 m	1.0 m
gravel layer with geogrid	25.0 cm	4.0 m	1.0 m
		8.0 m	1.5 m

The following bullet list provides an overview of the applied strategy.

- **single piles - 2D axisymmetric**
  - examination of different pile dimensions
  - examination of different tip shapes
  - examination of different pile shapes
- **infinite pile group - 2D axisymmetric**
  - examination of different load distributing layers
  - examination of different pile group configurations
- **single piles - 3D**
  - examination of different pile dimensions
- **infinite pile group - 3D**
  - examination of different plan views
- **entire pile group - 3D**
  - examination of different monolithic blocks including a shallow foundation
  - examination of different load distributing layers
  - examination of different pile shapes
  - examination of different pile group configurations

3.2 Material parameters

In Austria, some vast lacustrine clay deposits are located (e.g. ˝Salzburger Seeton˝). These soils are composed out of silt with an minor content of clay or fine sand (Waldherr B. [2010]). Such subsoil conditions offer perfect opportunities for the application of timber pile foundations. For this thesis, suitable parameters were assigned to model a subsoil consisting of soft lacustrine clay. The lacustrine clay was the only material resorted on an advanced constitutive model, namely the hardening soil model with small-strain stiffness (HSsmall-model). For all other materials, a linear elastic material behaviour was presumed as sufficiently accurate and adequate parameters were assigned. The stiffness of timber was pursuant to its high moisture content deduced from Niemz P. [2014]. A detailed description on the material models can be found in PLAXIS [2018b]. Furthermore, it has to be noted, that for all models the ground water table was on top of the subsoil. The analyses were performed under drained conditions, which to a certain extents is not the proper way to model the present circumstances. Since the main interest of this thesis is a comparison of different setups, this assumtion was made for the sake of shorter computation times.
A summary of material parameters used for the computations is given in table 3.2.

For the geogrid a $EA = 2\,500\ [kN/m^2]$ was assumed.

Table 3.2: *Material parameter*

	lacustrine clay ST	**wood** W	**concrete** Con	**gravel** Grav	
constitutive model	HSsmall	LE	LE	LE	
drainage type	drained	non-porous	non-porous	drained	
$E_{oed}^{ref} \mid {}^*E$	8	* 8 800	* 30 000	* 100	$[MPa]$
E_{50}^{ref}	10				$[MPa]$
E_{ur}^{ref}	30				$[MPa]$
ν_{ur}	0.2				$[-]$
ν		0.33	0.33	0.33	$[-]$
p_{ref}	100				$[kPa]$
OCR	1				$[-]$
G_0^{ref}	37.5				$[MPa]$
$\gamma_{0.7}$	$1.5 * 10^{-4}$				$[-]$
m	0.8				$[-]$
K_0^{nc}	0.546				$[-]$
γ_{unsat}	17.5	7.5	24	21	$[kN/m^3]$
γ_{sat}	19			23	$[kN/m^3]$
c'	3				$[kPa]$
φ'	27				$[^\circ]$
ψ'	0				$[^\circ]$
$k_x = k_y = k_z$	$8.64 * 10^{-4}$			86.4	$[m/day]$
R_{inter}	0.7				$[-]$

3.3 Model depth

In general the depth of numerical models is set in a way that the influence with respect to boundary conditions is negligible. When modelling a pile out of an infinite pile group, it is not possible to eliminate this problem. A simple explanation of this problem can be found in a reflection of $Hooke's\ law$ (eq. 3.1). The ratio between model width and model depth is so small that it can be seen as a 1D beam and from a certain model depth on there is no difference if a pile is installed or not.

$$\sigma = E * \varepsilon \qquad \hat{=} \qquad \frac{F}{A} = E * \frac{\Delta l}{l_0} \tag{3.1}$$

In eq. 3.1, Δl depicts the boundary condition of $125\ mm$ displacement, l_0 describes the model depth, E in the current case is stress dependent and increasing with the power of 0.8 and A is the area of the pile cell. The load is applied on the whole area of the cell and has to be transferred to the bottom of the model. Therefore in each horizontal section the same stress conditions due to additional stresses occur. Since a linear increase of model depth is coupled to a stiffness increase with the power of $m = 0.8$ it is not possible to eliminate this problem.

For that reason a lacustrine clay layer with an extent of $20\ m$ was presumed. All conducted analyses were performed with a model depth of $20\ m$.

3.4 Load application

Basically the load application was performed displacement controlled. To capture a precise load versus settlement behaviour of the shaft at small displacements, the initial load application was executed by applying displacements in a millimetre range. For the advancing calculation the displacement steps were increased step by step up to steps of $25\ mm$. The load application for the evaluation of the entire pile group was carried out stress controlled by applying load steps of $25\ kPa$.

3.5 Interface elements

To model the interaction between pile and adjacent soil, interface elements were used. The strength parameters for the shaft resistance were reduced by $R_{inter} = 0.7$. An interface extension at the pile tip is a common way to avoid stress concentrations. According to Engin H.K. [2013] the variation of extension length has no distinct influence in the overall behaviour. Due to a simple modelling procedure an extension length of one times the pile radius was used. Since reading out interface stresses is a convenient way of extracting data, for the 2D analyses interfaces were used as an intersection between each material change. For the latter two applications of interface elements, no strength reduction was applied and $R_{inter} = 1.0$ was used.

3.6 Interpretation

3.6.1 Representation of results

As a result of the computations, applied load versus settlement diagrams were generated. For a more detailed investigation, a subdivision into shaft resistance, base resistance and load which was directly transferred from the load distributing layer to the subsoil was carried out. Due to $actio = reactio$ the applied load has to equal the summation of the three resistances. The generated diagrams capture settlements up to displacements of $125\ mm$. This order of magnitude was chosen since it depicts $100\,\%$ or $50\,\%$ of the pile diameter respectively. The maximum of the axis depicting resistances was adjusted to the curves for each individual diagram. This enables a high readability for each chart instead of an optical comparability. Displacements are referred to the centre point of the pile head. Results presenting resistances are related to the indeed applied load. This implies that stresses as a consequence of executing the foundation were eliminated.

In addition an even more detailed interpretation of the shaft was carried out. For different load levels (the self weight of the construction was neglected) the mobilised shaft resistance τ_{mob} and the relative shear stress τ_{rel} were plotted and evaluated.

The interpretation of the entire pile group was mainly performed for the overall foundation. Resistances are in general depicted as the summation of individual pile resistances. For two comparable cases a detailed interpretation of three decisive piles out of the pile group was performed. Additionally to the load versus settlement curves, charts showing the load separation changing over the load application procedure were introduced. Therefore three new terms were defined which are expressed as described in eq. 3.2 to eq. 3.4. In these charts results of one foundation type are depicted with hatched areas. To enable a comparison, the transition borders of a second investigated foundation were attached as dash-dotted lines.

- **Proportion of base resistance:**

$$R^*_{base} = \frac{\sum R_{base}}{F_{z,tot}} \tag{3.2}$$

- **Proportion of shaft resistance:**

$$R^*_{shaft} = \frac{\sum R_{shaft}}{F_{z,tot}} \tag{3.3}$$

- **Proportion of force transferred directly to the subsoil:**

$$R^*_{soil} = \frac{\sum R_{soil}}{F_{z,tot}} \tag{3.4}$$

3.6.2 Extraction and interpretation of results - PLAXIS 2D

Due to the fact that the load application was performed displacement controlled the extraction of the applied load versus displacement curves was conveniently performed via the curves manager tool provided in the PLAXIS 2D OUTPUT application. For the interpretation of the different resistances, the interface elements were used to read out stresses. To prove the accuracy of the interpretation a crosschecking of $applied\ load \overset{!}{=} \sum resistances$ was conducted. Furthermore, it has to be noted that in PLAXIS 2D the vertical axis is designated by y whereas z is used in PLAXIS 3D. To avoid any confusion in the interpretation a renaming of 2D results was required ($y_{PLAXIS\ 2D} \overset{\wedge}{=} z_{interpretation}$). 2D computations were performed solely in respect of axial symmetry (circular plan view). The following equations (eq. 3.5 to eq. 3.8) demonstrate the post processing procedure:

- **Applied load:**

$$F_{z,tot} = 2\pi * F_{y(PLAXIS\ 2D)} \tag{3.5}$$

- **Resistance of a horizontal interface like R_{base} or R_{soil}:**

$$R_{base} = R_{soil} = \sum_{i=1}^{n} \pi * \left(x_{i+1}^2 - x_i^2\right) * \left(\frac{\sigma_{i+1} + \sigma_i}{2}\right) \tag{3.6}$$

- **Resistance of a vertical interface like R_{shaft}:**

$$R_{shaft} = \sum_{i=1}^{n} 2\,r\,\pi * (y_{i+1} - y_i) * \left(\frac{\tau_{i+1} + \tau_i}{2}\right) \tag{3.7}$$

  Where r is the radius of the pile.

- **Resistance of an inclined interface like R_{base} for different tip shapes or R_{shaft} for tapered piles:**

$$\begin{aligned} R_{base} = R_{shaft} = \sum_{i=1}^{n} \pi * (x_{i+1} + x_i) * \frac{(x_{i+1} - x_i)}{cos(\alpha)} * \dots \\ \dots * \left[\left(\frac{\sigma_{i+1} + \sigma_i}{2}\right) cos(\alpha) + \left(\frac{\tau_{i+1} + \tau_i}{2}\right) sin(\alpha)\right] \end{aligned} \tag{3.8}$$

  Where α is the angle of the interface with respect to the horizontal.

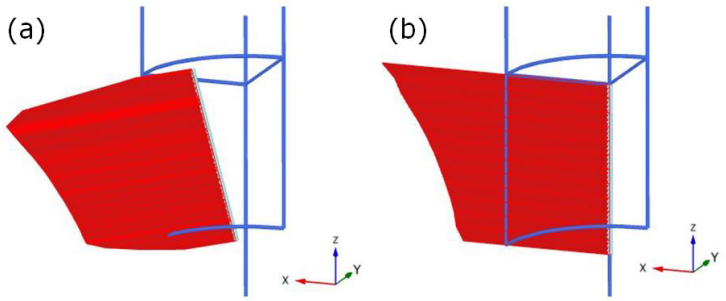

Figure 3.1: *Structural forces in volumes: (a) faulty centre line (b) correct centre line*

3.6.3 Extraction and interpretation of results - PLAXIS 3D (single piles and infinite pile group)

The extraction of the applied load versus settlement behaviour was likewise as previously performed with the curves manager tool. The shaft resistance was obtained by the integration of the interface along a vertical section by applying eq. 3.7. To assess the base resistance of the pile, the structural forces in volumes tool was used. The author had quite bad experiences by applying this tool in terms of automatically adding centre lines and thus correctness of results. These problems occurred already for small models consisting out of $\sim$ 35 000 elements. To overcome these problems a soil volume with a height of $10\ cm$ and the same cross section as the pile was modelled below the actual pile. In figure 3.1 a faulty and a correctly added centre line of the auxiliary volume is shown. One can say that the faulty one is a kind of space diagonal, but by checking the coordinates the arbitrariness of the position became visible. Data were extracted at the top of the volume, which depicts the transition to the pile. The force which was transferred directly to the soil was deduced out of the applied load and the pile resistances ($R_{soil} = F_{z,tot} - R_{base} - R_{shaft}$).

3.6.4 Extraction and interpretation of results - PLAXIS 3D (entire pile group)

For the interpretation of the entire pile group different methods as explained above were applied. Since the load application was performed in consecutive load steps the applied load versus settlement behaviour was generated via ΣM_{stage} as shown in eq. 3.9.

$$F_{z,tot} = (F_i - F_{i-1}) * \Sigma M_{stage} + F_{i-1} \tag{3.9}$$

Where F_i is the maximum applied load of the current calculation phase and F_{i-1} the maximum applied load of the previous phase.

To perform an evaluation of the shaft and base resistance it was not possible to use the structural forces in volumes tool due to the above mentioned problems. The option of manual adding of centre lines was not used due to a significant increase of required time

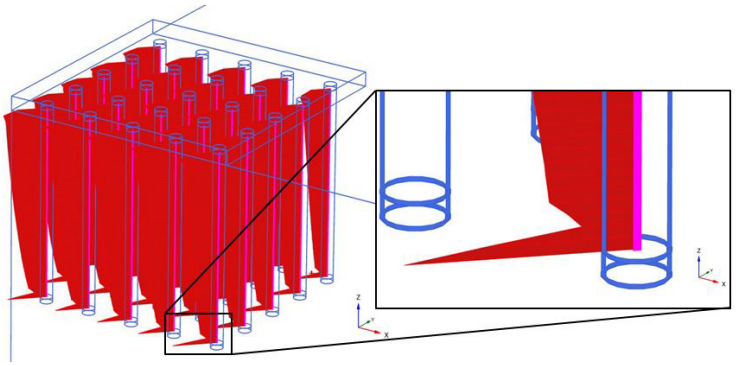

Figure 3.2: *Stress concentration at the pile end*

and effort (up to 55 piles per model and at least 5 minutes per pile). Therefore, additionally to the piles, beam elements were modelled. For the computation the stiffness of the beam material was reduced by a factor of $1\ 000$ compared to the actual pile stiffness. In a further step the beam elements were used for the interpretation. As base resistance, the resultant normal force of the beam element at the bottom was used. Moreover, the shaft resistance was deduced by the subtraction of normal force at the base to the normal force at the pile head. Due to stress concentrations at the ends of the beam elements (figure 3.2), adequate stress points with a distance of $10-25\ cm$ above the end of the pile were selected manually. This measure caused a slight inaccuracy.

4 2D axisymmetric studies

4.1 Single piles - Model

4.1.1 Investigation of different pile dimensions

The investigation of single piles in 2D was carried out by means of an axisymmetric model. The model size has a depth of $20\ m$, which is the assumed extant of the lacustrine clay layer. To ensure the elimination of boundary conditions, the model width was set to $20\ m$. The x_{min} boundary depicts the symmetry axis of the model as well as the pile axis. To keep the number of elements as small as possible but to gain on the other hand the best possible discretisation, some extra soil clusters were modelled where a local mesh refinement was applied. An exemplary connectivity plot of a single pile model is demonstrated in figure 4.1. In the present case, approximately 2 000 to 3 000 $15-$noded elements were used. An overview of examined pile dimensionsis given in table 4.1.

Table 4.1: *Single piles*

diameter	length
12.5 cm	2.5 m
12.5 cm	4.0 m
25.0 cm	4.0 m
25.0 cm	8.0 m

4.1.2 Investigation of different tip shapes

The pile tips of timber piles frequently exhibit a conical shape. An evaluation of the impact due to a conical tip shape to the load versus settlement behaviour was conducted. Therefore, four different cone angles were considered. α, the cone angle is specified as shown in figure 4.2. An elongation of the pile by the height of the cone was conducted to preserve the same shaft area and thus a good comparability. The examination was carried out for two different pile dimensions. In principle the model was the same as in section 4.1.1 except the execution of the pile tip which is shown in detail in figure 4.3. The examined pile dimensions and different tip shapes are summarised in table 4.2.

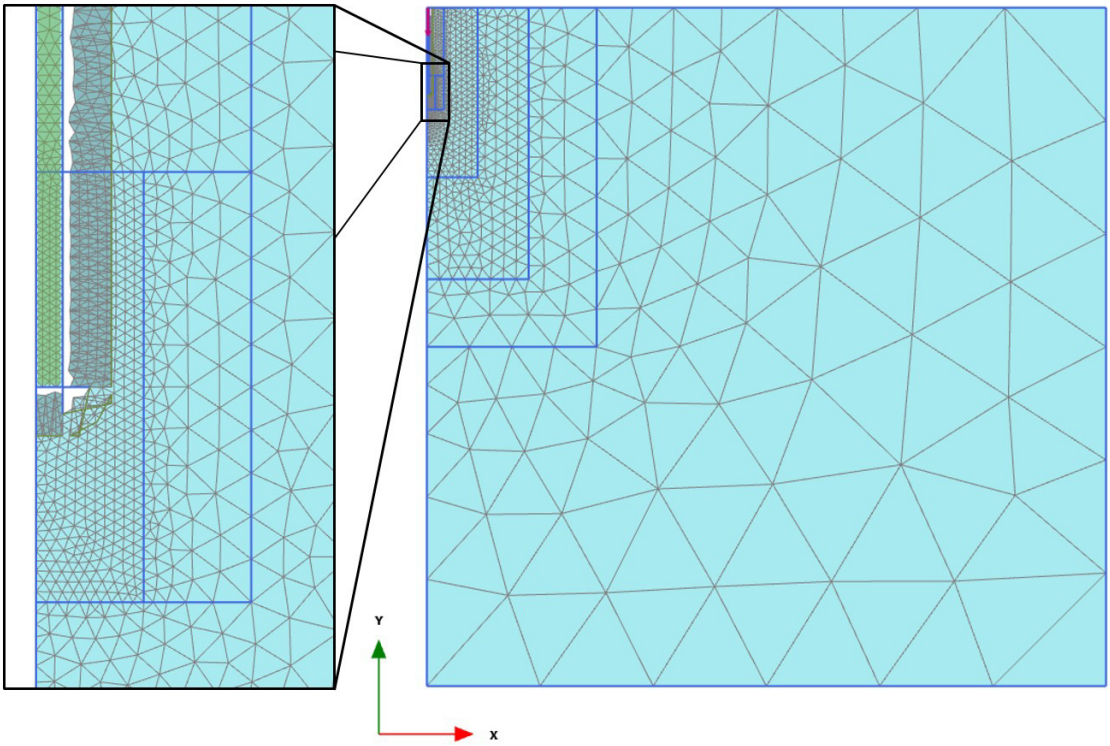

Figure 4.1: *Connectivity plot of a single pile model*

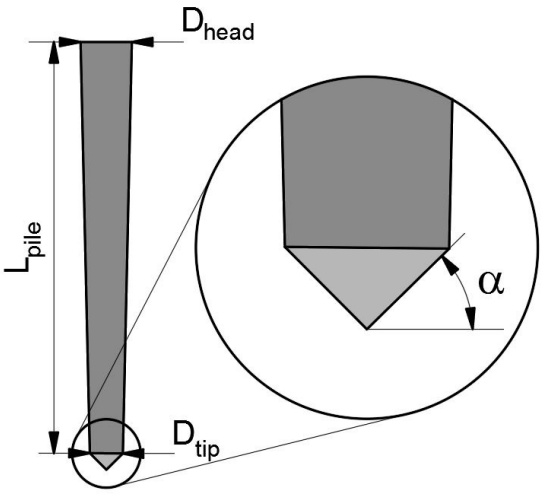

Figure 4.2: *Specification of the tip shape and the shaft shape*

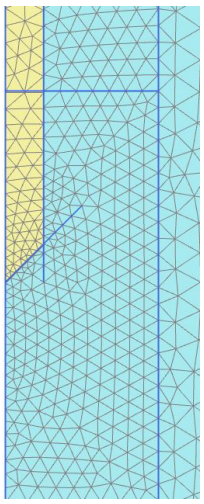

Figure 4.3: *Exemplary detail of a connectivity plot*

Table 4.2: *Tip shapes*

D	L	α
$12.5\ cm$	$2.5\ m$	$0°$
		$30°$
		$45°$
		$60°$
$25.0\ cm$	$8.0\ m$	$0°$
		$30°$
		$45°$
		$60°$

Table 4.3: *Ratio of taper*

D_{head}	D_{tip}	ROT
$25\ cm$	$25\ cm$	$0\ cm/m$
$25\ cm$	$21\ cm$	$0.5\ cm/m$
$25\ cm$	$17\ cm$	$1.0\ cm/m$
$25\ cm$	$13\ cm$	$1.5\ cm/m$
$31\ cm$	$19\ cm$	$1.5\ cm/m$

4.1.3 Investigation of different pile shapes

Since timber has an inherent conical shape, the impact of taper was evaluated. The basic model was sourced from section 4.1.1. For a pile comprising a diameter of $25\ cm$ and a length of $8.0\ m$, different tapers were examined. The ratio of taper is expressed as the change in diameter per pile length ($ROT = (D_{head} - D_{tip})/L_{pile}\ [cm/m]$ as shown in figure 4.2). In general, the diameter at the pile head was kept constant. Additionally a computation using an equal shaft area as the uniform pile and a high ratio of taper was conducted. In table 4.3 the used ratios of taper and the corresponding pile head diameters of the conducted verifications are depicted.

4.2 Single piles - Results

4.2.1 Validation of different pile dimensions

The present studies refer mainly to four pile dimension. To be aware of the capacity of these piles, investigations executed as single piles were carried out. In figure 4.4 the obtained results of the examination are shown. According to expectations, the largest pile yields the most. By comparing different lengths at same diameters, longer piles provide in each case a higher base resistance. This fact is based on the stiffness increase over depth due to the stress dependent stiffness. Furthermore it is clearly visible that the full shaft resistance is mobilised already after a few millimetres of displacement, whereas the base resistance increases with ongoing displacements.

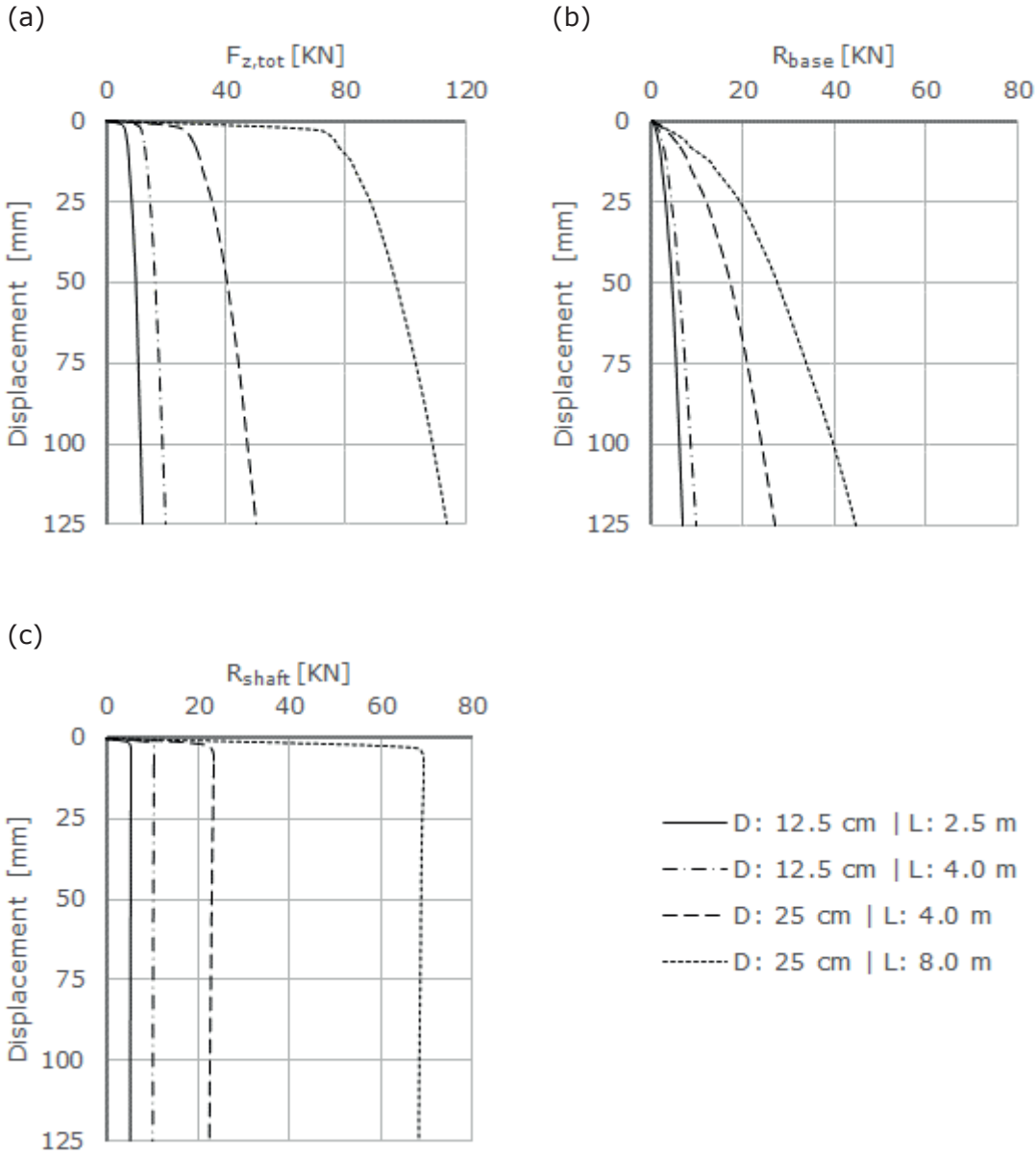

Figure 4.4: *Results of single piles:*
(a) total applied load, (b) base resistance, (c) shaft resistance

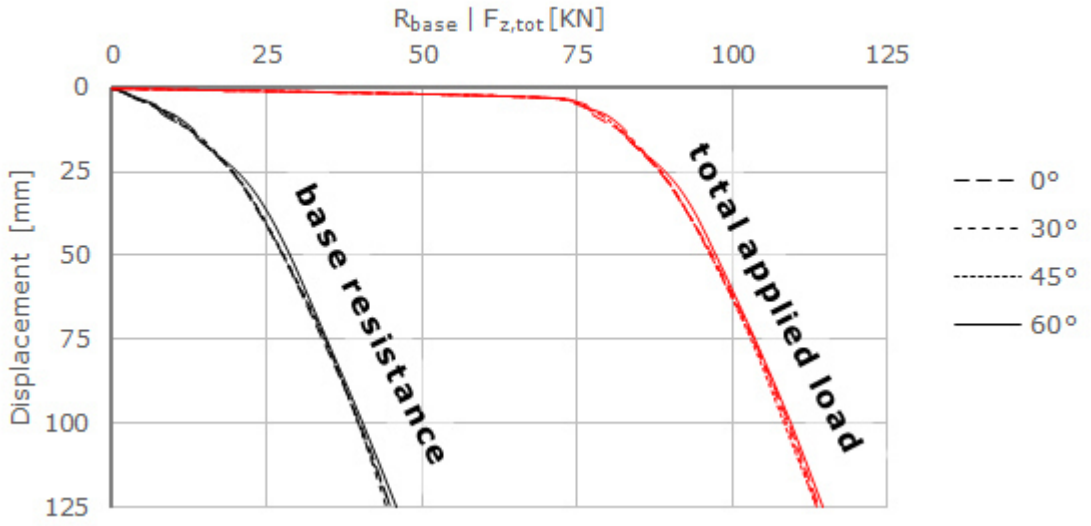

Figure 4.5: *Validation of different tip shapes:*
D: 25 cm | L: 8.0 m

4.2.2 Validation of different tip shapes

The evaluation of the impact due to different tip shapes was conducted for the largest and smallest pile dimension. In both cases no difference was observed. The results of a pile with a length of $8\ m$ and a diameter of $25\ cm$ are shown in figure 4.5. On the one hand the base resistance is shown, where no difference (beyond numerical accuracy) occurs and on the other hand the total applied load is plotted, to notice the proportion of the base resistance. Results of the second examined pile can be found in section 8.1.

4.2.3 Validation of different pile shapes

It has to be noted, that for the validation of tapered pile shapes, the same diameter at the pile head and thus a changing shaft area was used. In addition, one pile exhibiting an equal shaft area as the uniform pile was examined. In figure 4.6 the obtained results are depicted. As (a) shows, a higher ratio of taper results in a decrease of bearing capacity. This fact is obviously connected to the decrease of tip and shaft area. More interesting is the almost parallel shift of the load versus settlement curves from tapered piles. It can be said, that already a slight tapering leads to a more ductile behaviour. The combination of decreasing base resistance due to a smaller tip area and a more ductile behaviour of the shaft resistance results in the encountered parallel shift. Furthermore, in figure 4.6 (c) it is visible, that for piles with an equal shaft area the characteristic kink in the shaft resistance, where a ˝full mobilisation˝ is reached, lies approximately at the same point.

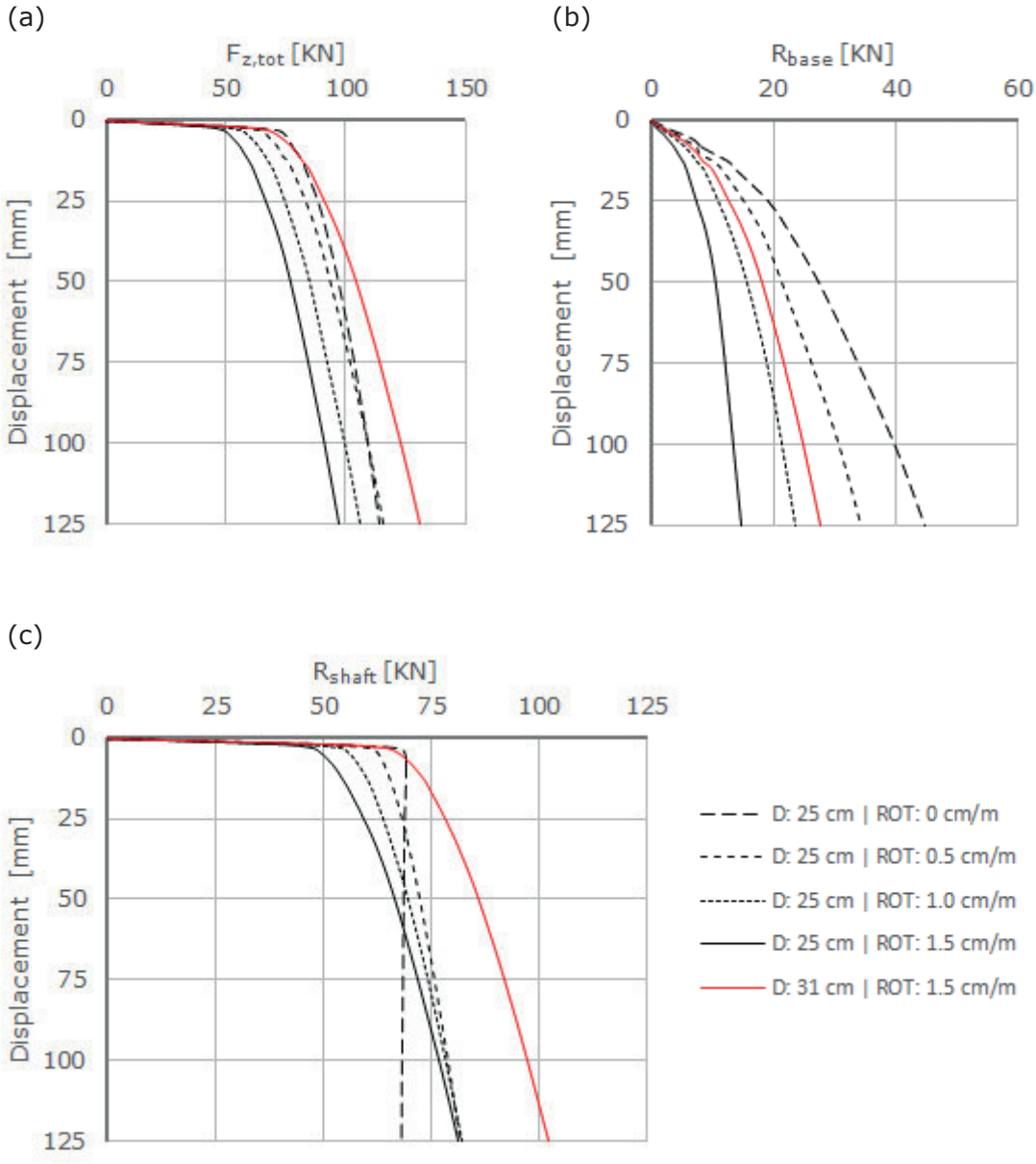

Figure 4.6: *Validation of tapered pile shapes:*
(a) total applied load, (b) base resistance, (c) shaft resistance

4.3 Infinite pile group - Model

4.3.1 General

The investigation of an infinite pile group was carried out by modelling a unit cell of one pile. Therefore the model width has to be equal to half of the pile spacing. The model depth was set to $20\ m$ and the water table was assumed on top of the subsoil. Boundary conditions were fixed in respect of horizontal displacements, which allows modelling the interaction of individual piles. On the contrary, in vertical direction an unrestrained movement was assigned. Around the pile tip the mesh was locally refined. An exemplary connectivity plot of a pile out of an infinite pile group is depicted in figure 4.8. The models comprised approximately 2 000 to 3 000 15−noded elements. It has to be remarked once again that especially for the current model configuration the model depth plays an essential role and effects the load versus settlement behaviour significantly. For an explanation it is referred to section 3.3.

4.3.2 Load distributing layer

In the present studies a load distributing layer was modelled. Therefore a $30\ cm$ thick concrete slab was assumed. To investigate the impact of the stiffness, in the contrary to the fairly stiff concrete slab, a rather soft gravel layer was modelled. Additionally to the gravel, a geogrid was inserted at the bottom of the layer. The difference of the two applied variants is shown in figure 4.7.

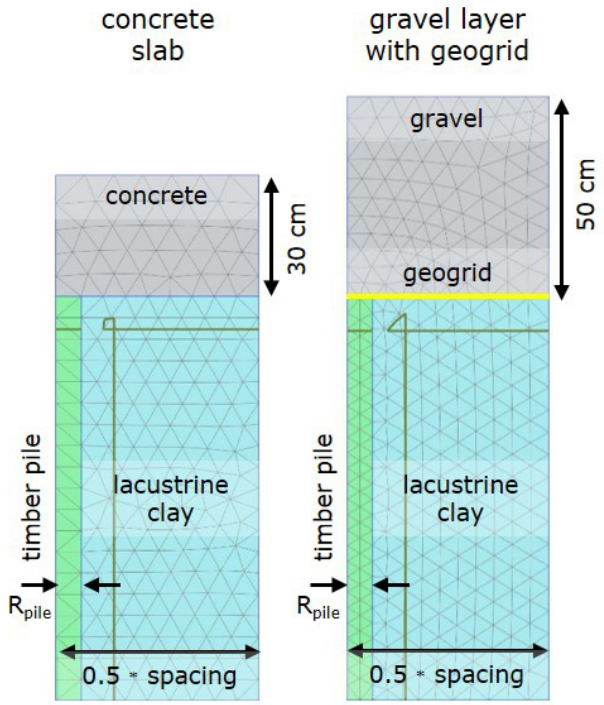

Figure 4.7: *Variants of load distributing layer*

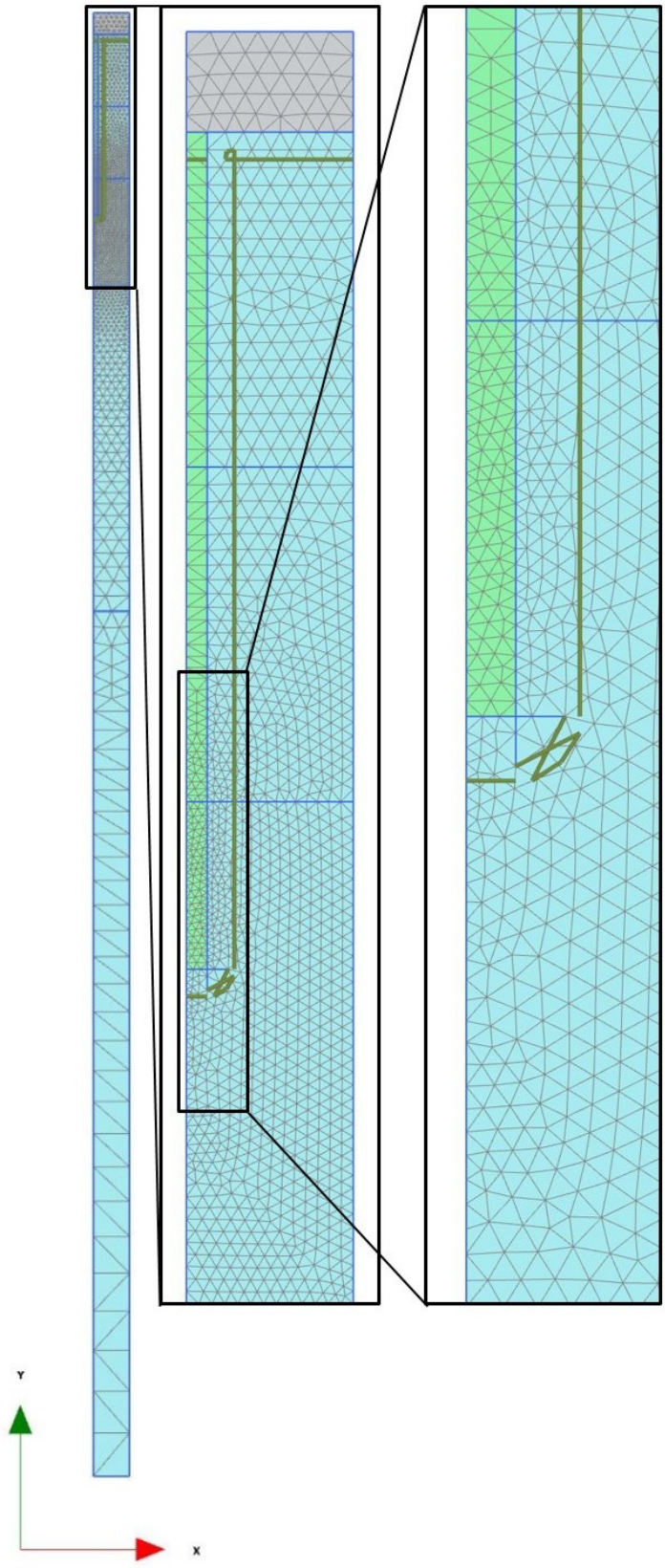

Figure 4.8: *Exemplary connectivity of a pile out of an infinite group*

4.4 Infinite pile group - Results

4.4.1 Validation of different load distributing layers

Two common versions of load distributing layers were examined. The main difference of the two designs was the stiffness. In figure 4.9 the obtained results are presented, where it can be seen, that no significant difference in the overall behaviour occurs. In figure 4.9 (c) a decrease in shaft resistance is revealed for the softer configuration whereas to the contrary in (d) it is visible that the softer layer transfers more load directly to the soil. This is a result based on displacements of the load distributing layer between the individual piles. The ˝sagging˝effect can be confirmed in the detailed interpretation of the shaft, depicted in figure 4.10 and figure 4.11. $(x.1)$ charts depict the mobilised shaft resistance plotted over the real depth whereas $(x.2)$ charts show the corresponding utilisation of the shaft resistance (τ_{rel}), plotted over the normalised depth. Due to ˝sagging˝of the gravel layer negative skin friction in the upper $20\,\% - 25\,\%$ of the pile occurs. This phenomena does not emerge for the stiff concrete slab. Hence the lower shaft resistance of piles using a softer distributing layer is explained.

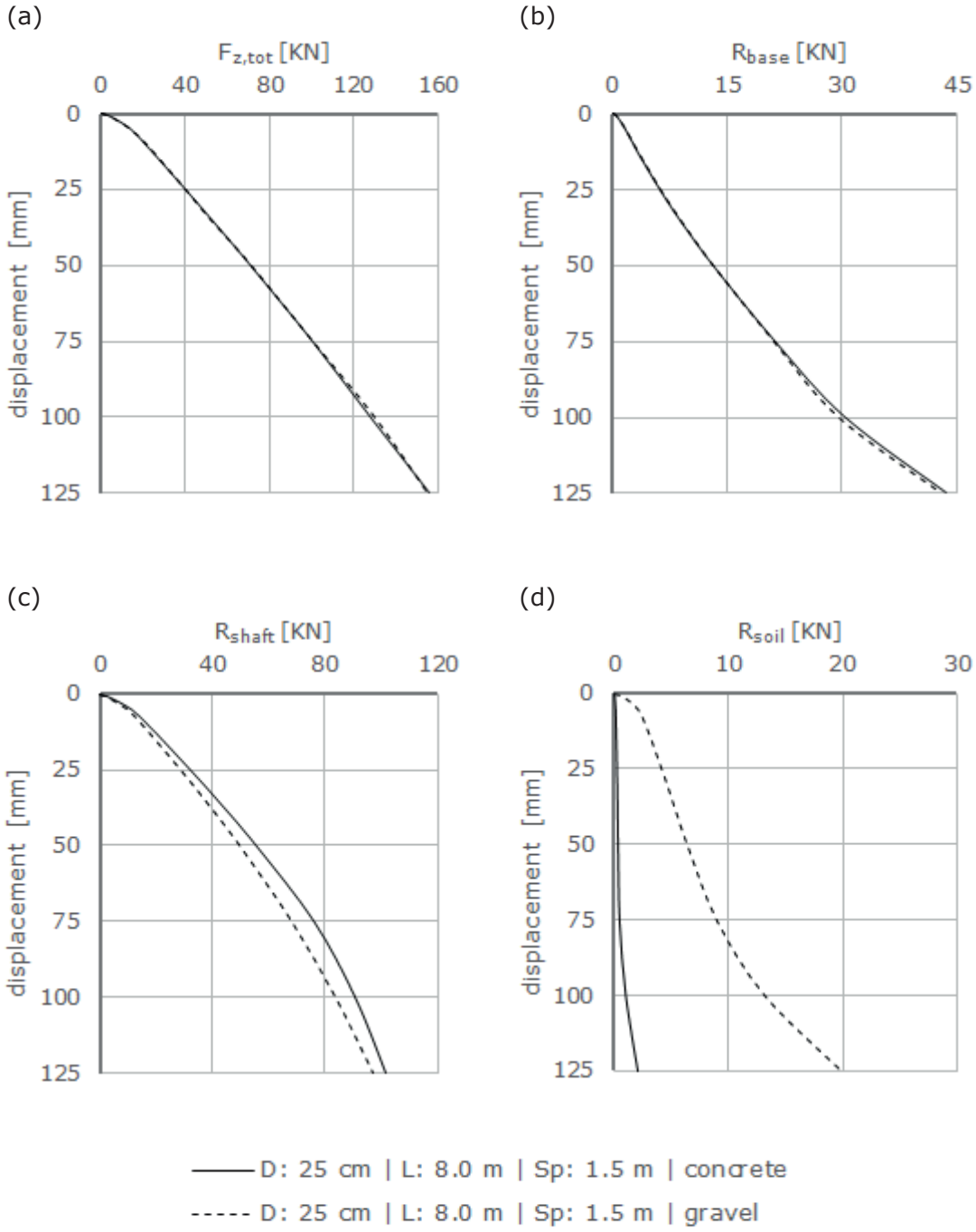

Figure 4.9: *Validation of different load distributing layers:*
D: 12.5 cm | L: 2.5 m | Sp: 1.5 m;
(a) total applied load, (b) base resistance, (c) shaft resistance,
(d) load transferred directly to the soil

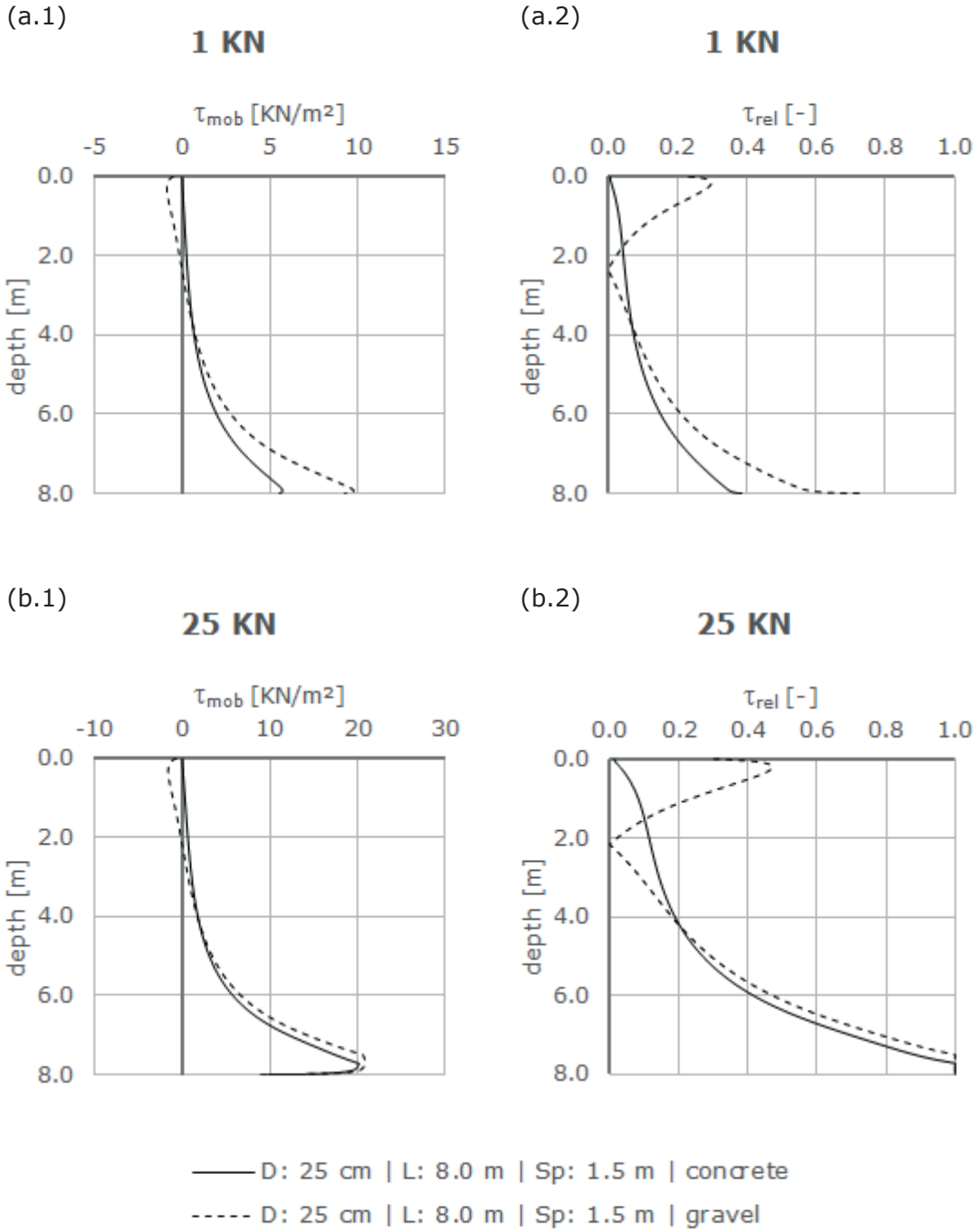

Figure 4.10: *Validation of different load distributing layers, detailed interpretation of the shaft: (a) load step 1 KN, (b) load step 25 KN*

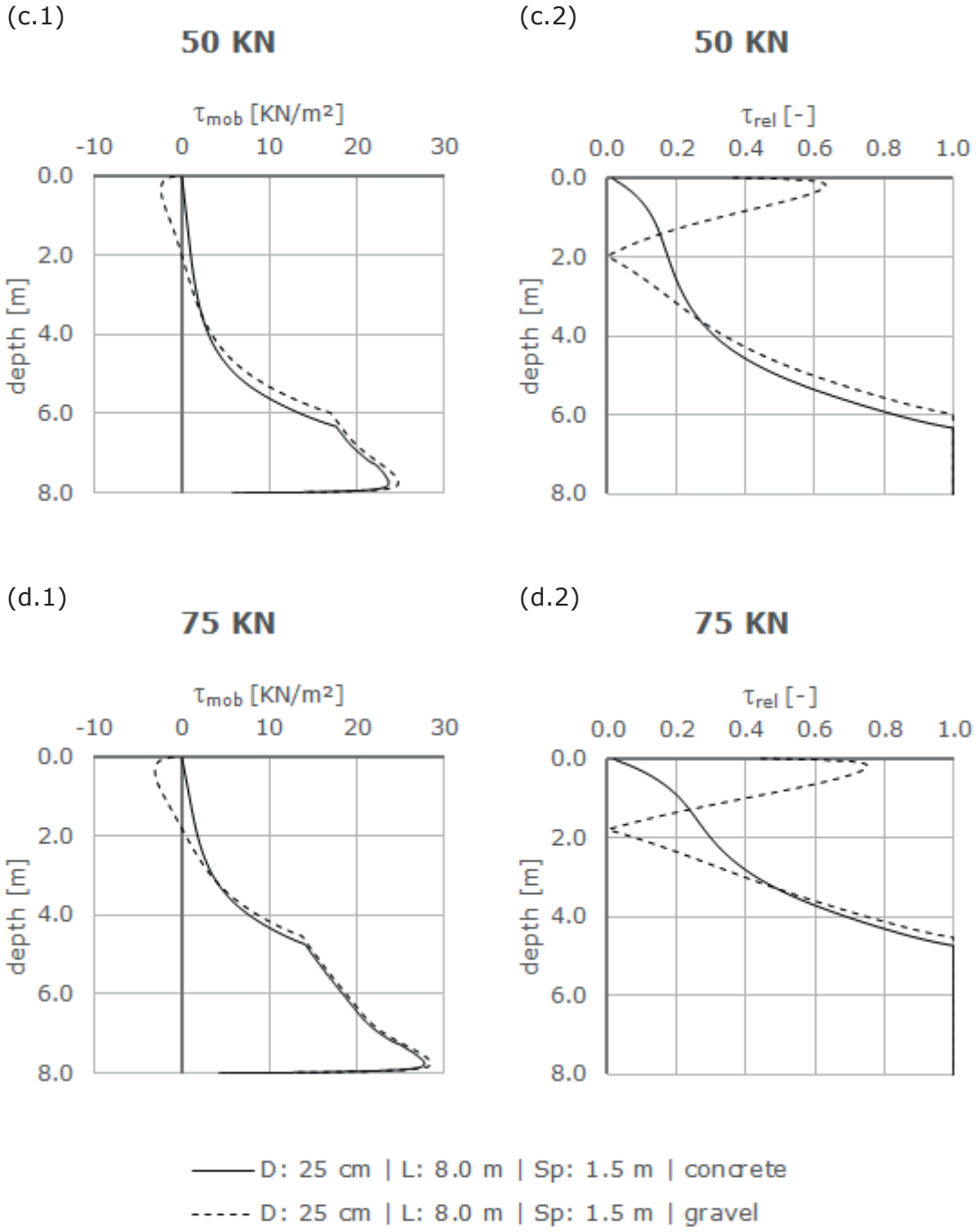

Figure 4.11: *Continuation of figure 4.10: (c) load step 50 KN, (d) load step 75 KN*

4.4.2 Validation of different pile group configurations

The main aim of the 2D preliminary studies was the evaluation of different pile group configurations. An overview of the variation of dimensions is given in table 3.1. In this section results of piles exhibiting a diameter of $12.5\ cm$ are shown. Supplementary results of the piles with a diameter of $25\ cm$ are depicted in section 8.1. Nevertheless, the discussion counts for all examined pile group configurations. Moreover one has to bear in mind that the evaluation was not conducted in a normalised manner since a normalised shaft or base resistance is not a meaningful measure.

In figure 4.12 the results of the studies are plotted. Additionally to the results from infinite pile groups, the outcome of single piles were added. By carrying out a detailed examination of the obtained results it can be seen that all three resistances are connected to each other. A full mobilisation of the shaft resistance leads to a kink in figure 4.13 (c) which can be confirmed in figure 4.15 (b). After the mobilisation of the shaft resistance is completed the additional load has to be transferred directly from the concrete slab to the soil, as figure 4.13 (d) shows. Following the activation of the soil resistance with a small distance the base resistance changes (figure 4.13 (b)).

To be able to carry out a detailed examination of the shaft resistance a subdivision into the two different spacings was performed as depicted in figure 4.13 to figure 4.15. It can be seen that for a small spacing it is not possible to utilise the shaft on a high percentage. Whereas for a larger spacing the utilisation is relatively high at the beginning of the load application procedure. From this fact it can be deduced, that too less relative displacements occur to obtain a better mobilisation of the shaft for a small spacing. This indicates that the soil and the piles displace almost jointly.

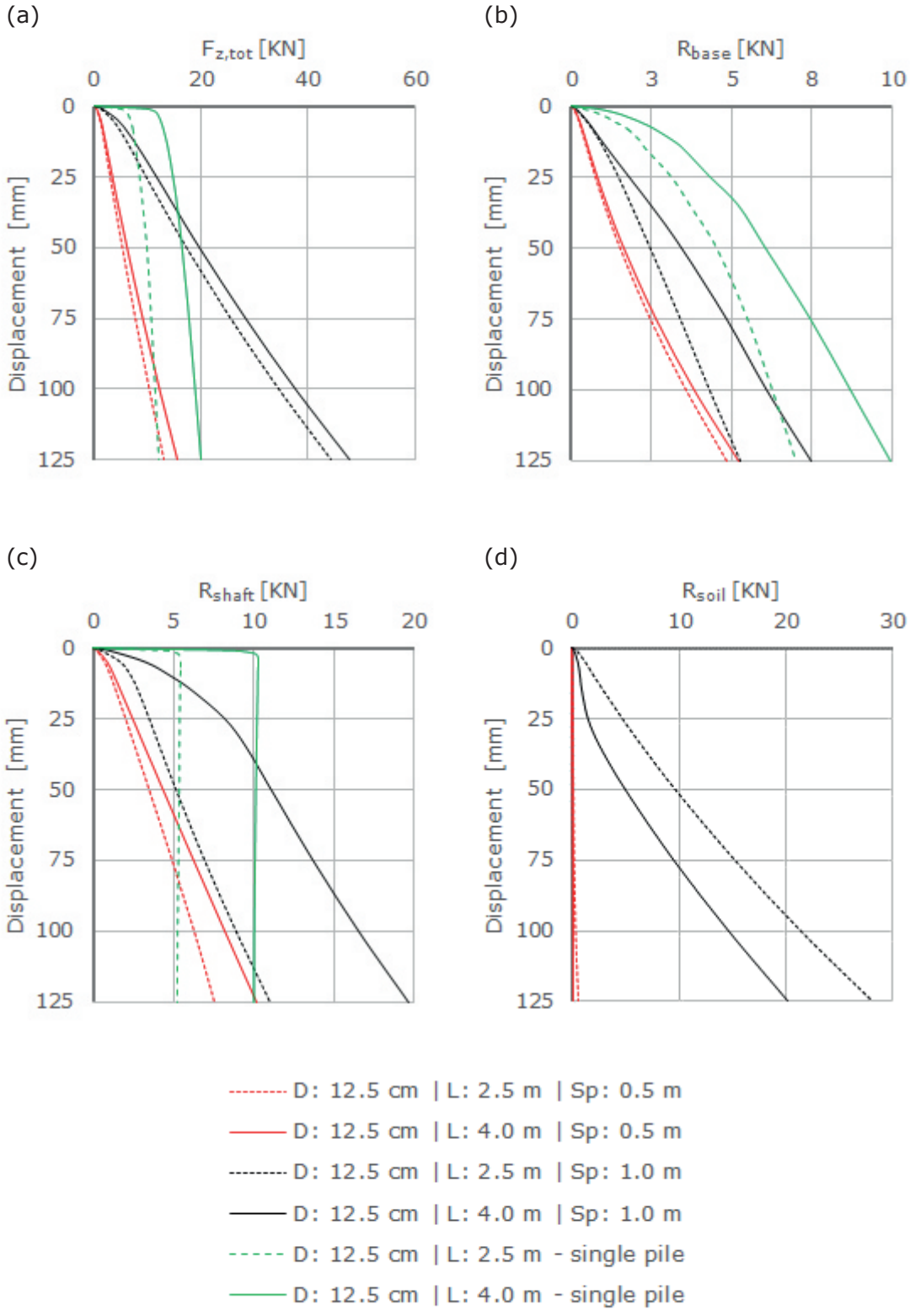

Figure 4.12: *Validation of different pile group configurations - D: 12.5 cm: (a) total applied load, (b) base resistance, (c) shaft resistance, (d) load transferred directly to the soil*

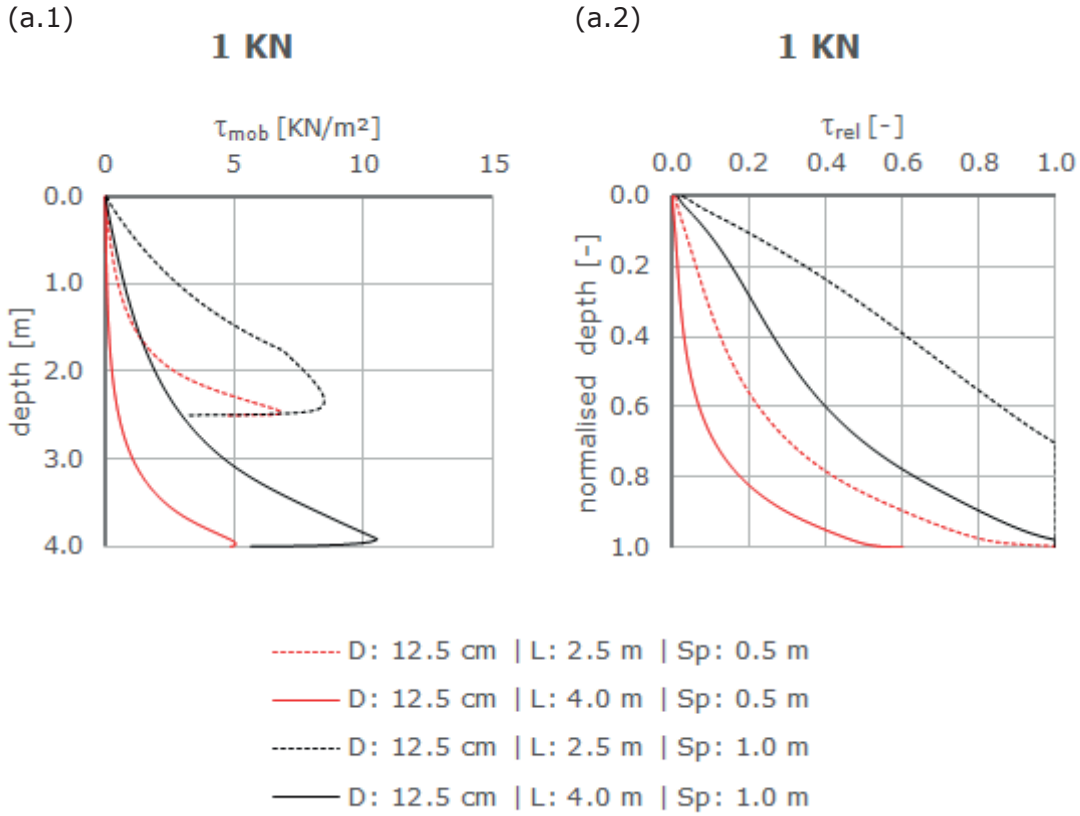

Figure 4.13: *Validation of different pile group configurations - D: 12.5 cm, detailed interpretation of the shaft:*
(a) load step 1 KN

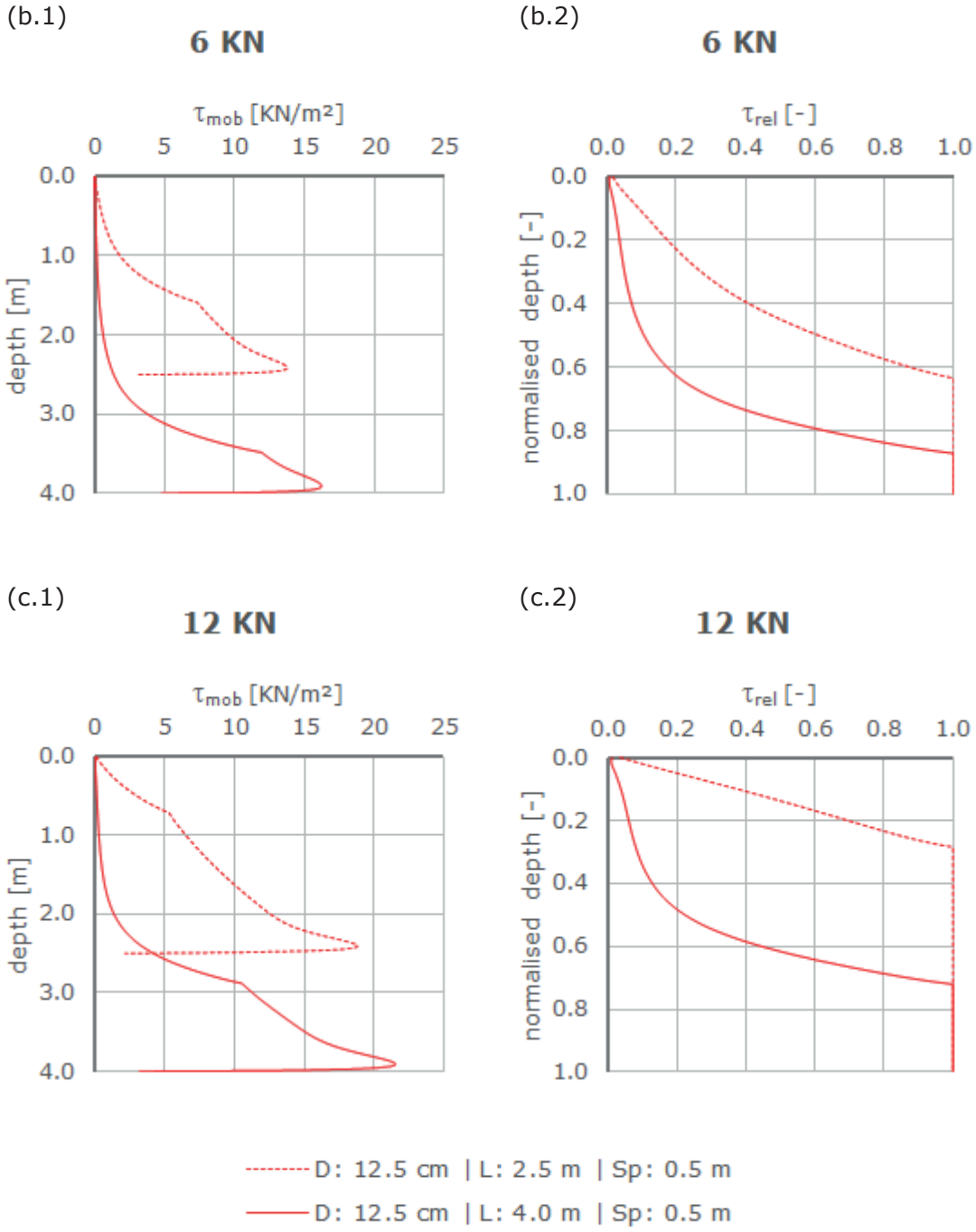

Figure 4.14: *Continuation of figure 4.13: (b) load step 2 KN, (c) load step 12 KN*

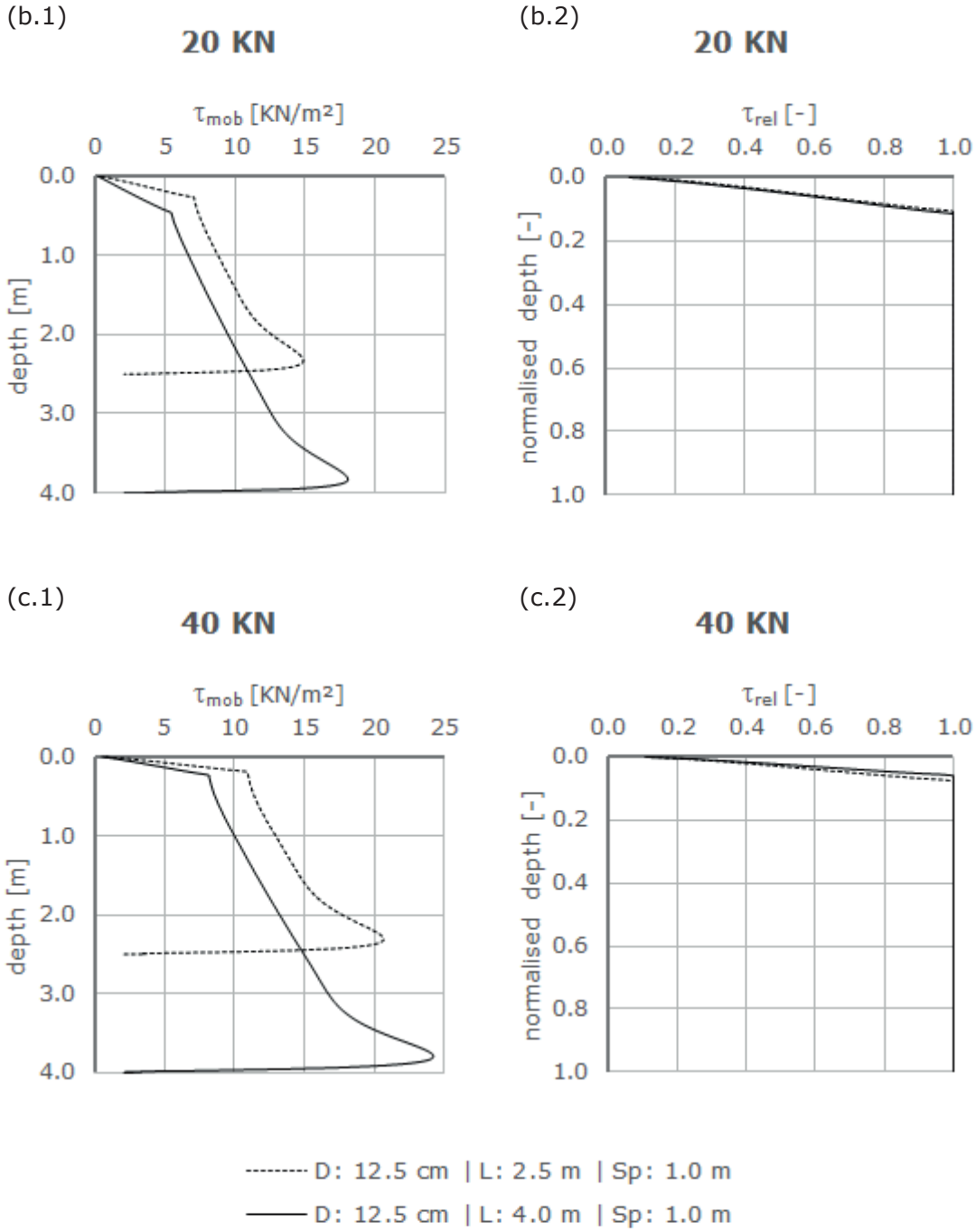

Figure 4.15: *Continuation of figure 4.13: (b) load step 20 KN, (c) load step 40 KN*

5 3D studies

5.1 Single piles - Model

Thus far all computations were carried out using axial symmetry, which is a proper feature to model single piles or piles out of an infinite pile group (as long they are loaded vertically). To be able to capture the overall behaviour of an entire pile group, 3D computations have to be performed. To confirm the equality of 2D and 3D computations, in a first step two single piles were examined under 3D conditions. The dimensions of the examined piles are provided in table 5.1.

3D models were not performed as full models, But two symmetry planes were implied and only one quarter was modelled. In the same way as in the 2D case, the model width amounted $20\ m$ and the model depth was set to $20\ m$. The used material parameters are discussed in table 3.2. The two models comprised $\sim$ 55 000 $10-$noded elements. An exemplary connectivity plot is depicted in figure 5.1.

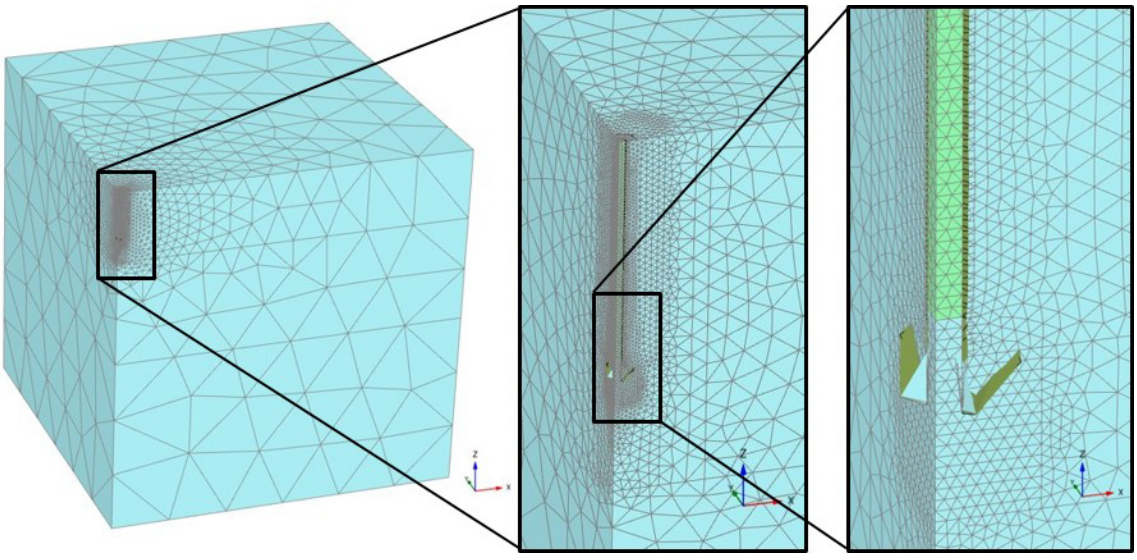

Figure 5.1: *Connectivity plot of a single pile model*

Table 5.1: *Single piles - 3D*

diameter	length
12.5 cm	2.5 m
25.0 cm	8.0 m

5.2 Single piles - Results

The examination of single piles modelled in 3D shows conformity with the obtained 2D results as depicted in figure 5.2. Supplementary results follow in section 8.2.

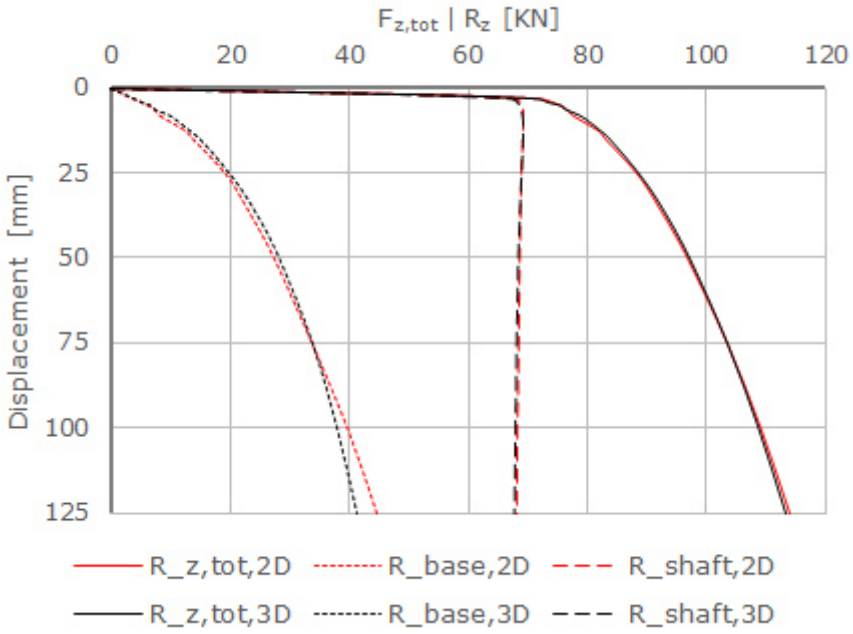

Figure 5.2: *Results of a single pile in 3D:*
D: 25 cm | L: 8.0 m

5.3 Infinite pile group - Model

The examination of piles out of an infinite pile group in 3D was carried out on the one hand to confirm equality of 2D and 3D computations and on the other hand to investigate the impact of the simplification owing to axial symmetry. 2D axis-symmetric modells exhibit a circular plan view whereas physical pile groups have a square or hexagonal plan view respectively as depicted in figure 5.3. The verification was performed for two layouts as delineated in table 5.2. Generally speaking the 3D models were the same as the 2D models, except the variation of top view. The models comprised 35 000 to 50 000 10−noded elements using two symmetry planes. An exemplary connectivity plot of the entire model is shown in figure 5.4. Furthermore connectivity plots of the different plan views are depicted in figure 5.5. The detailed interpretaion of the shaft resistance was carried out at a vertical section at 45° of the modelled quarter.

Table 5.2: *Infinite pile group - 3D*

diameter	length	spacing
12.5 cm	2.5 m	1.0 m
25.0 cm	8.0 m	1.5 m

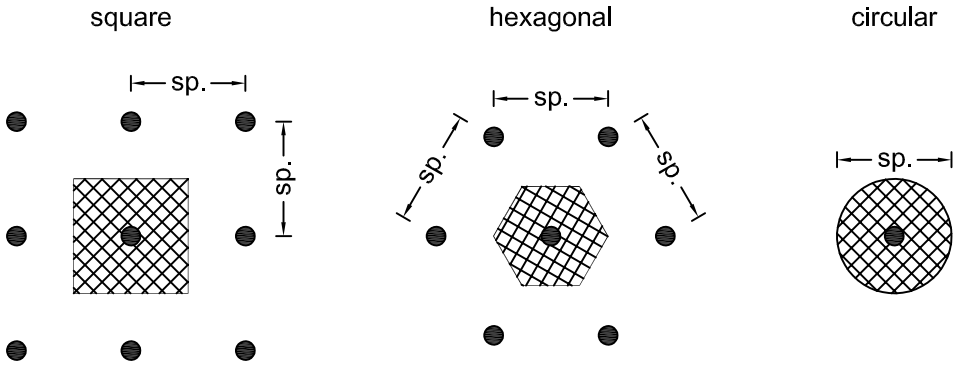

Figure 5.3: *Physical and theoretical plan views*

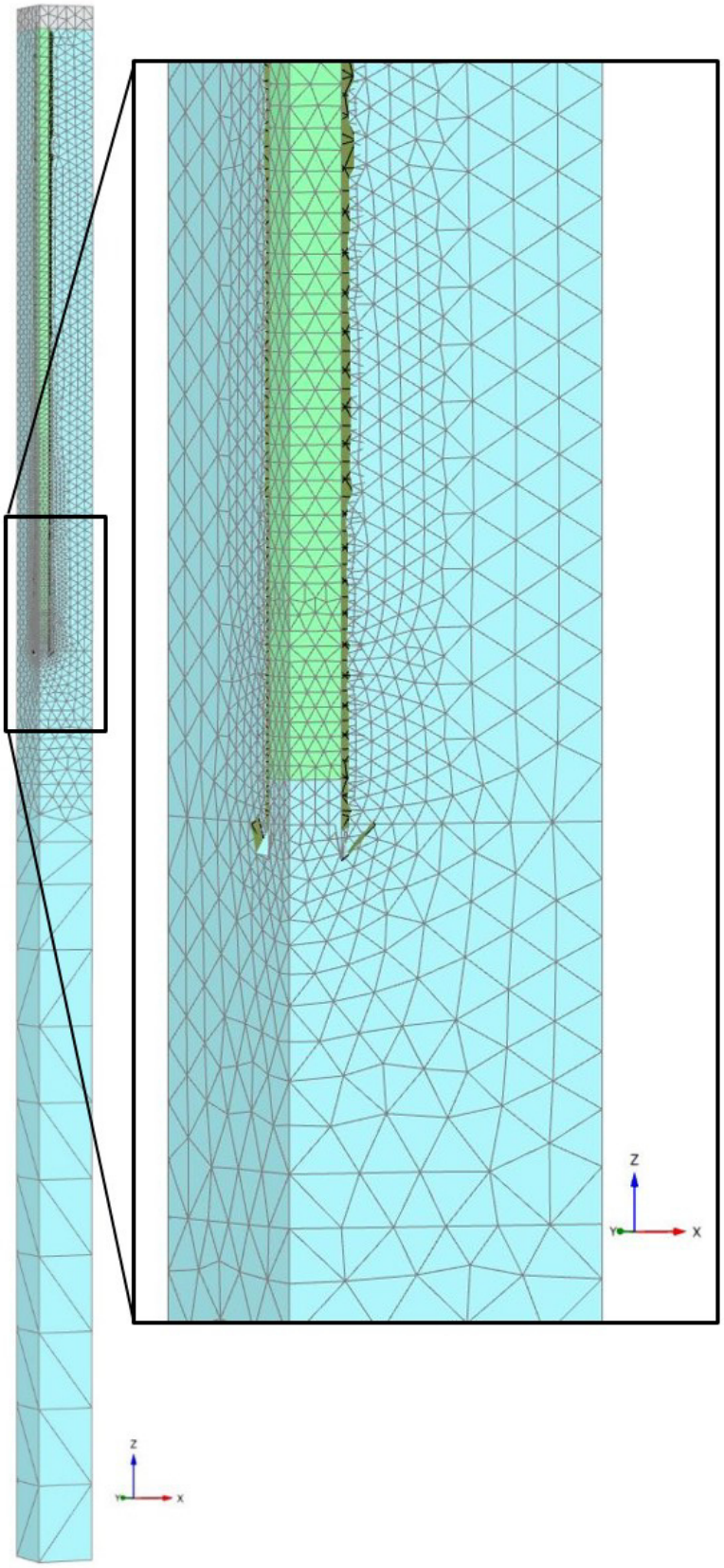

Figure 5.4: *Connectivity plot of an infinite pile group*

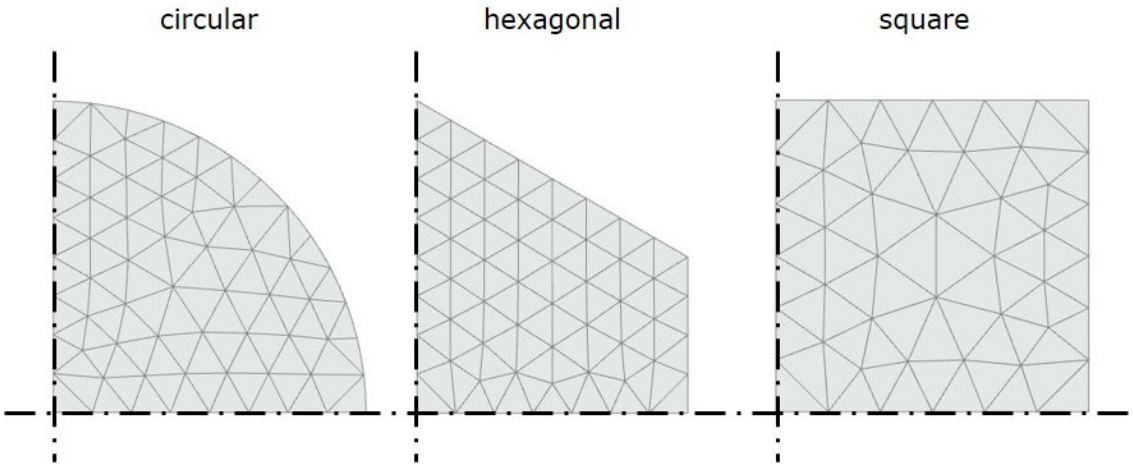

Figure 5.5: *Connectivity plot of different plan views*

5.4 Infinite pile group - Results

At the beginning of the examination of infinite pile groups, a validation of conformity between 2D and 3D computations was performed. By comparing results of the 2D axis-symmetric model with 3D results exhibiting a circular plan view in figure 5.6 it can be observed that both finite element analyses compute same results.

For the examination of different plan views it can be deduced from figure 5.6 that the size of the pile cell is the main issue which governs the bearing behaviour. Due to the bigger area and a larger distance to the adjacent pile in diagonal direction, models with a square plan view have the ability to transfer more load directly to the subsoil. As a further consequence the normal stress acting on the shaft is higher and thus the shaft resistance as well, which can be observed in figure 5.7 and figure 5.8. In general it has to be remarked that it requires a relatively high load level to achieve a reasonable utilisation of the shaft resistance.

For the actual investigation a normalisation of results was carried out. The normalised total applied load for different plan views is depicted in figure 5.9. As it can be deduced, a hexagonal arrangement of the piles provides the highest capacity whereas a quadratic arrangement bears $\sim 20\ \%$ less. The simplified 2D computation is located somewhere between.

Since the examination was performed for two different pile group setups a comparison of these was carried out. As a finding from figure 5.10 it can be seen that for a small pile spacing the difference in bearing capacity due to pile arrangement is less significant than for larger ones. Further results of the second examined configuration are given in section 8.2.

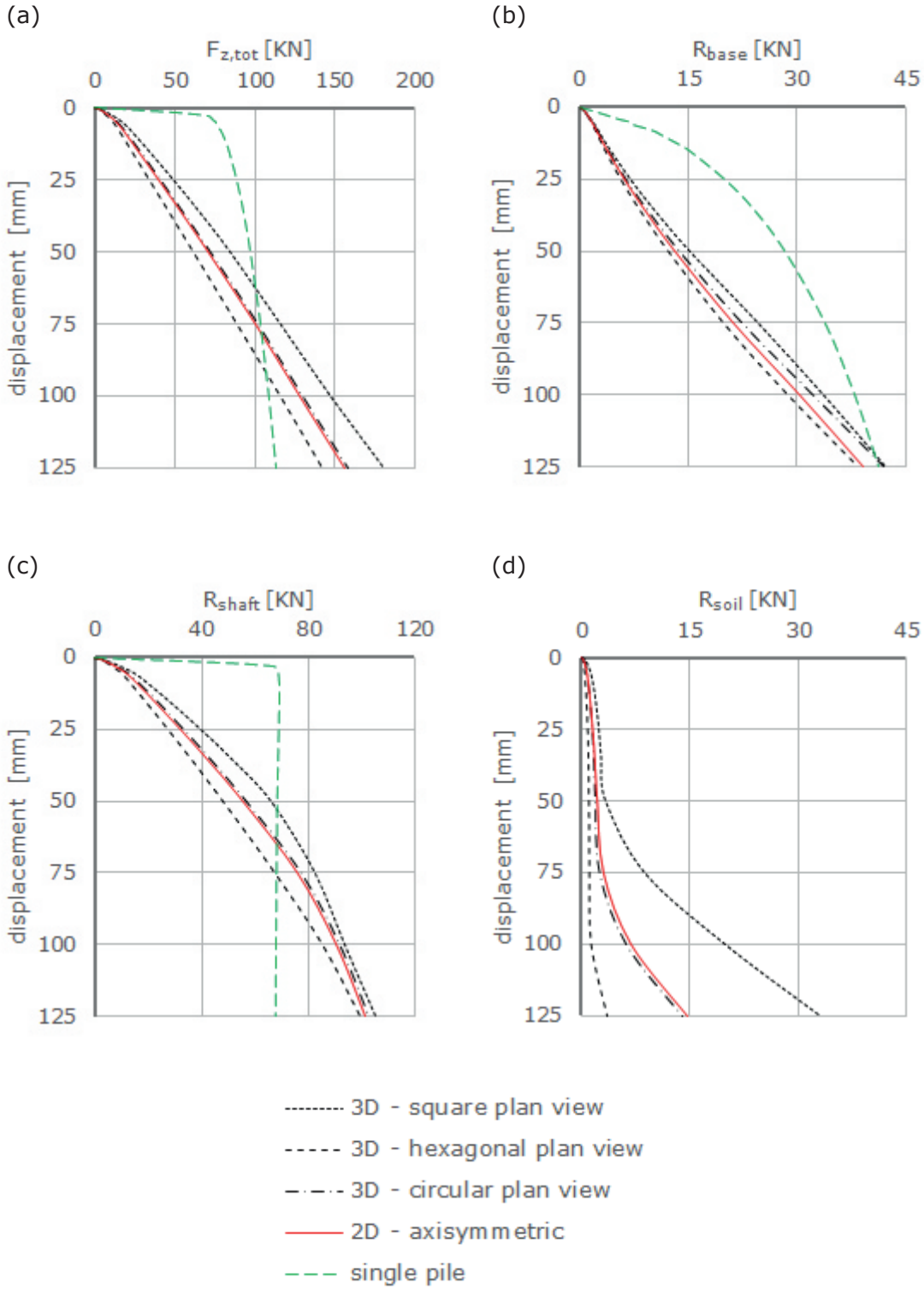

Figure 5.6: *Validation of different plan views:*
(a) total applied load, (b) base resistance,
(c) shaft resistance, (d) load transferred directly to the soil
D: 25 cm | L: 8.0 m | Sp: 1.5 m

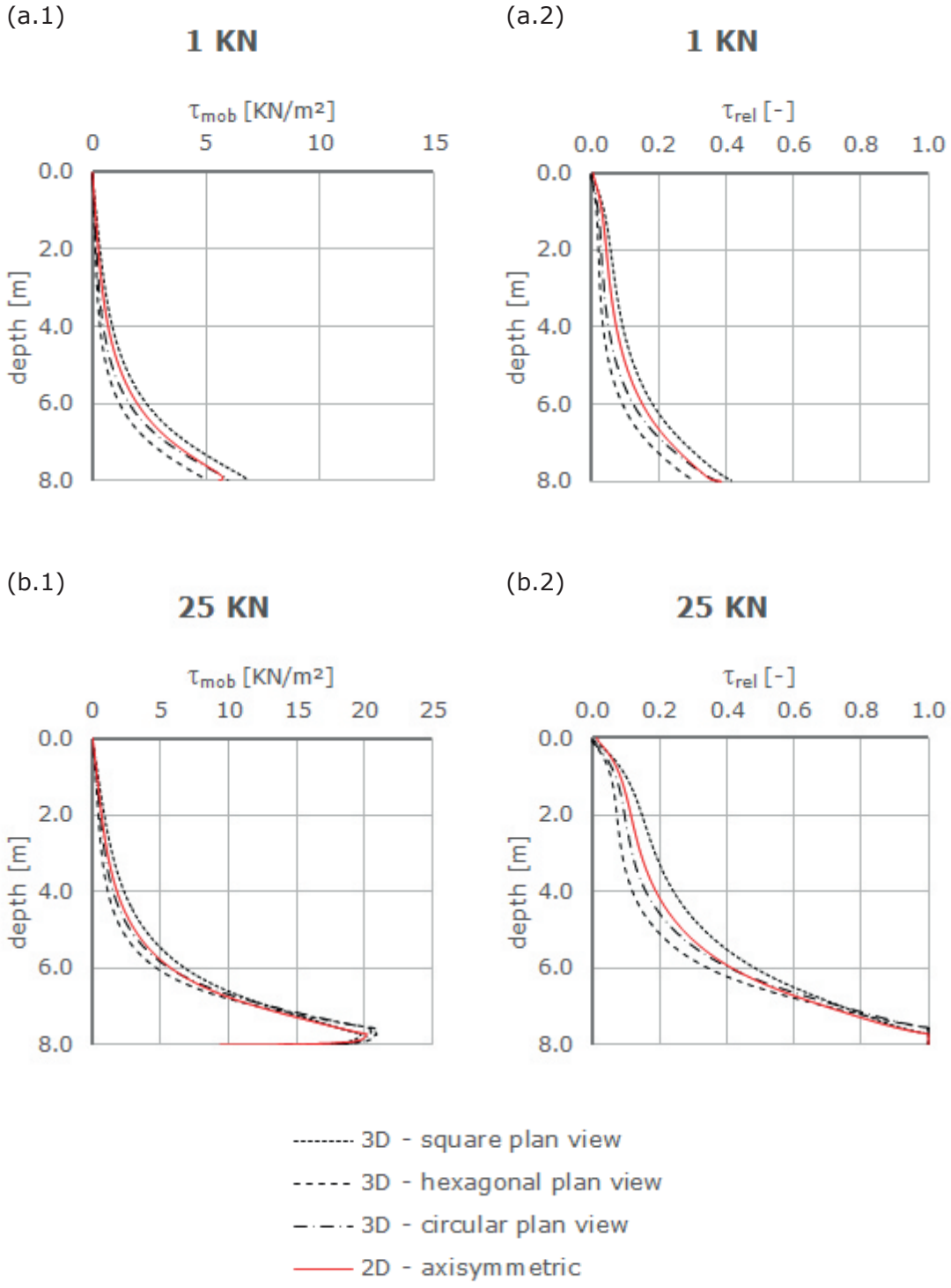

Figure 5.7: *Validation of different plan views, detailed interpretation of the shaft: (a) load step 1 KN, (b) load step 25 KN*

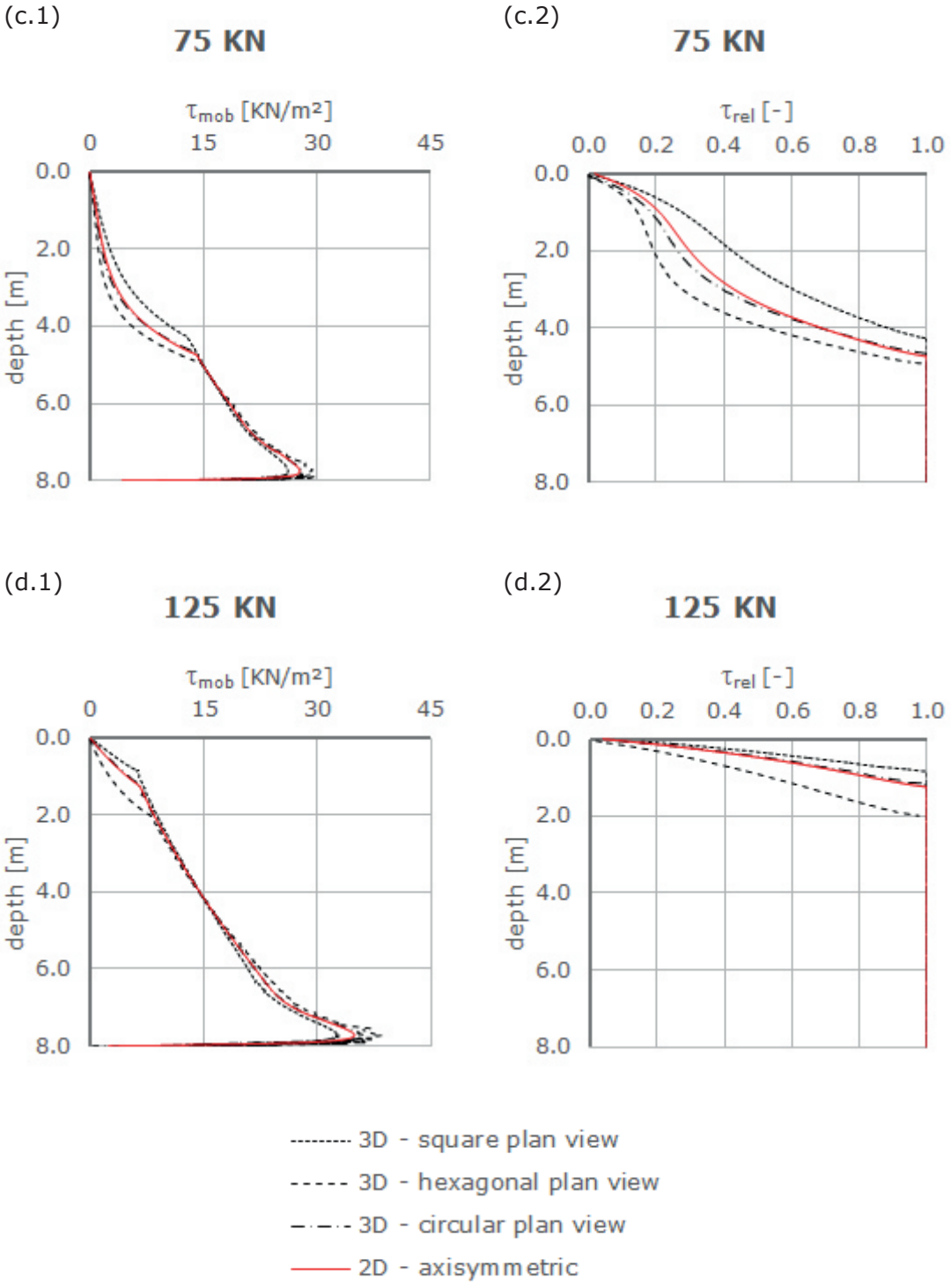

Figure 5.8: *Continuation of figure 5.7: (c) load step 75 KN, (d) load step 125 KN*

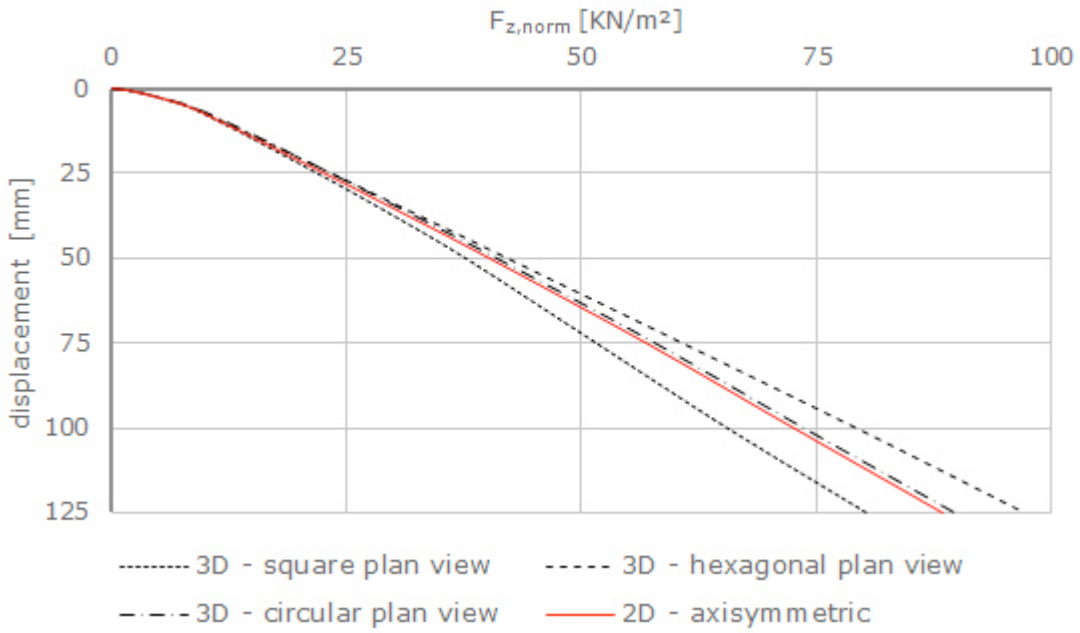

Figure 5.9: *Normalised depiction of different plan views:*
D: 25 cm | L: 8.0 m | Sp: 1.5 m

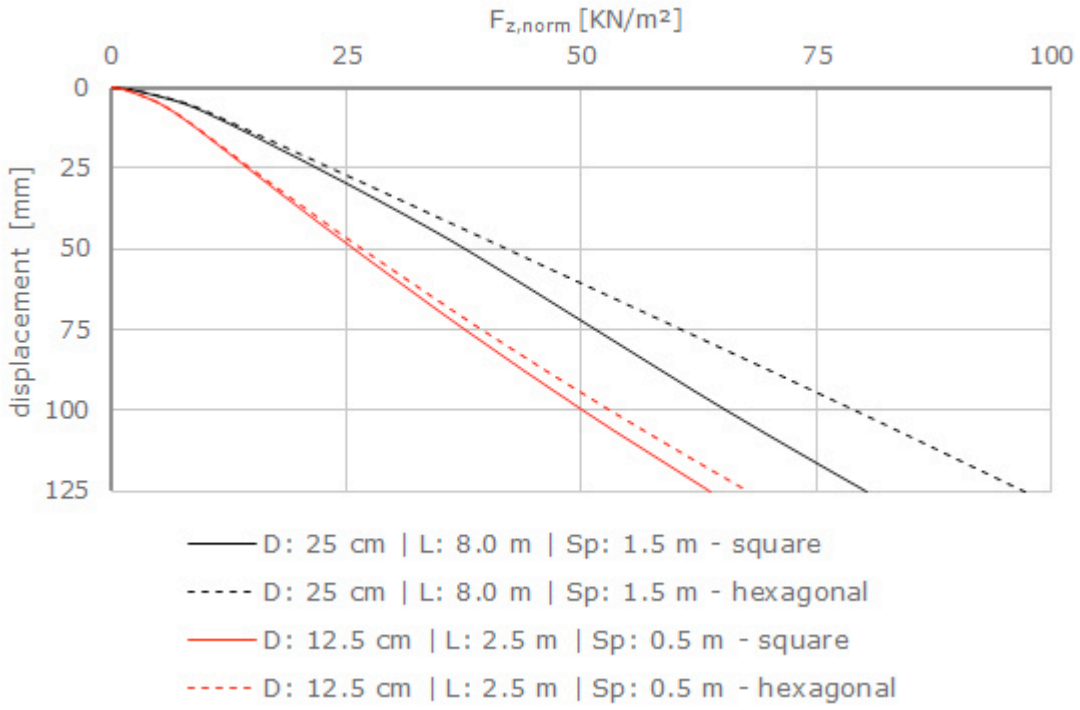

Figure 5.10: *Normalised depiction of different pile group setups*

5.5 Monolithic block - Model

For practical purposes it can be quite useful to simplify the entire pile group as a monolithic block. In the present section three different blocks, depicting the envelop of the pile groups were investigated. The dimensions of the examined pile foundation are delineated in section 5.7.

There are two common approaches to estimate an equivalent stiffness of a monolithic block. First EA equality can be applied and secondly an approach using EI equality, suggested by Bernecker O. and Ries s. [2012] can be used as demonstrated in eq. 5.1. A validation of the impact based on different block stiffnesses was carried out. Therefore four models of varying stiffness were examined for a block with a depth of $4\ m$. The highest, lowest and the approximate mean value were used. In addition a four times smaller stiffness as the lowest computed value was investigated. In a last step an adjusted stiffness was used to obtain equal results as an actual pile foundation. An overview of the investigated stiffnesses is given in table 5.3. A linear elastic constitutive model was assigned for the block material.

Furthermore, a shallow foundation (foundation slab without piles) was investigated to perceive a general feeling of the improvement due to piles. The model had a dimension of $20 * 20 * 20\ m$ and benefited of two symmetry planes. It comprised $\sim$130 000 10$-$noded elements.

$$E_{eq.}^{EI} = \frac{E_{pile}}{Sp} * \sqrt{\frac{A_{pile}^3}{12 * I_{pile}}} \tag{5.1}$$

Table 5.3: *Equivalent block stiffness*

diameter	**spacing**	$\boldsymbol{E_{eq.}^{EA}}\ [kPa]$	$\boldsymbol{E_{eq.}^{EI}}\ [kPa]$
$12.5\ cm$	$0.5\ m$	$\mathbf{4.32 * 10^5}$	$\mathbf{2.0 * 10^6}$
	$1.0\ m$	$\mathbf{1.08 * 10^5}$	$9.98 * 10^5$
$25\ cm$	$1.0\ m$	$\mathbf{4.32 * 10^5}$	$\mathbf{2.0 * 10^6}$
	$1.5\ m$	$1.92 * 10^5$	$1.33 * 10^6$

5.6 Monolithic block - Results

The validation of different stiff monolithic blocks showed, that both ways of computing an equivalent stiffness deliver a far too stiff response of the simplified foundation. From figure 5.11 it can also be deduced, that from a certain stiffness on there is no change in the bearing behaviour anymore. All computed stiffnesses are located in this range of no change, although they differ in a factor of 20. The lowest computed stiffness depicts more or less the lower boundary. By adjusting the stiffness to obtain similar results as an according pile foundation, it was possible to show that in terms of EI equality a correction factor of $1/200$ and for EA equality a correction factor of $1/45$ had to be used.

The obtained results of the investigation of different block depths are quite unspectacular and thus not depicted separately. In section 5.9 the results are incorporated in figure 5.28.

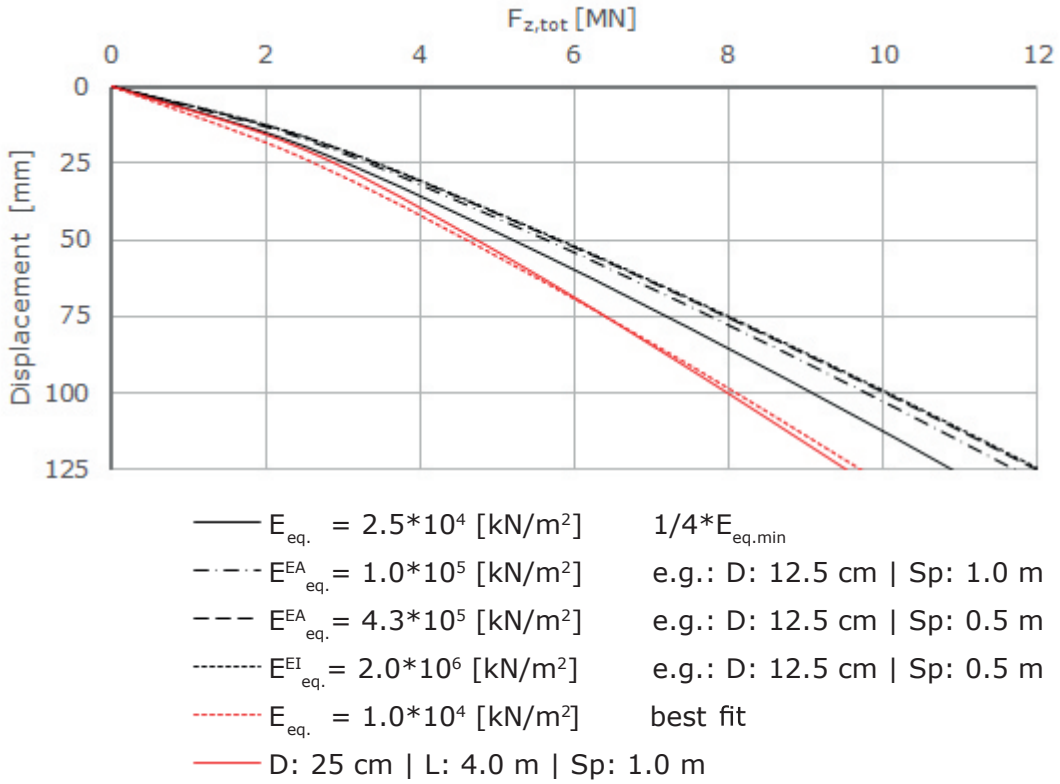

Figure 5.11: *Validation of block stiffness variation*

5.7 Entire pile group - Model

To capture the overall behaviour of different pile foundations, models of entire pile groups were generated. A quadratic foundation slab with a length of $10 * 10\ m$ was investigated. The extent of the piles amounted to $9 * 9\ m$. The different examined pile group configurations are shown in table 5.4 and figure 5.12 depicts a cross section of the foundation including the pile arrangement of different spacings. Two symmetry planes, cutting the entire model into a quarter were used. For the pile group exhibiting a spacing of $0.5\ m$ this model was still very big. Therefore one symmetry plane was defined which creates an eight part of the foundation. Hereinafter this model is designated as a ˝slice of cake˝. The entire model had a size of $20 * 20 * 20\ m$ and comprised approximately 300 000 to 850 000 10−noded elements. An exemplary connectivity plot of the quarter model is shown in figure 5.13 and of the ˝slice of cake˝in figure 5.14. For the validation of mesh fineness a ˝slice of cake˝model with ∼1 000 000 10−noded elements was used.

The pile group exhibiting the following dimensions: $D:\ 25\,cm\ |\ L:\ 4.0\,m\ |\ Sp:\ 1.0\,m$ was used to perform several validations. First of all a validation of equality between the quarter models and the ˝slice of cake˝model was conducted. Since it was possible to keep the amount of elements for the slice of cake model relatively small, additionally a validation of mesh fineness was performed. Furthermore an evaluation of the impact due to a different load distributing layer was performed. A cross section of the alternative gravel layer is displayed in figure 5.12. As a next validation the effect of a tapered pile shape was investigated. The piles had a ratio of taper of $ROT = 1.5\ cm/m$ (see section 4.1.3) and were modelled as conical volumes. The diameter at the pile head was equal to uniform piles. For the detailed interpretation of the base resistance the implemented beam elements were used. Since the properties of these elements are uniform along the entire length a correction factor of $A_{pile\ tip}/A_{pile\ head}$ had to be incorporated to obtain correct results.

Table 5.4: *Entire pile foundation*

diameter	length	spacing
12.5 cm	2.5 m	0.5 m
12.5 cm	2.5 m	1.0 m
25.0 cm	4.0 m	1.0 m
25.0 cm	8.0 m	1.5 m

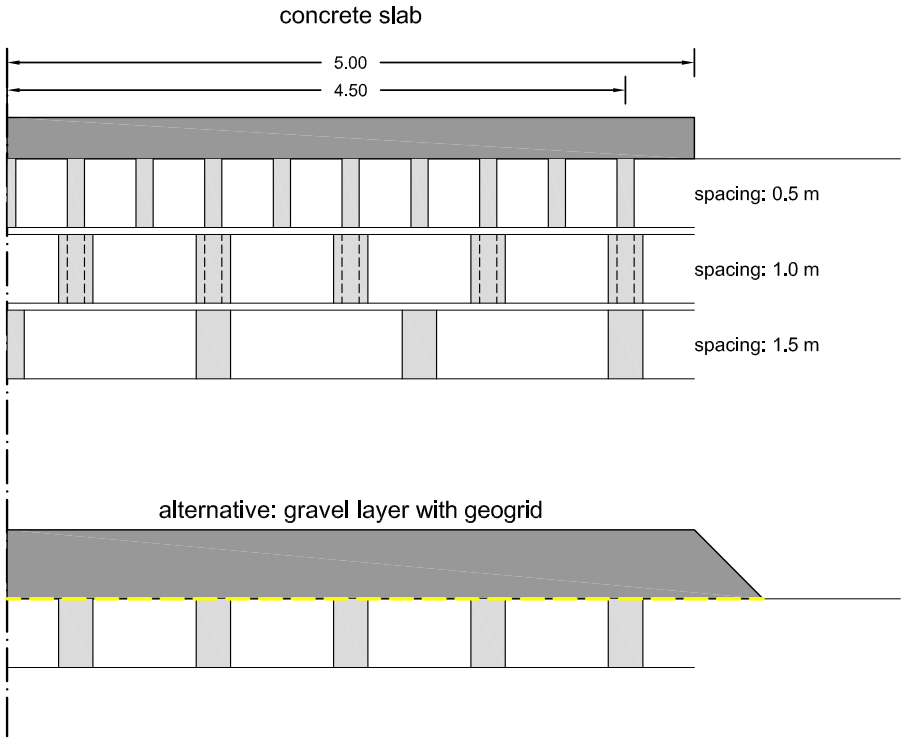

Figure 5.12: *Design of the entire pile group*

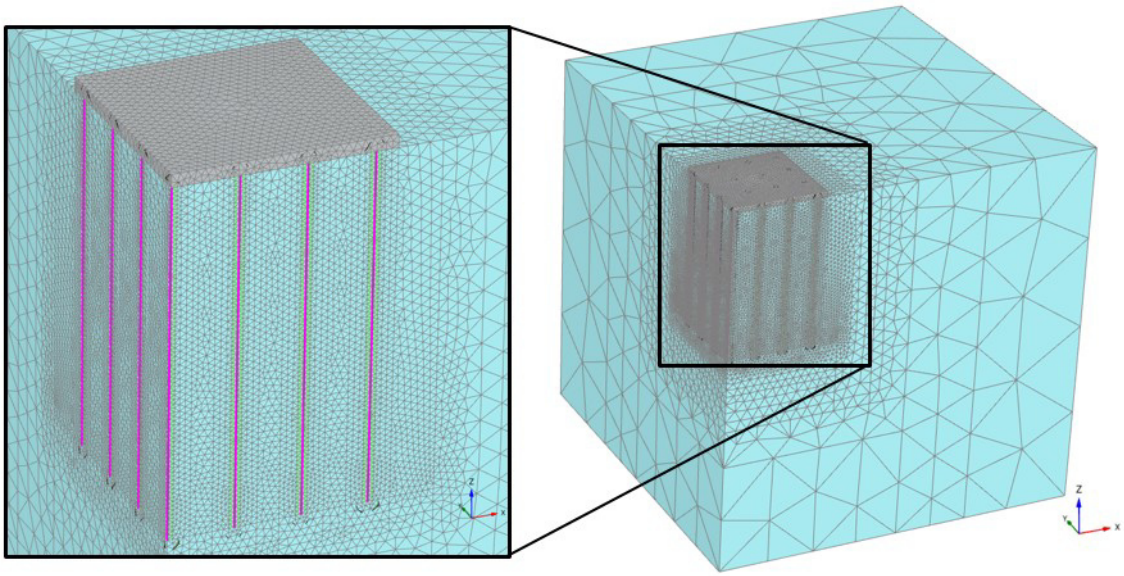

Figure 5.13: *Exemplary connectivity plot of a quarter model*

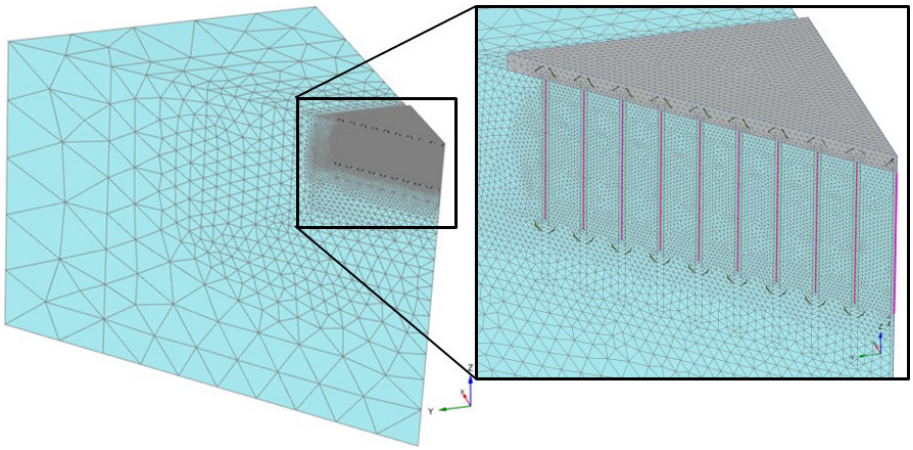

Figure 5.14: *Exemplary connectivity plot of a ˝slice of cake˝model*

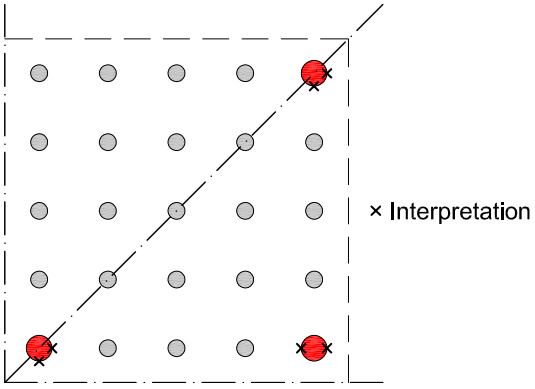

Figure 5.15: *Position of detailed shaft interpretation*

The detailed interpretation of the shaft was carried out for three decisive piles and for each at two positions as shown in figure 5.15. For the centre pile located in the actual centre of the model only one section was evaluated. The pile located in the middle of the foundation edge was investigated at an inlying and an outlying vertical section of the pile (x_{min} and x_{max}). Since a stress decrease of the interface occurred along the intersection of interface and model boundary, the interpretation of the corner pile was not carried out under $45°$ which would have resulted in the highest shaft resistance. It was performed as for the edge pile at the $x_{min} = y_{min}$ and x_{max} position. To obtain awareness of the inaccurate interpretation of the corner pile an even more detailed interpretation was conducted for one example. The pile was split in $45°$ sections and was interpreted individually. I has to be noted in advance, that for some detailed interpretations of the shaft resistance oscillations occurred which comes from the interface elements but does not effect the results. In general the pile resistances are depicted as the summation of all individual piles. Since the three above mentioned piles usually show a different response when loaded, an interpretation of the individual piles was performed. This additional interpretation was conducted for two pile groups, which differ only in the stiffness of the load distributing layer.

5.8 Entire pile group - Results

5.8.1 Validation of model geometry and mesh fineness

The validation of different model geometry resulted in well conformity as it can be seen in figure 5.16. Furthermore it can be concluded that the discretisation of the models was carried out with a sufficient number of elements. The slight inaccuracy of the base and thus soil resistance is most probably a result of manual selection of stress points for the interpretation. An explenation of this theme can be found in section 3.6.4.

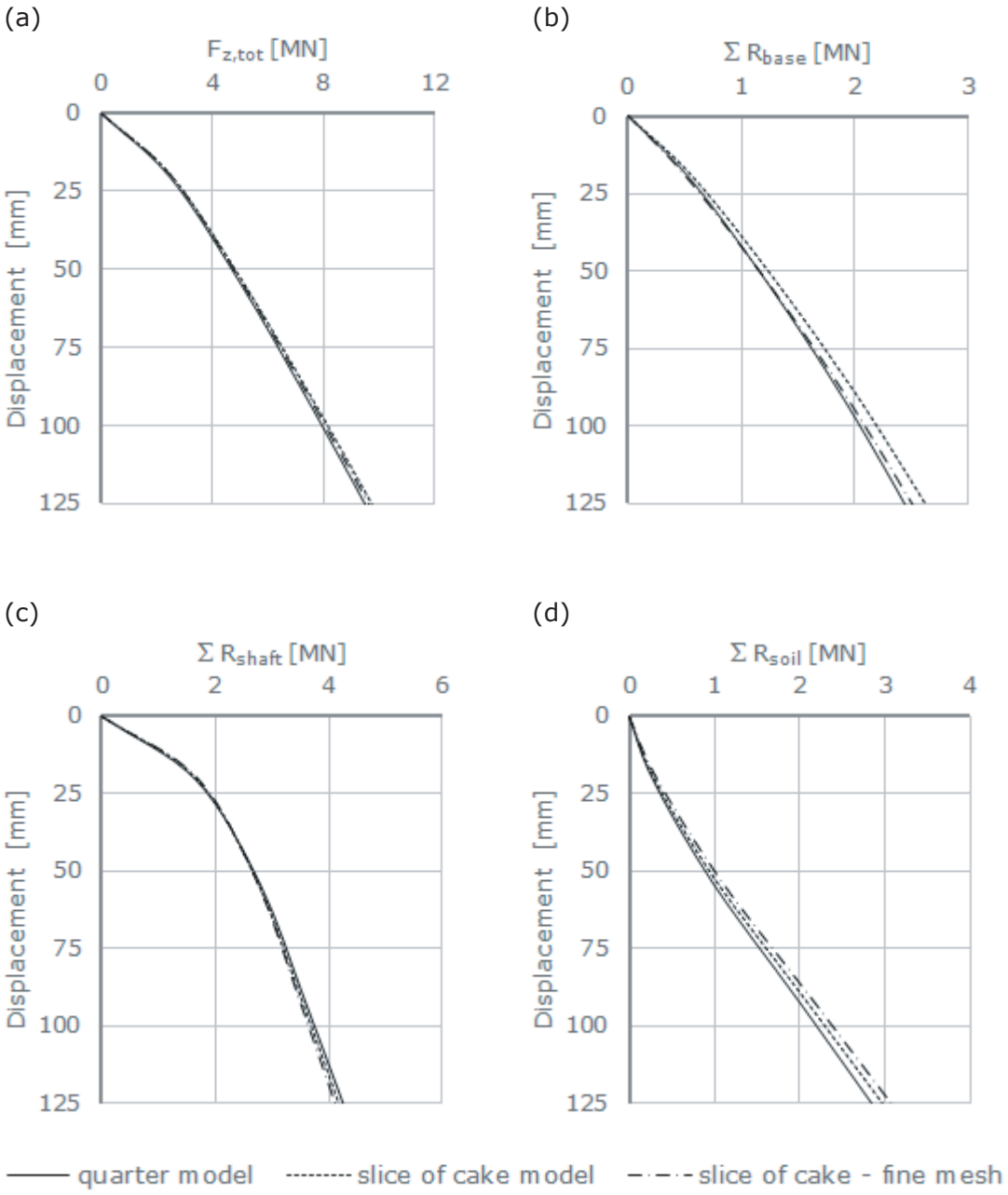

Figure 5.16: *Validation of model shape and mesh fineness:*
(a) total applied load, (b) sum of base resistance,
(c) sum of shaft resistance, (d) load transferred directly to the soil

5.8.2 Validation of different load distributing layers

It has to be mentioned that loads and resistances are referred to the centre pile. For the foundation exhibiting a concrete slab this is not that important since differential settlements are very small. Whereas for the gravel layer differential settlements of $\sim 4.0\ cm$ occurred for a load level of $100\ kPa$ ($F_{y,tot} = 10\ MN$).

In general it can be stated that a softer load distributing layer results in a slight reduction of the bearing capacity as shown in figure 5.18 (a). As the load separation in figure 5.17 shows, the main difference is the reduction of the shaft resistance. This result is based on negative skin friction due to displacements of the gravel layer which can be deduced from the detailed shaft interpretation displayed in figure 8.10. On the other hand ˝sagging˝of the gravel layer leads to a higher load transfer directly to the subsoil as depicted in figure 5.18 (d) and thus a higher stress level in the soil. As a further consequence an increase of base resistance is obtained as well as a slight increase of normal stresses acting on the pile shaft.

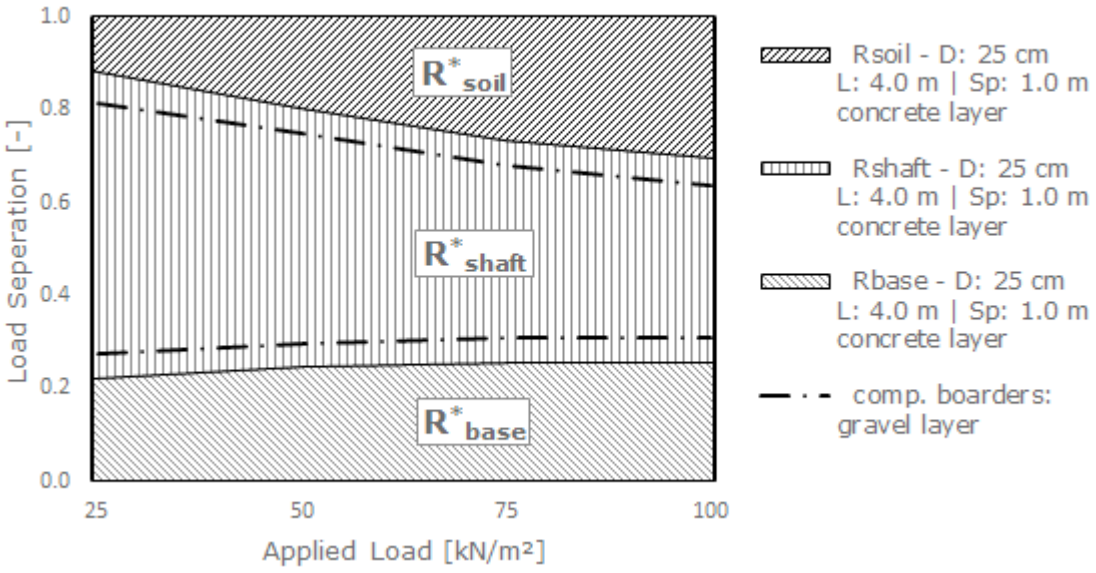

Figure 5.17: *Load separation*

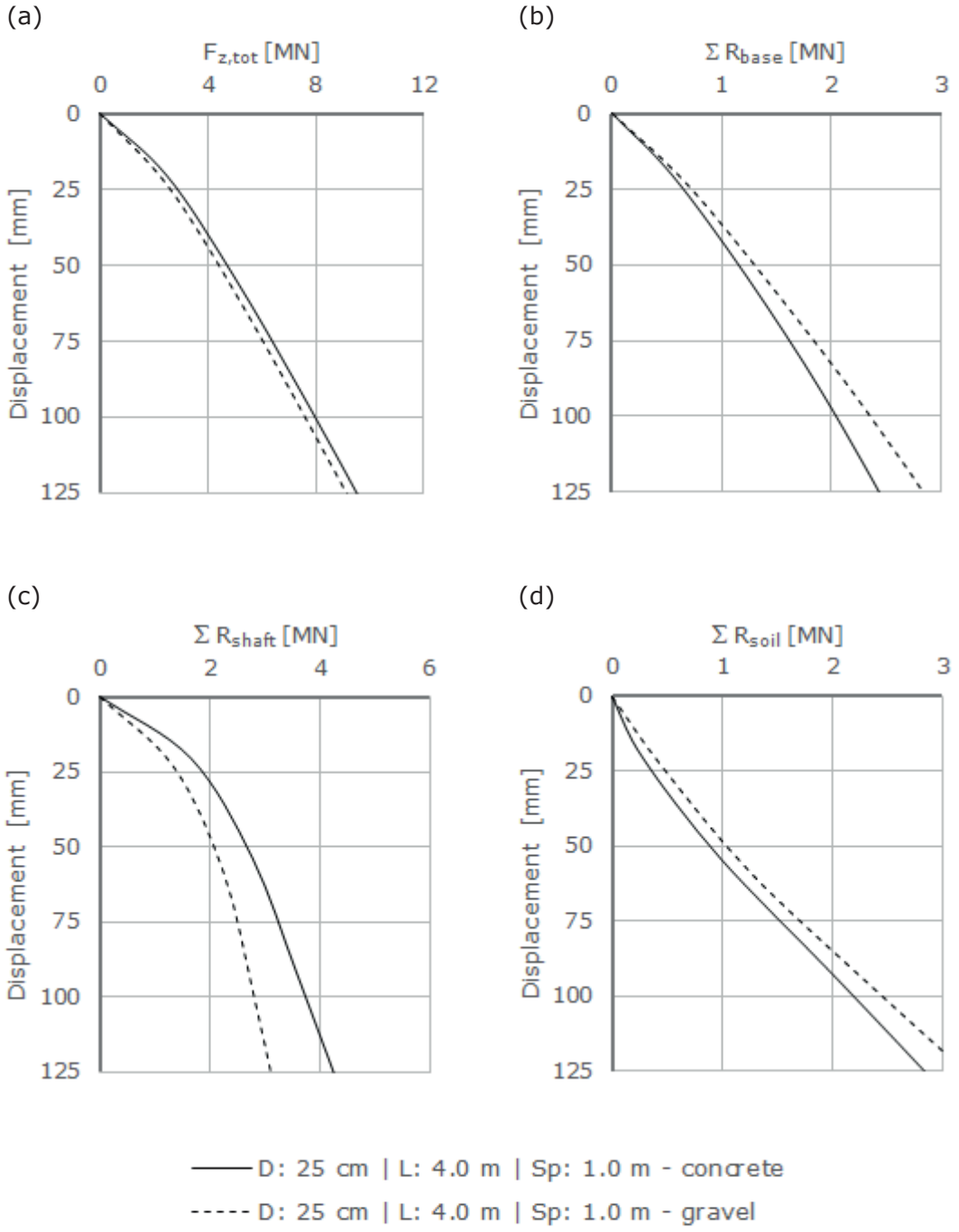

Figure 5.18: *Validation of different load distributing layers: (a) total applied load, (b) sum of base resistance, (c) sum of shaft resistance, (d) load transferred directly to the soil*

For detailed investigation of decisive piles, loads and resistances were referred to the individual pile.

In both cases (of different load distributing layer), it can be seen in figure 5.19 that piles located along the edges initially show a stiffer response as centre piles. For a concrete slab as load distributing layer this effect is more pronounced. In the posterior behaviour (higher loading) piles located in the centre take an obvious advantage of the higher stress level in the subsoil compared to piles located along the edges.

Based on a higher stress level in the soil due to ˝sagging˝of the gravel layer a higher base resistance can be mobilised for all piles out of the pile group using a softer load distributing layer. This fact can be seen in figure 5.19 (b).

By comparing the shaft resistance of piles with different locations (figure 5.19 (c)), in both cases the centre pile is initially not able to utilise the shaft on a high degree since too little relative displacements occur (figure 5.23 and figure 8.10). During the ongoing load application full mobilisation of the piles along the edge is reached approximately at the same time. Compared with the centre pile much more displacement is needed to reach this point. The further behaviour is mainly governed by the additional stresses in the soil, thus the centre pile is able to bear much more as piles located along the edges. Furthermore by comparing the shaft resistances using different load distributing layers it can be seen, that for a softer layer initially less shaft resistance can be mobilised due to negative skin friction (figure 8.10 and figure 8.11)

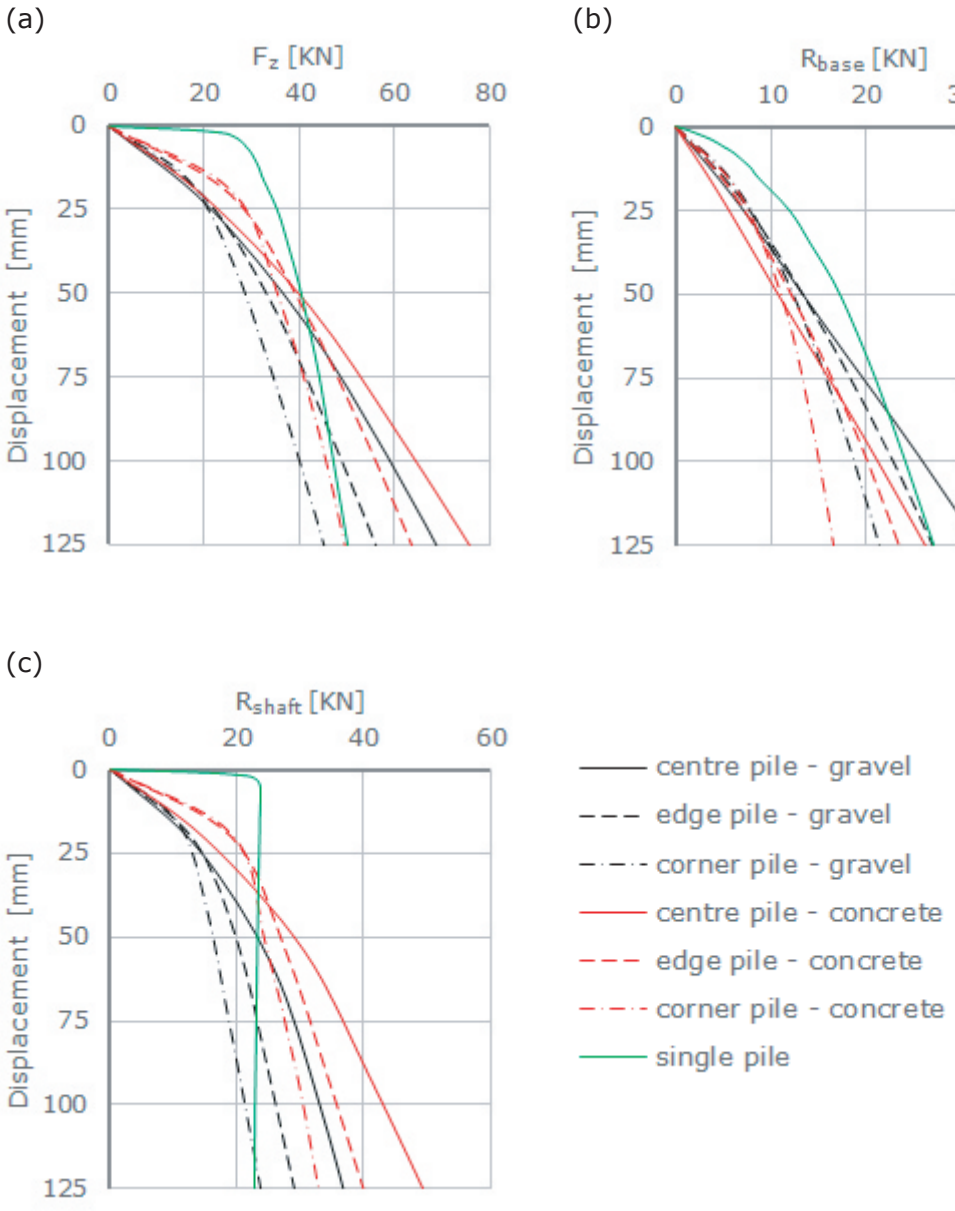

Figure 5.19: *Detailed interpretation of three decisive piles: (a) total applied load, (b) base resistance, (c) shaft resistance*

5.8.3 Validation of different pile shapes

The investigation of different pile shapes revealed a lower bearing capacity of tapered piles compared to uniform piles as shown in figure 5.21 (a). However, it has to be noted that all piles exhibit the same diameter at the pile head and hence the tapered piles have a smaller shaft and base area.

According to this fact, the base and shaft resistance has to be smaller for tapered piles as depicted in figure 5.21 (b) and (c). On the other hand more load is transferred directly to the subsoil. From figure 5.20 it can be deduced that the proportion of base resistance stays almost constant for tapered piles whereas for a uniform shape a slight increase occurs. Furthermore the activation of the proportion sustained by the soil is more distinct and activated more rapidly for a tapered pile shape.

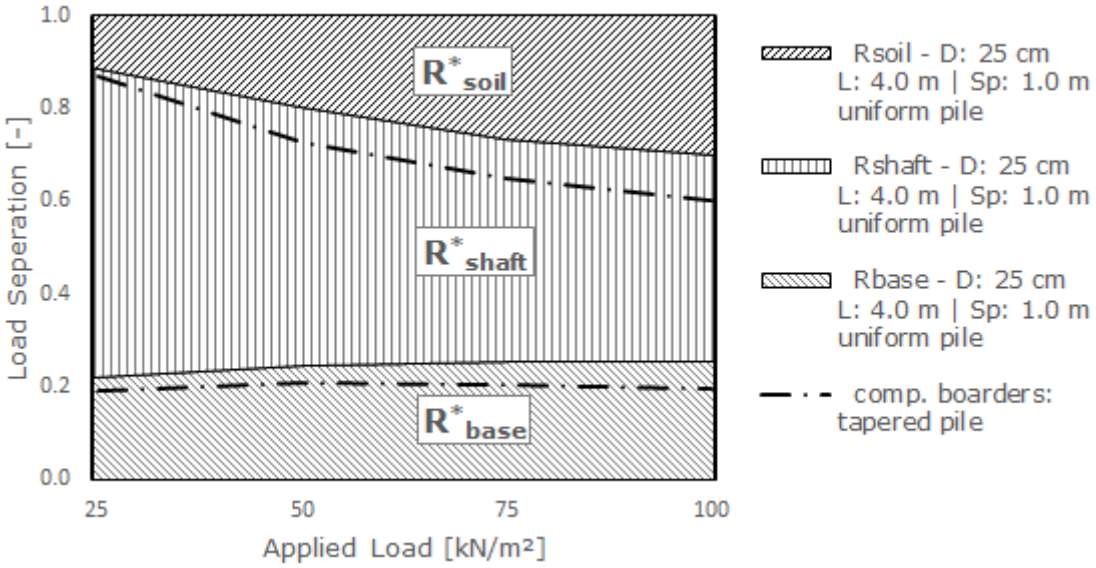

Figure 5.20: *Load separation*

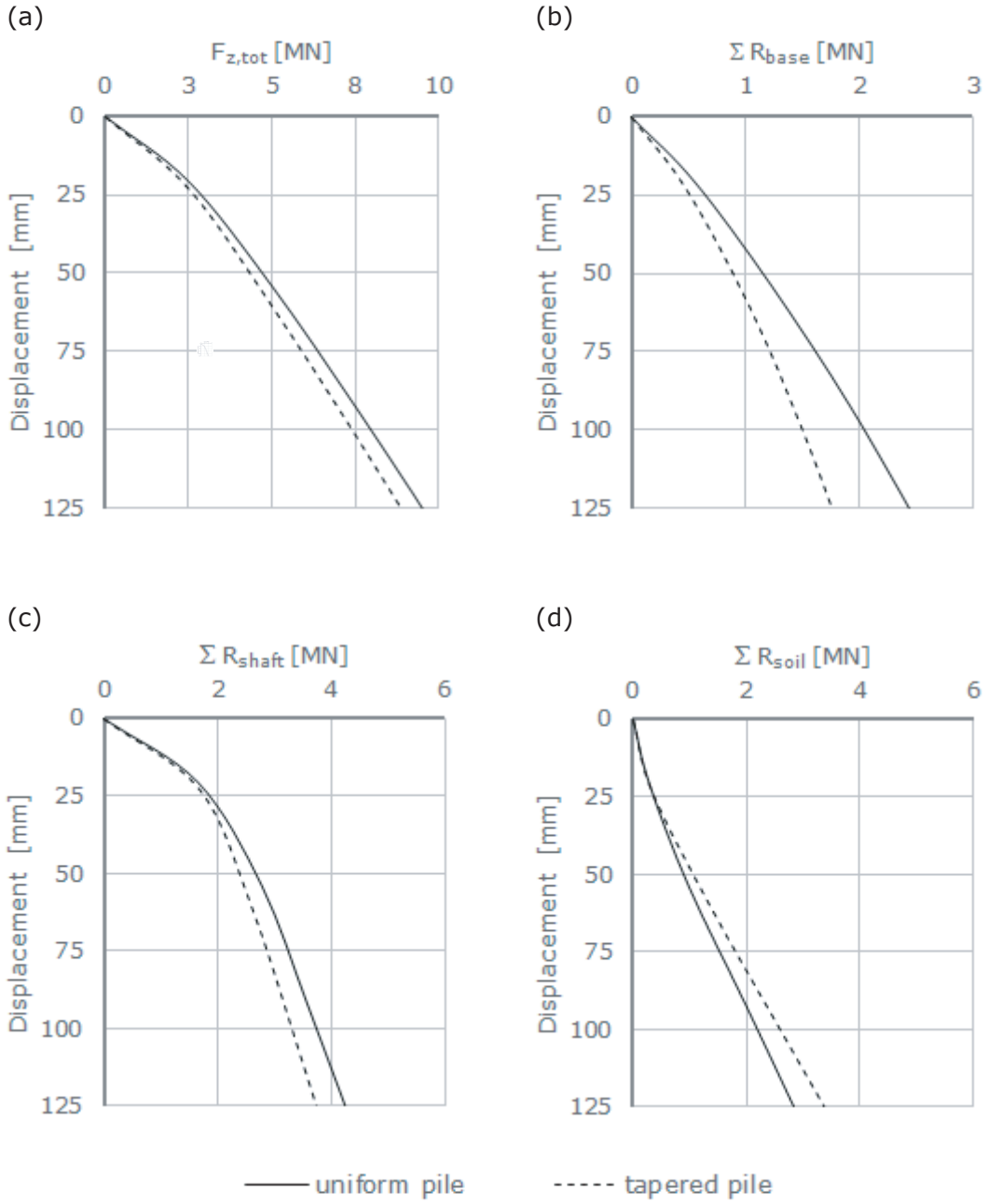

Figure 5.21: *Validation of different pile shapes:*
(a) total applied load, (b) summation of base resistance,
(c) summation of shaft resistance,
(d) load transferred directly to the soil

5.8.4 Validation of different pile group configurations

An investigation of figure 5.22 (a) reveals expected results. Pile groups comprising larger pile dimensions and a wider spacing provide a higher capacity compared to other configurations. For obtaining the same amount of settlements an improvement of applicable load up to $\sim 25\,\%$ was achieved in the best case. For the pile group comprising a diameter of $D = 12.5\ cm$, a length of $L = 2.5\ m$ and a spacing of $Sp = 1.0\ m$ it can be clearly seen that almost no improvement was possible. The piles were far too small to bear a considerable load. Almost the entire load was transferred directly to the subsoil.

In figure 5.22 (b) the pile group exhibiting a diameter of $D = 12.5\ cm$, a length of $L = 2.5\ m$ and a spacing of $Sp = 0.5\ m$ is presented which has the same total base area as the pile group exhibiting a diameter of $D = 25\ cm$, a length of $L = 4.0\ m$ and a spacing of $Sp = 1.0\ m$. Even though the latter consists of longer piles and thus a higher stiffness below the pile tip, the summation of pile resistances results in a lower resistance as the other pile group. From this fact it can be assumed, that the arching effect at the pile base is strongly dependent on the spacing of individual piles.

According to expectations larger pile dimensions result in a higher shaft resistance as depicted in figure 5.22 (c). Despite the fact that the pile group exhibiting a diameter of $D = 25\ cm$, a length of $L = 8.0\ m$ and a spacing of $Sp = 1.5\ m$ has a smaller total shaft area as the other two noteworthy configurations, it is still able to provide a higher shaft resistance. This result is based on a higher stress level in greater depth, thus a higher normal stress acting on the shaft. This can be proved by comparing figure 5.23 (b.1) and figure 8.19 (b.1). In figure 5.23 and figure 5.24 it is shown that piles located in the centre of the foundation initially have a much lower utilisation (can be seen by the mobilisation of resistance) as piles located along the edges. This is based on the settlement of soil, hence too little relative displacement. To a lesser extent this can also be observed for the inner side of piles located along the edges. From figure 8.15 to figure 8.20 further detailed results are displayed. Basically it can be stated, that the shafts of all evaluated pile groups exhibit a similar behaviour which is strongly dependent on the spacing and the pile length. If the spacing is big enough in relation to the length an ˝immediate˝high degree of utilisation is computed for all piles. Due to a larger stress level in the soil centre piles provide the highest shaft resistance with ongoing loading. Vice versa the lower part of the pile located at the corner is surrounded by almost primary conditions and hence the pile is not able to provide a high resistance.

After a full mobilisation of the shaft resistance, hence an activation of the load transfer to the soil the improvement due to piles is more or less completed. This can be deduced from figure 5.22 (a) where from $\sim 50\ mm$ settlements on a parallel trend can be observed. For some configurations this point is reached earlier.

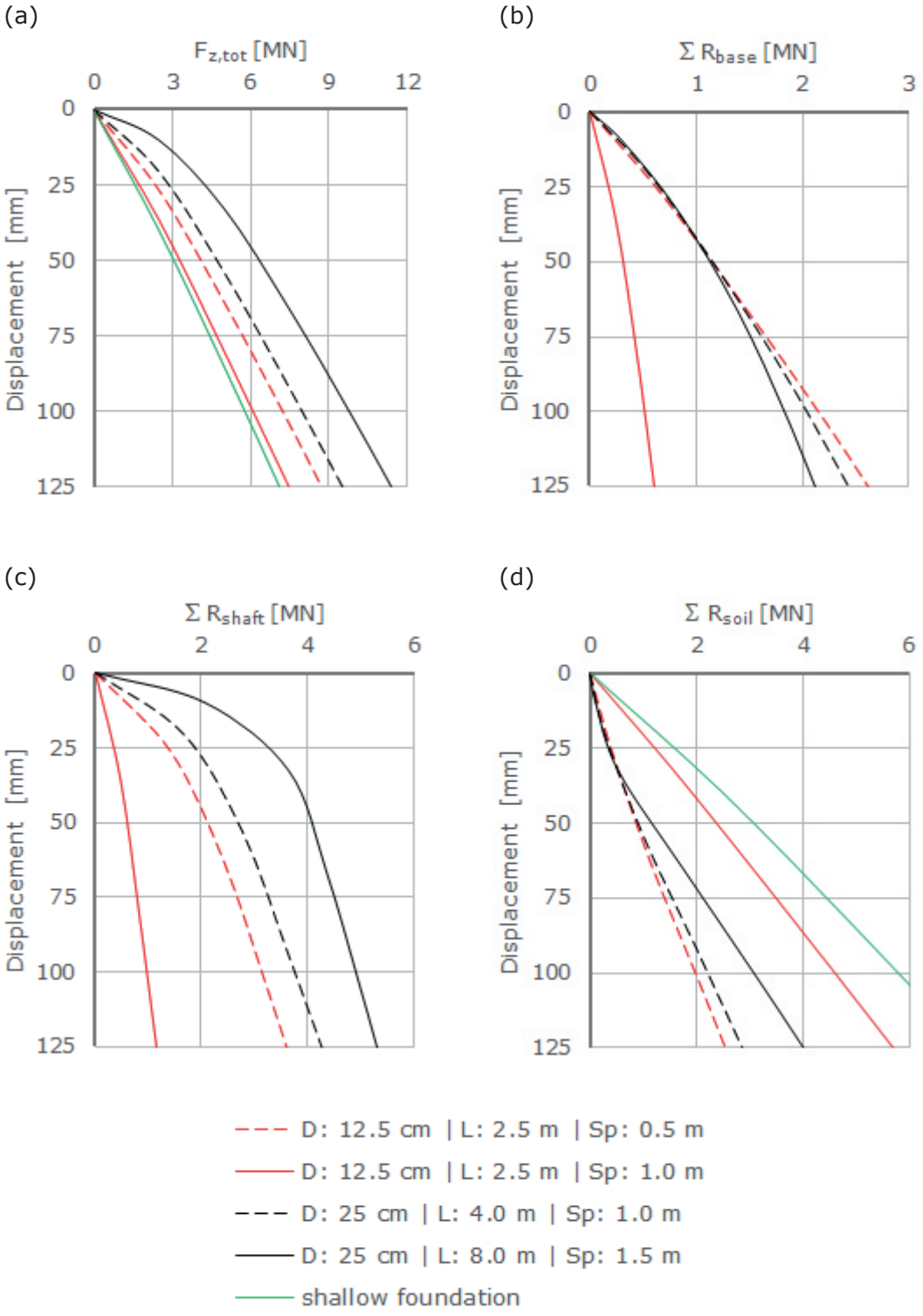

Figure 5.22: *Validation of different pile group configurations: (a) total applied load, (b) sum of base resistance, (c) sum of shaft resistance, (d) load transferred directly to the soil*

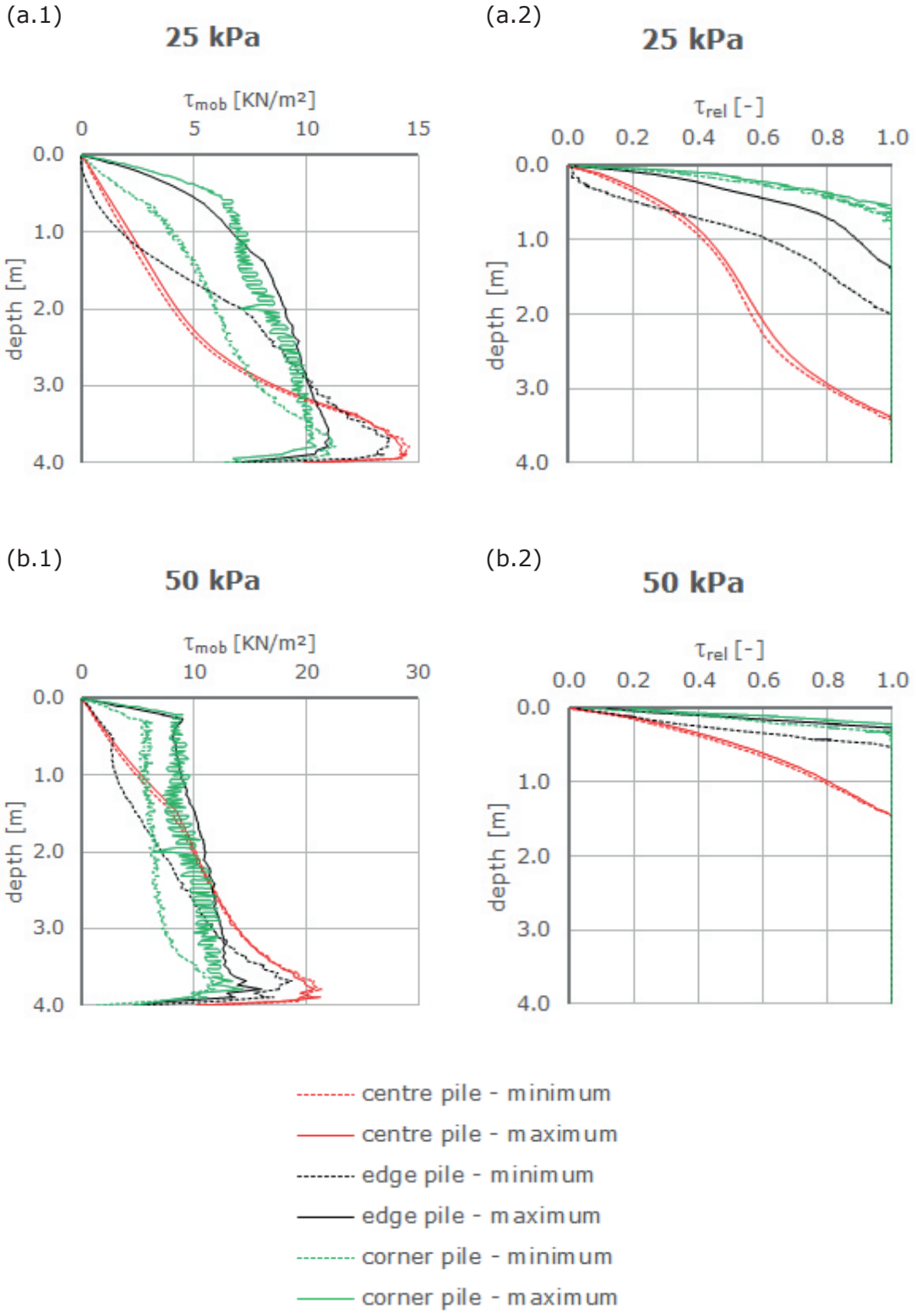

Figure 5.23: *Detailed interpretation of the shaft:*
(a) load step 25 kPa, (b) load step 50 kPa
D: 25 cm | L: 4.0 m | Sp: 1.0 m

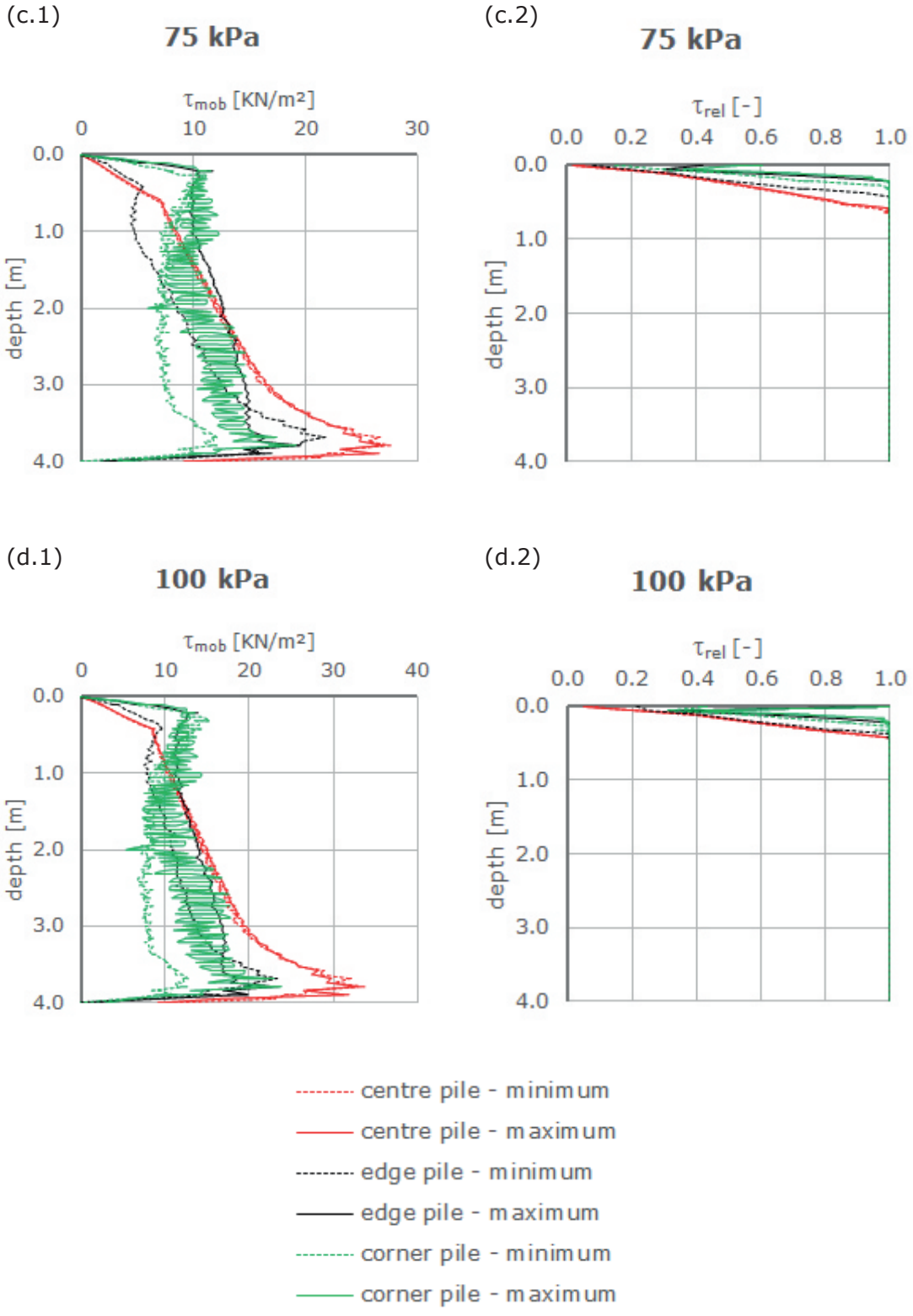

Figure 5.24: *Continuation of figure 5.23:*
(c) load step 75 kPa, (d) load step 100 kPa
D: 25 cm | L: 4.0 m | Sp: 1.0 m

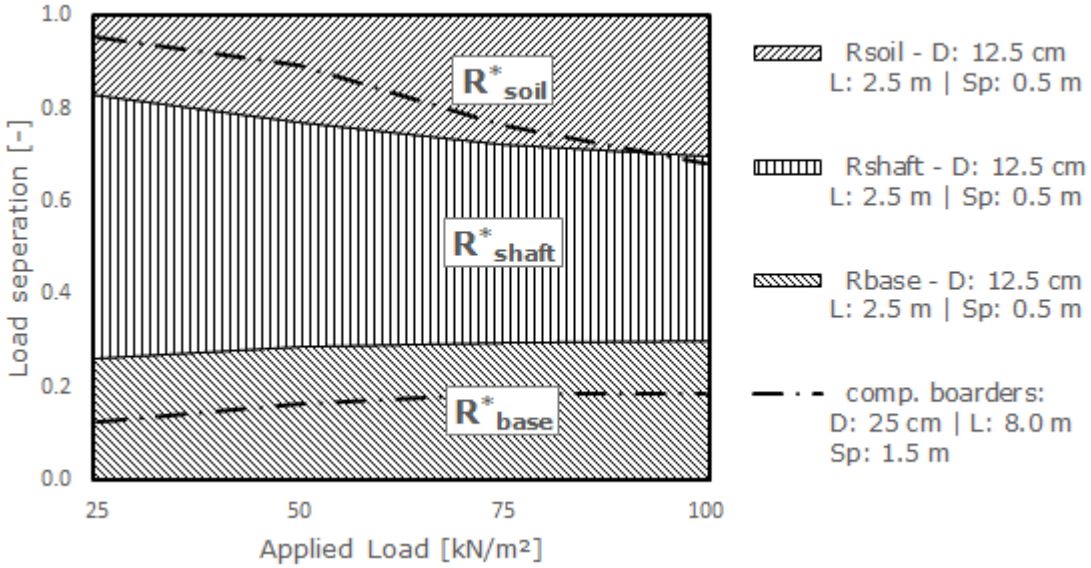

Figure 5.25: *Load separation*
D: 12.5 cm | L: 2.5 m | Sp: 0.5 m
D: 25 cm | L: 8.0 m | Sp: 1.5 m

From the load separation charts, as exemplarily depicted in figure 5.25 it can be seen that a pile group exhibiting a diameter of $D = 25\ cm$, a length of $L = 8.0\ m$ and a spacing of $Sp = 1.5\ m$ initially transfers $\sim 95\,\%$ of the load by the pile. During further load application a notable part is shifted to R_{soil}. Further depictions can be found in section 8.2 (figure 8.12 to figure 8.14).

To asses the impact of (the not perfectly carried out) interpretation of the shaft resistance of corner piles, a more detailed post processing is demonstrated in figure 5.26 and figure 5.27. For the interpretation the pile was split into $45°$ sections which enables an all around depiction of the mobilised shaft resistance. Due to symmetry the points B, C and D can be mirrored along a diagonal axis.

It follows, that for all points around the pile the shaft resistance is almost fully mobilised and an approximate uniform utilisation of the pile is given.

Point A, which is located in the inside is subjected to a high stress level at the lower part of the pile, hence provides a high shaft resistance, whereas in the upper part relatively low stresses are transferred. The influence of adjacent piles can be seen in point B since just a low shaft resistance is mobilisable. By pivoting around the pile (from A to E) in figure 5.27, the pronounced peak at the pile tip of point A disappears. In return the middle part bulges out. For point E there is almost no influence of the pile group, thus a typical shaft resistance profile is obtained (e.g. figure 5.27 (d)).

Interesting are the more or less same stress conditions of point B and C for higher load levels. This can just be coincidence or a result of the foundation slab which protrudes half a meter beyond the piles as depicted in figure 5.12.

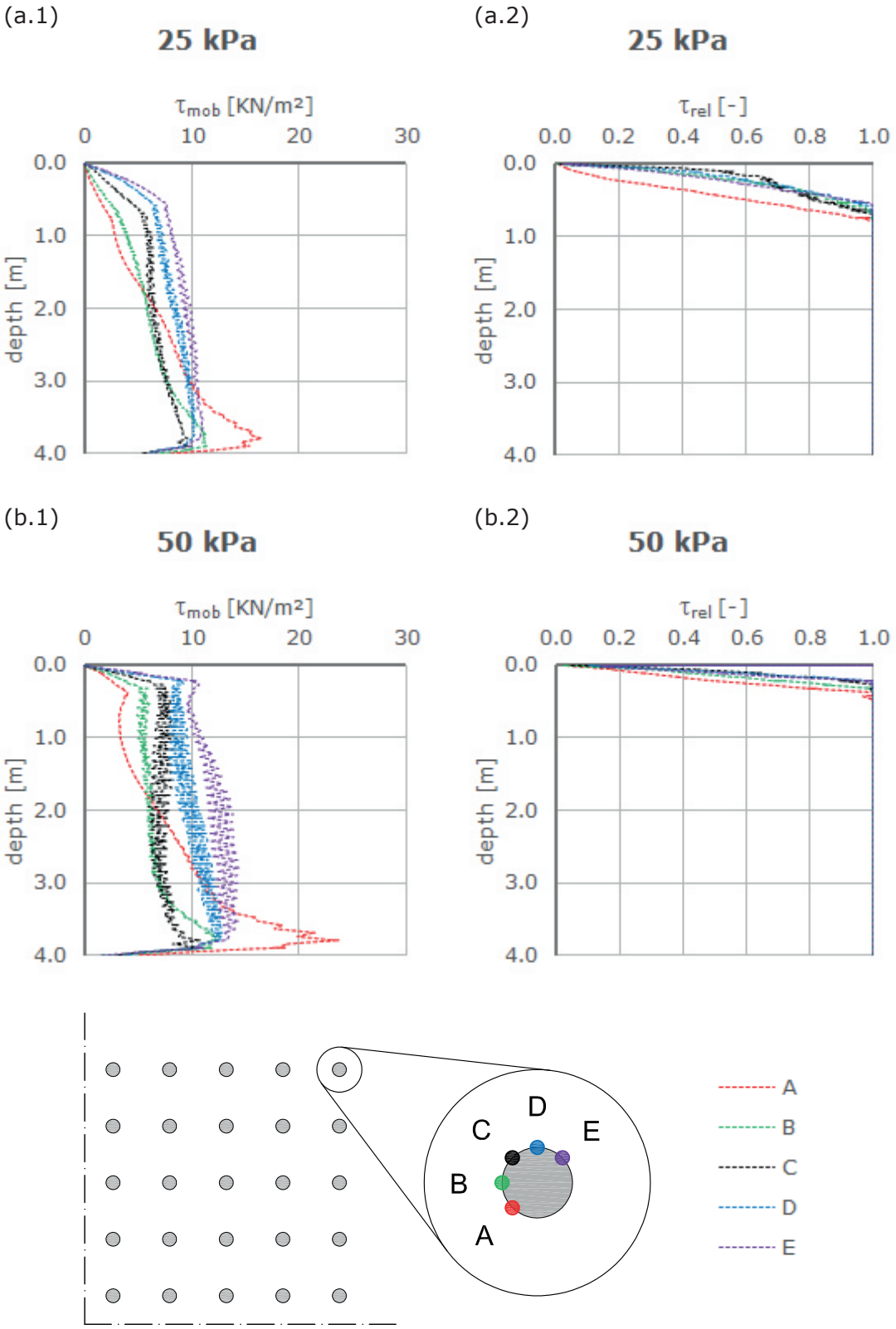

Figure 5.26: *Detailed interpretation of the corner pile:*
(a) load step 25 kPa, (b) load step 50 kPa
D: 25 cm | L: 4.0 m | Sp: 1.0 m

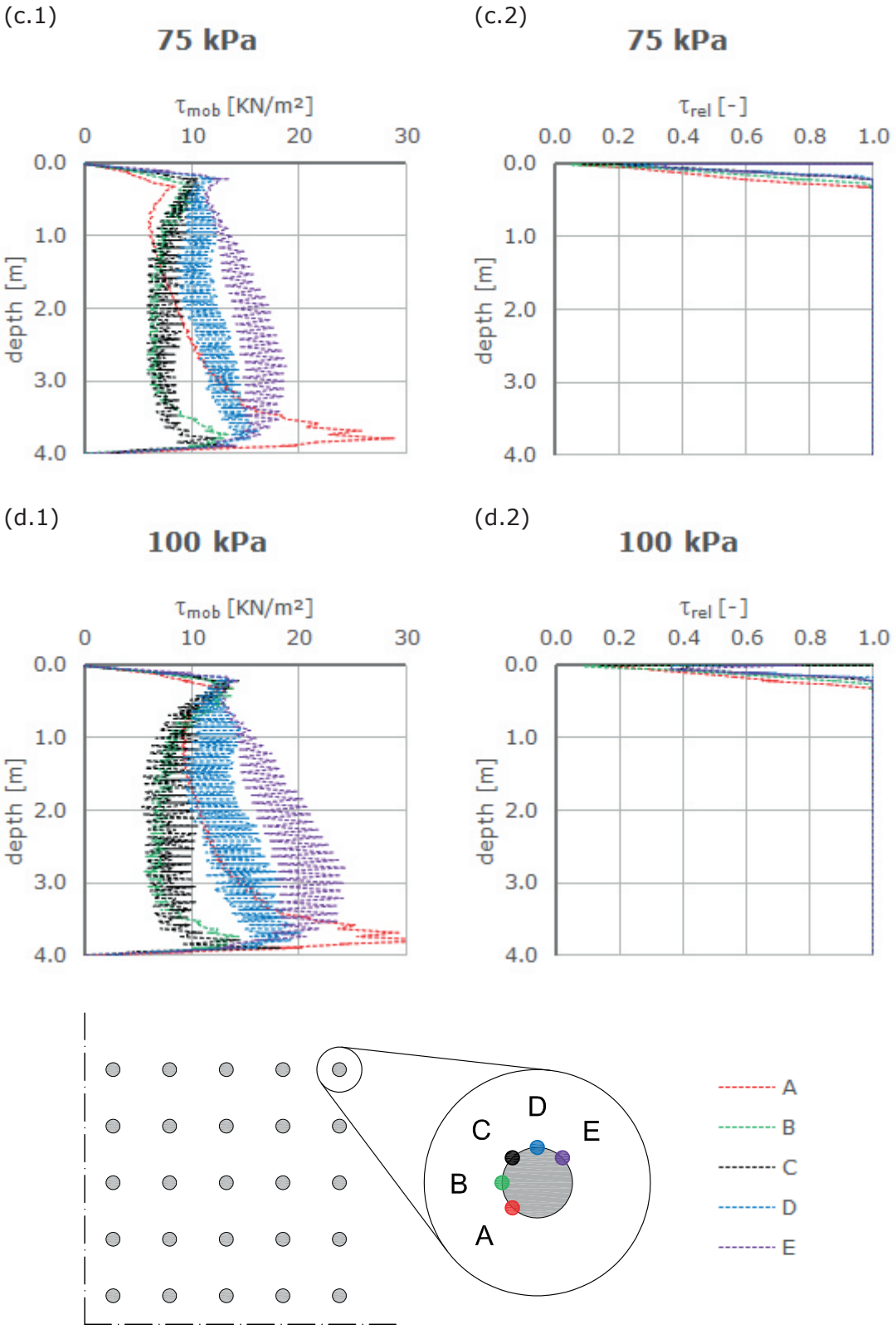

Figure 5.27: *Continuation of figure 5.26:*
(c) load step 75 kPa, (d) load step 100 kPa
D: 25 cm | L: 4.0 m | Sp: 1.0 m

5.9 Comparison of results

In the final section the different computations were compared as demonstrated in figure 5.28. It can be seen, that by executing simplified 2D computations, the entire load versus settlement behaviour is underestimated by far. Basically the assumption of an infinite pile group counts most for pile groups exhibiting a spacing of $Sp = 0.5\ m$. By carrying out a summation of ˝unit cell˝ resistances an even lower total applicable load was obtained compared to the load versus settlement behaviour of a shallow foundation modelled in 3D. On the contrary, a simplification as monolithic block results in a much too high load versus settlement behaviour.

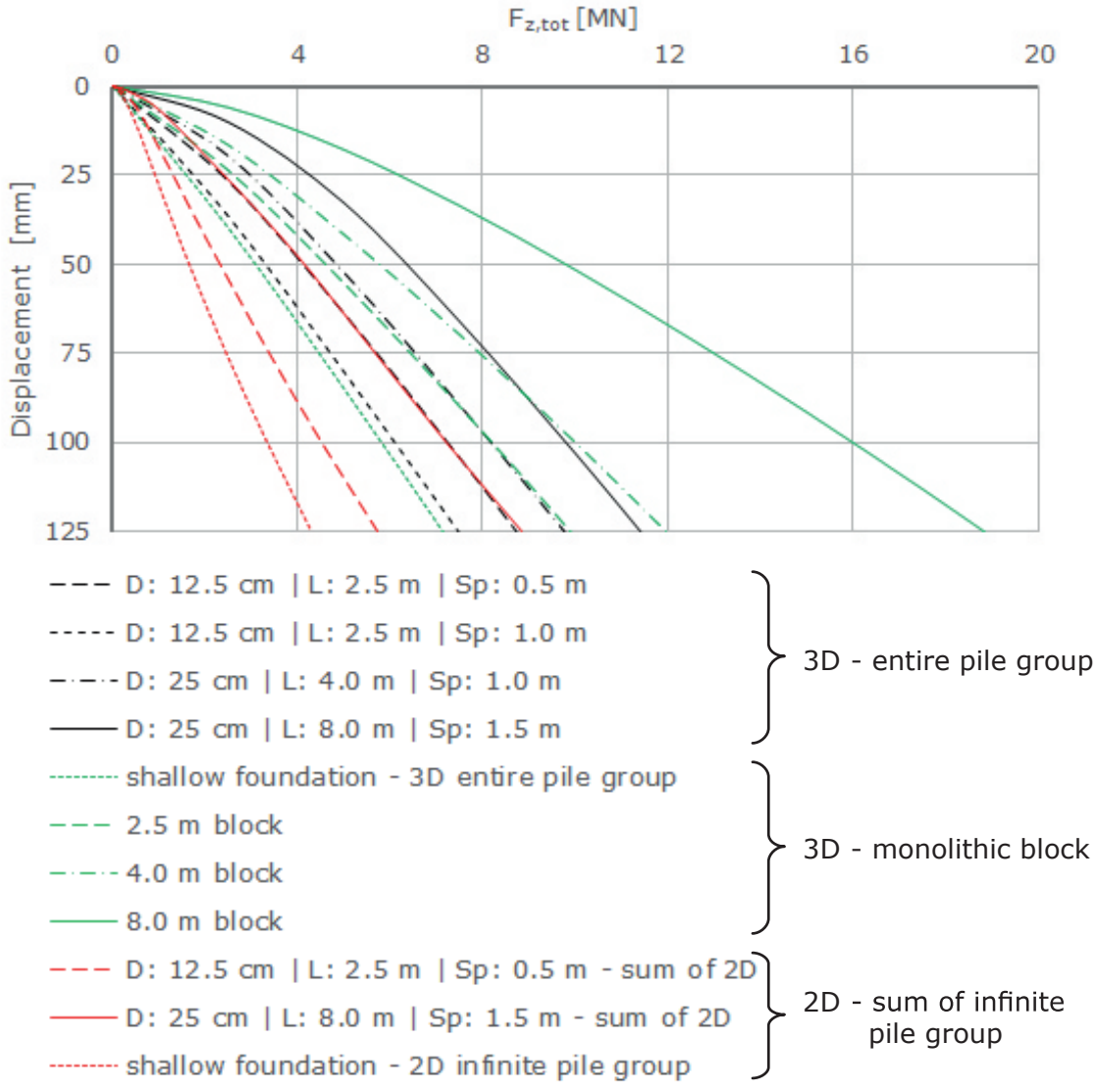

Figure 5.28: *Comparison of different computation methods*

6 Summary

In the following, some key findings of the numerical studies are summarised.

It was possible to show that there is no impact in the load versus settlement behaviour due to a varying tip shape of piles. Furthermore, a conical pile shape generally shows a softer response as uniform piles. Tapered piles with an equal shaft area as uniform piles take advantage in larger displacements.

Equality of 2D and 3D computations could be confirmed for simple geometries. A verification of the simplified circular plan view as used in 2D axisymmetric models and plan views from real pile group arrangements showed, that by plotting results in a normalised manner, simplified models are located somewhere between actual models. By comparing a hexagonal and a square plan view the difference in bearing capacity for small spacings is not as big as for larger spacings.

Owing to the studies of different pile group configurations using 3D models it was possible to gain an idea about the load transfer mechanisms. The results obtained for a pile group exhibit a very small spacing show that an advantage can be taken from the arching effect below the pile tips. As a consequence an improvement can be achieved with very small piles.

A simplification of the entire pile group as a monolithic block with an equivalent stiffness obtained by two different common approaches of conversion results in both cases in far too high load versus settlement behaviour. On the other hand by conducting simplified infinite pile group models, the load versus settlement behaviour is underestimated.

7 Outlook

This thesis certainly is a good basis concerning the research of timber pile foundations. Practical issues as e.g. installation effects or the water absorption ability of timber are touched in short. Furthermore, the numerical studies delineate the impact of different pile group configurations.

In a next step these two issues have to be combined. Model tests should be executed for the calibration of numerical models.

To gain more information about speeding up consolidation due to the water absorption of wood and bracing of the piles based on swelling, full scale model tests which compare timber piles with other impermeable piles using the same dimensions have to be executed. Thereby a detailed observation of the pore water pressure and load versus settlement behaviour over time should be conducted.

In terms of numerical investigation the focus should be on small lengths ($\leq\ 3\ m$) and a gradual decrease of spacing. With this measure it might be possible to capture the arching effect below the pile tips.

Bibliography

Bernecker O. and Ries s. 2D oder 3D? vergleichende finite elemente Berechnungen für komplexe Gründungssysteme. *8. Kolloquium Bauen in Boden und Fels*, page 465, 2012.

Michael Borrmann. *Historische Pfahlgründungen: Untersuchung zur Geschichte einer Fundamentierungstechnik, dargestellt an römischen, mittelalterlichen und neuzeitlichen Beispielen, hauptsächlich aus dem süddeutschen Raum: Zugl.: Karlsruhe, Univ., Diss., 1991*, volume 3 of *Materialien zu Bauforschung und Baugeschichte*. Inst. für Baugeschichte der Univ. Karlsruhe, Karlsruhe, 1992.

Cambefort H. La force portante des groupes de pieux: The bearing capacity of pile groups. *Procceedings, 3rd International Conference on Soil Mechanics and Foundation Engineering*, Vol. 2:22–28, 1953.

Collin J.G. *Timber Pile: Design & Construction Manual*. 2015.

Coyle H.M. and Sulaiman I.H. Bearing capacity of foundation piles: State of the art. *49th Annual Meeting of the Highway Research Board*, pages 87–103, 1970.

Dean M. Timber piles: A brief overview. *Piledriver*, 2006(Q4):12–20, 2006.

Dejog J.T. and Frost J.D. A multisleeve friction attachment for the cone penetrometer. *Geotechnical Testing Journal*, (No.2):111–127, 2002.

Engin H.K. *Modelling Pile Installation Effects: A Numerical Approach*. 2013. ISBN 978-94-6186-140-5.

Hans-Georg Kempfert and Berhane Gebreselassie. *Excavations and Foundations in Soft Soils*. Springer-Verlag Berlin Heidelberg, Berlin, Heidelberg, 2006. ISBN 9783540328940. doi: 10.1007/3-540-32895-5. URL `http://dx.doi.org/10.1007/3-540-32895-5`.

Kothe E. Holzpfahlgründungen tragen häufig auch nach 100 Jahren noch. *Der Prüfingenieur*, (8):30–38, 1996.

Mahutka K.P., König F., and Grabe J. Numerical modelling of pile jacking, driving and vibratory driving. In Theodoros Triantafyllidis, editor, *Numerical modelling of construction processes in geotechnical engineering for urban environment*, Balkema - Proceedings and monographs in engineering, water and earth sciences, pages 235–246. Taylor & Francis, London u.a., 2006. ISBN 978-0-415-39748-3.

Ni P., Mangalathu S., and Zhao Y. Permeable piles: An alternative to improve the performance of driven piles. *Computers and Geotechnics*, (84):78–87, 2017.

Niemz P. *Physik des Holzes und der Holzwerkstoffe*. DRW-Verlag, 1993.

Niemz P. *Holz un Holzwerkstoffe: Skript zur Vorlesung Werkstoffe I*. 2011.

Niemz P. Einfluss der Holzfeuchte auf E-modul und Biegefestigkeit ausgewählter heimischer Holzarten. (11):65–67, 2014. URL `www.hob-magazin.com`.

Niemz P. Wasseraufnahmefaehigkeit von holz: E-mail, 2018.

Niemz P., Mannes D., Kock W., and Herbers Y. Untersuchung zum Wasseraufnahmekoeffizienten von Holz bei variation von Holzart und Flüssigkeit. *Bauphysik 32*, (3): 149–153, 2010.

PLAXIS. *PLAXIS 3D Reference Manual*. 2017.

PLAXIS. *PLAXIS 2D Reference Manual 2018*. 2018a.

PLAXIS. *PLAXIS 2D Material Models Manual 2018*. 2018b.

Randolph M. Science and empiricism in pile foundation design. *Geotechnique 53*, (No. 10), 2003.

Ressel J. *Werkstoff Holz: Physikalische Eigenschaften von Holz und Holzwerkstoffen*. 1992.

Rudolf M. *Beanspruchung und Verformung von Gründungskonstruktionen auf Pfahlrosten und Pfahlgruppen unter Berücksichtigung des Teilsicherheitskonzeptes*. Heft 17. Kassel, 2005. ISBN 3-89958-168-7.

Sayed M. and Bakeer M. Efficiency formula of pile groups. *Journal of Geotechnical Engineering*, 118:278–299, 1992.

Schickhofer G. *Holzbau: Der Roh- und Werkstoff Holz*. 2006.

Smettan K. Holzpfahlgründungen - heute noch technisch und wirtschaftlich sinnvoll? *Pfahl Symposium*, (71):96–114, 2003.

Waldherr B. Der Salzburger Seeton. *bvfs Forschungsnews*, (12):1–2, 2010.

White R.T. and Bolton M.D. Observing friction fatigue on a jacked pile. In *Centifuge and Constitutive Modelling: Two extremes*, pages 347–354. 2002.

List of Figures

List of Tables

8 Appendix

8.1 Additional results of 2D studies

8.1.1 Validation of different tip shapes

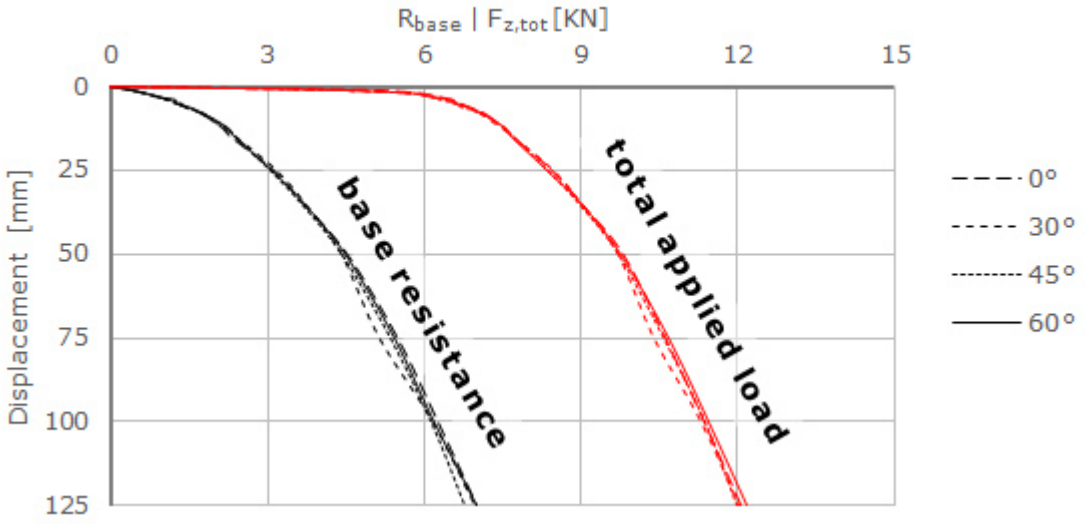

Figure 8.1: *Validation of different tip shapes; D: 12.5 cm | L: 2.5 m*

8.1.2 Validation of different load distributing layers

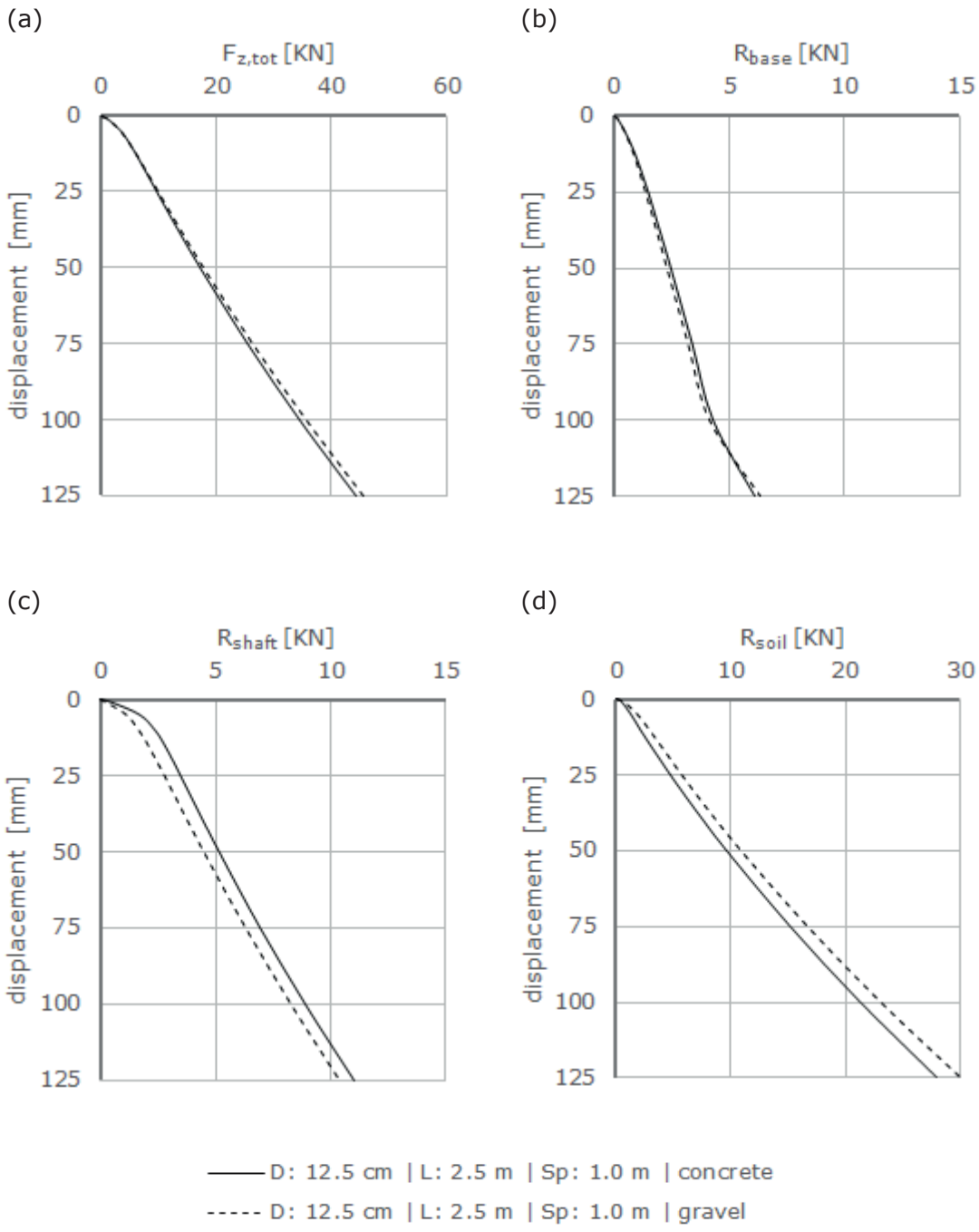

Figure 8.2: *Validation of different load distributing layers; D: 12.5 cm | L: 2.5 m | Sp: 0.5 m*

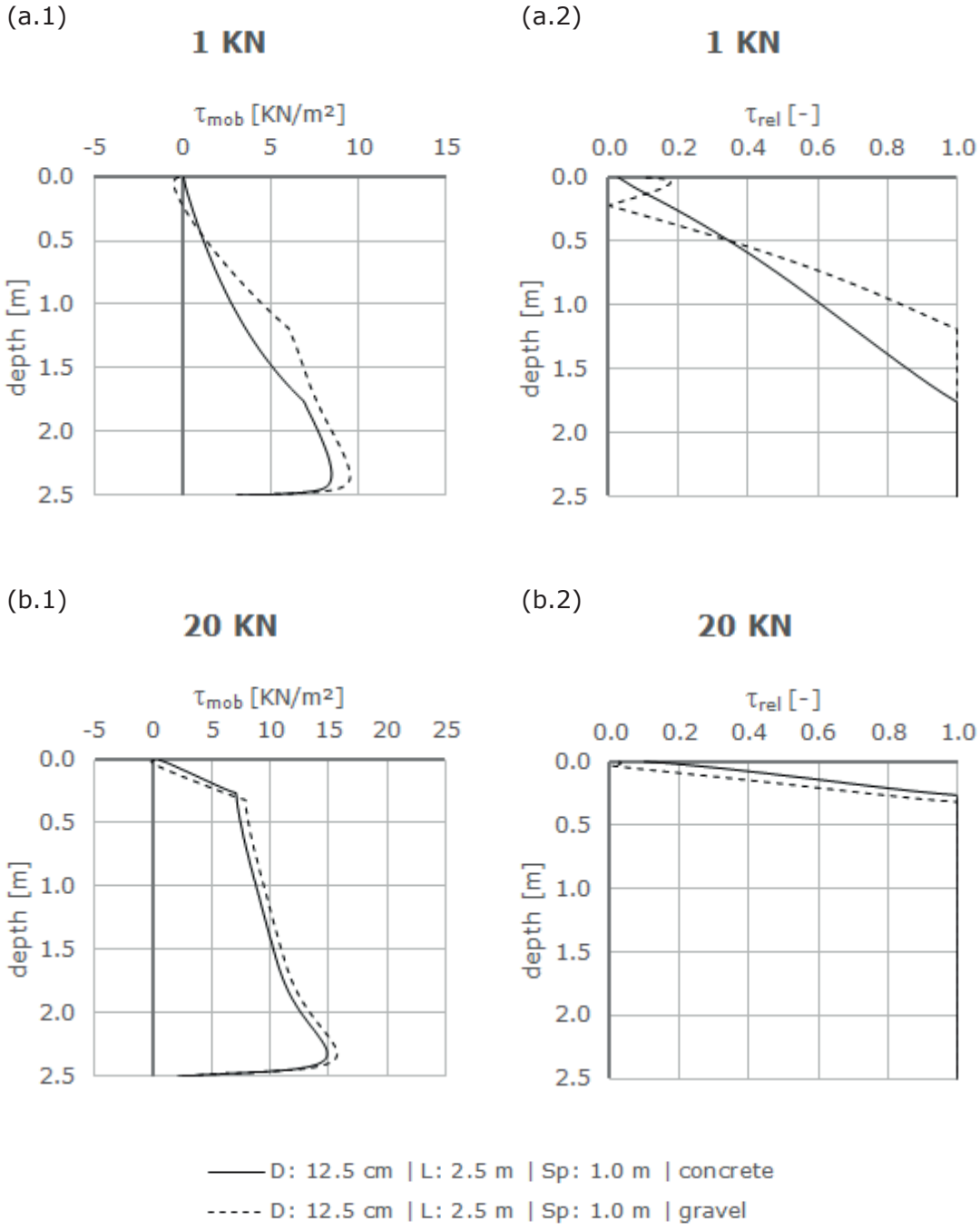

Figure 8.3: *Validation of different load distributing layers, detailed interpretation of the shaft: (a) load step 1 KN, (b) load step 20 KN D: 12.5 cm | L: 2.5 m | Sp: 0.5 m*

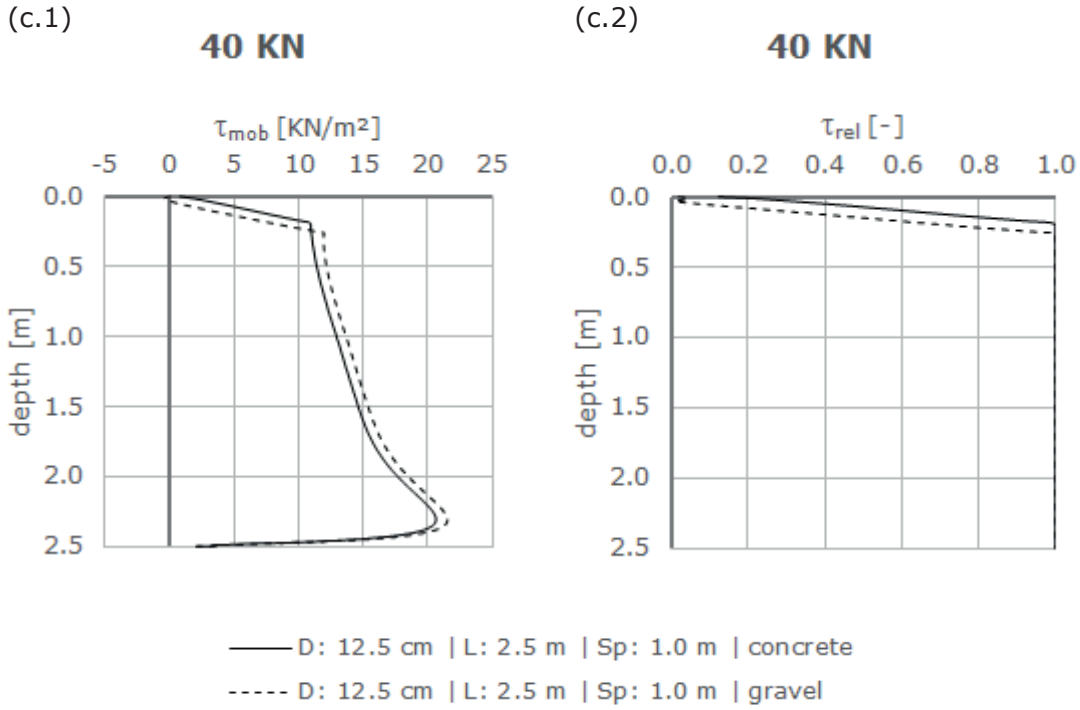

Figure 8.4: *Continuation of figure 8.3*
(c) load step 40 KN
D: 12.5 cm | L: 2.5 m | Sp: 0.5 m

8.1.3 Validation of different pile group configurations

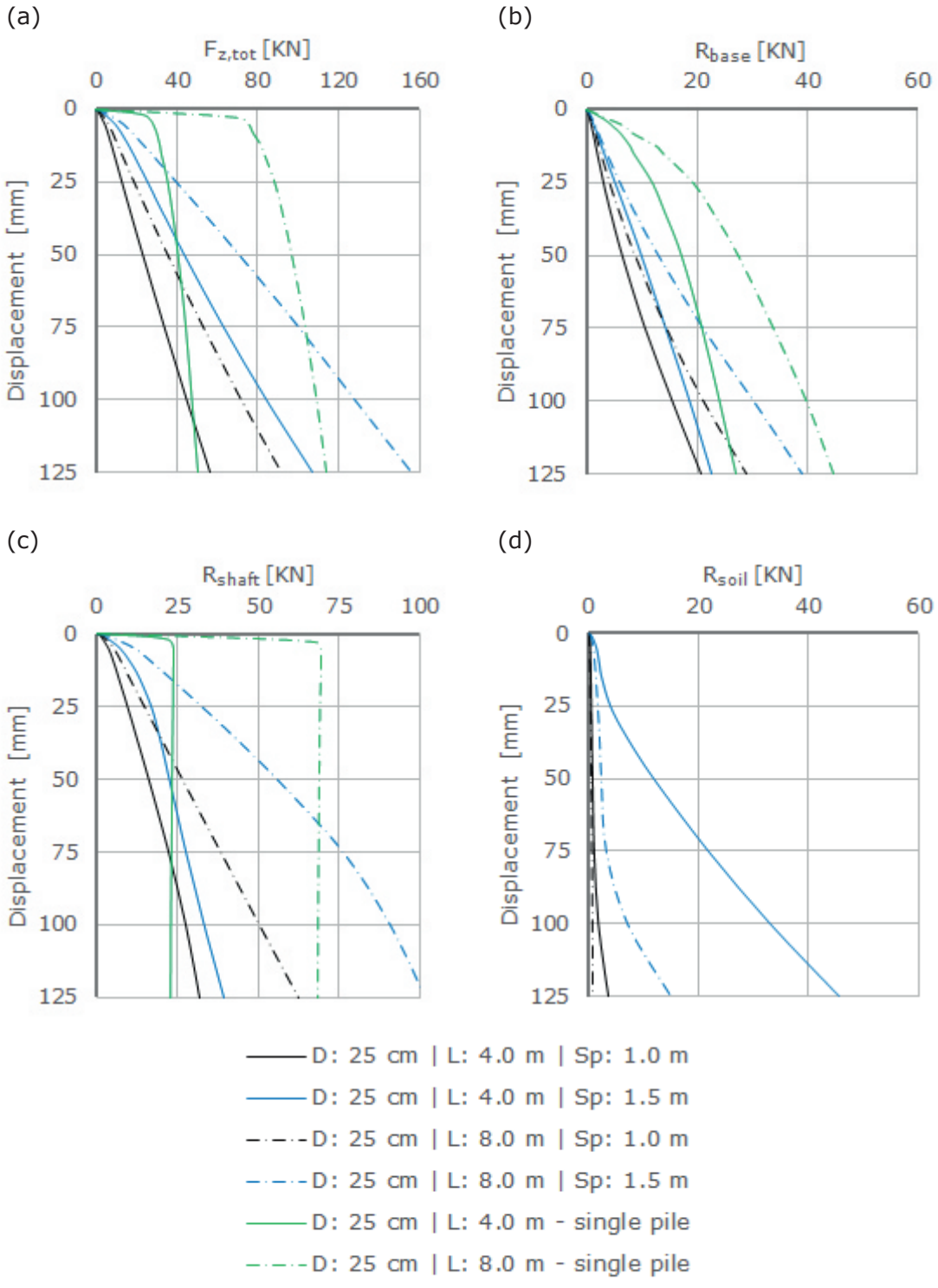

Figure 8.5: *Validation of different pile group configurations - D: 25 cm: (a) total applied load, (b) base resistance, (c) shaft resistance, (d) load transferred directly to the soil*

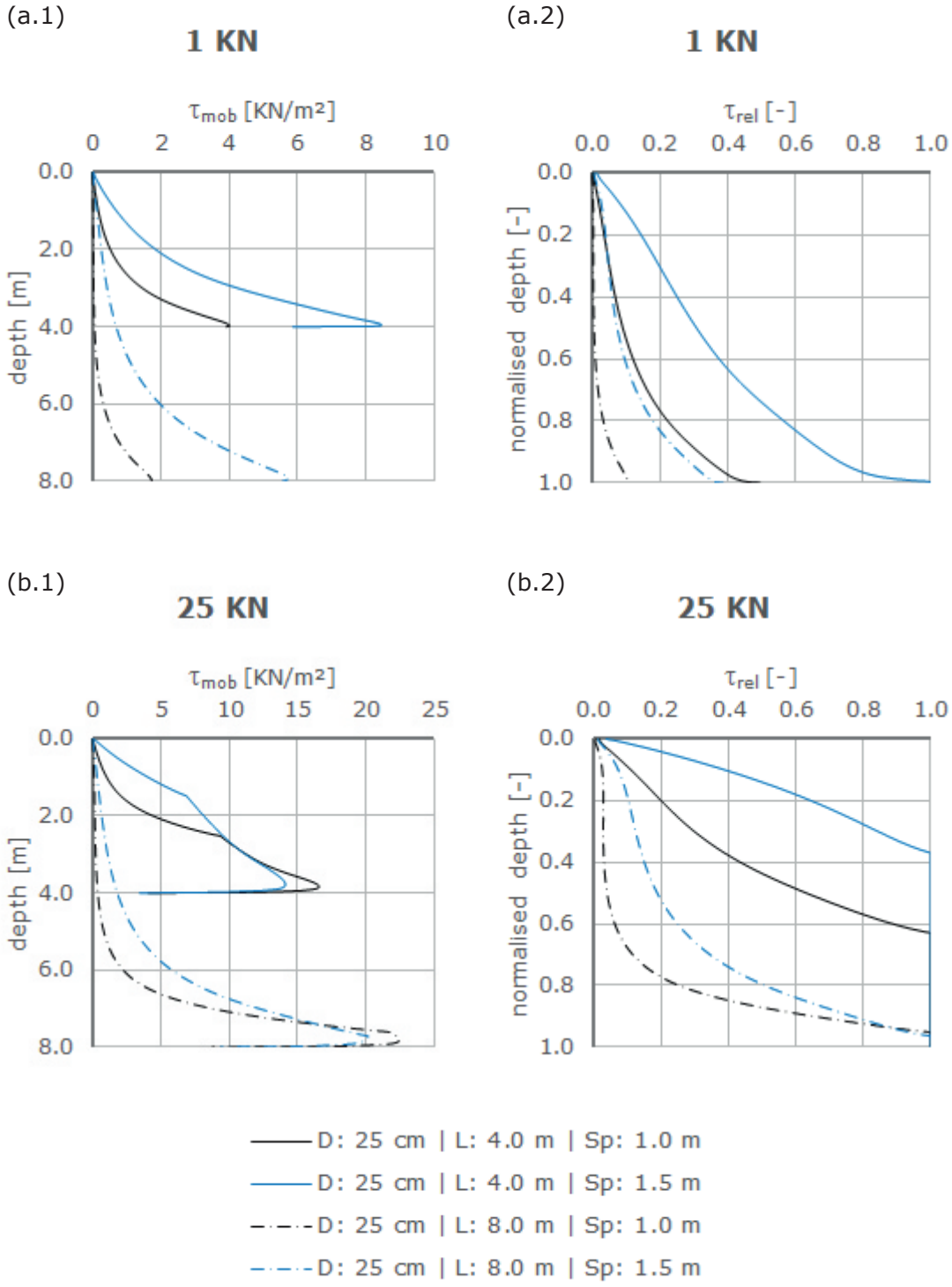

Figure 8.6: *Validation of different pile group configurations - D: 25 cm, detailed interpretation of the shaft: (a) load step 1 KN, (b) load step 25 KN*

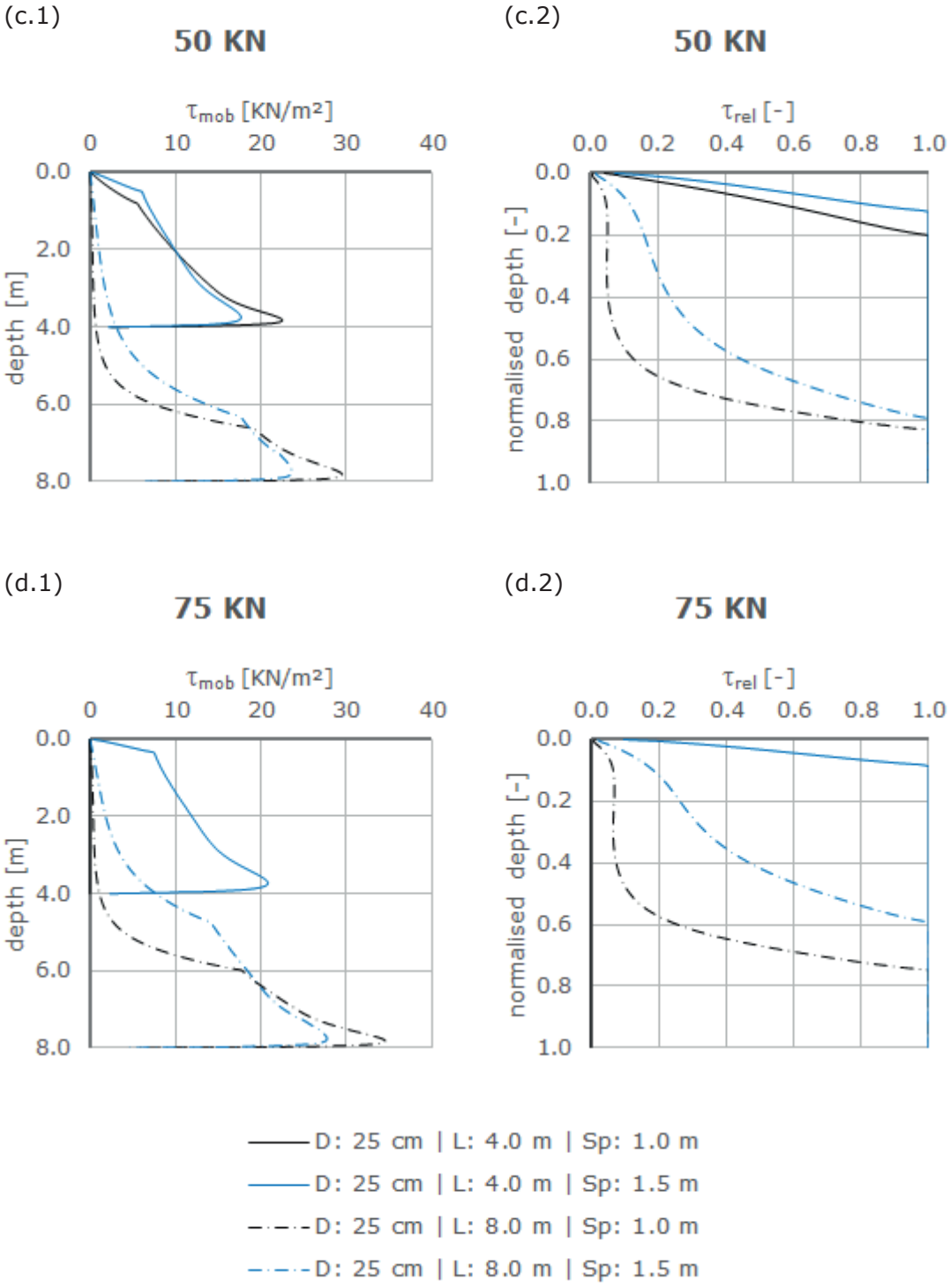

Figure 8.7: *Continuation of figure 8.6: (c) load step 50 KN, (d) load step 75 KN*

8.2 Additional results of 3D studies

8.2.1 Single piles

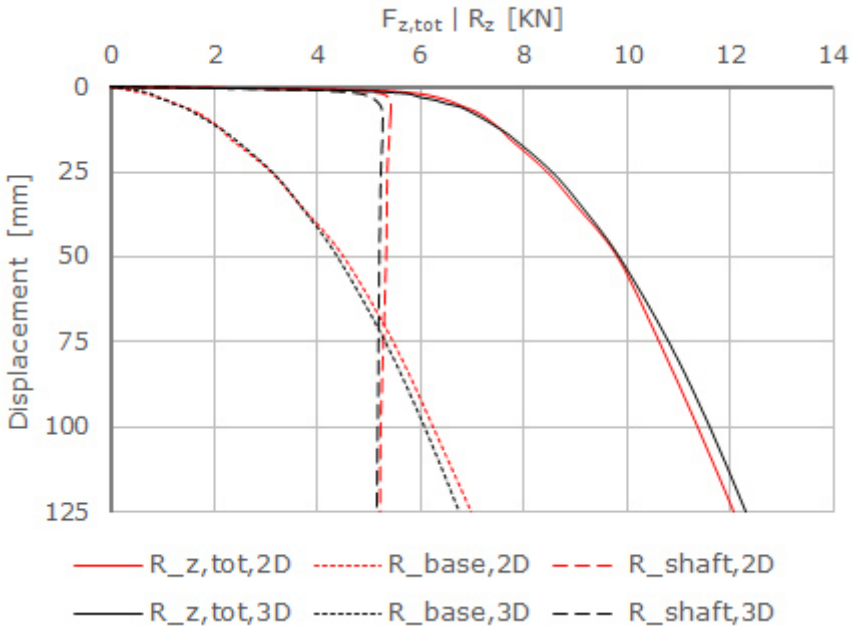

Figure 8.8: *Results of single pile in 3D:*
D: 12.5 cm | L: 2.5 m

8.2.2 Validation of different plan views - infinite pile group

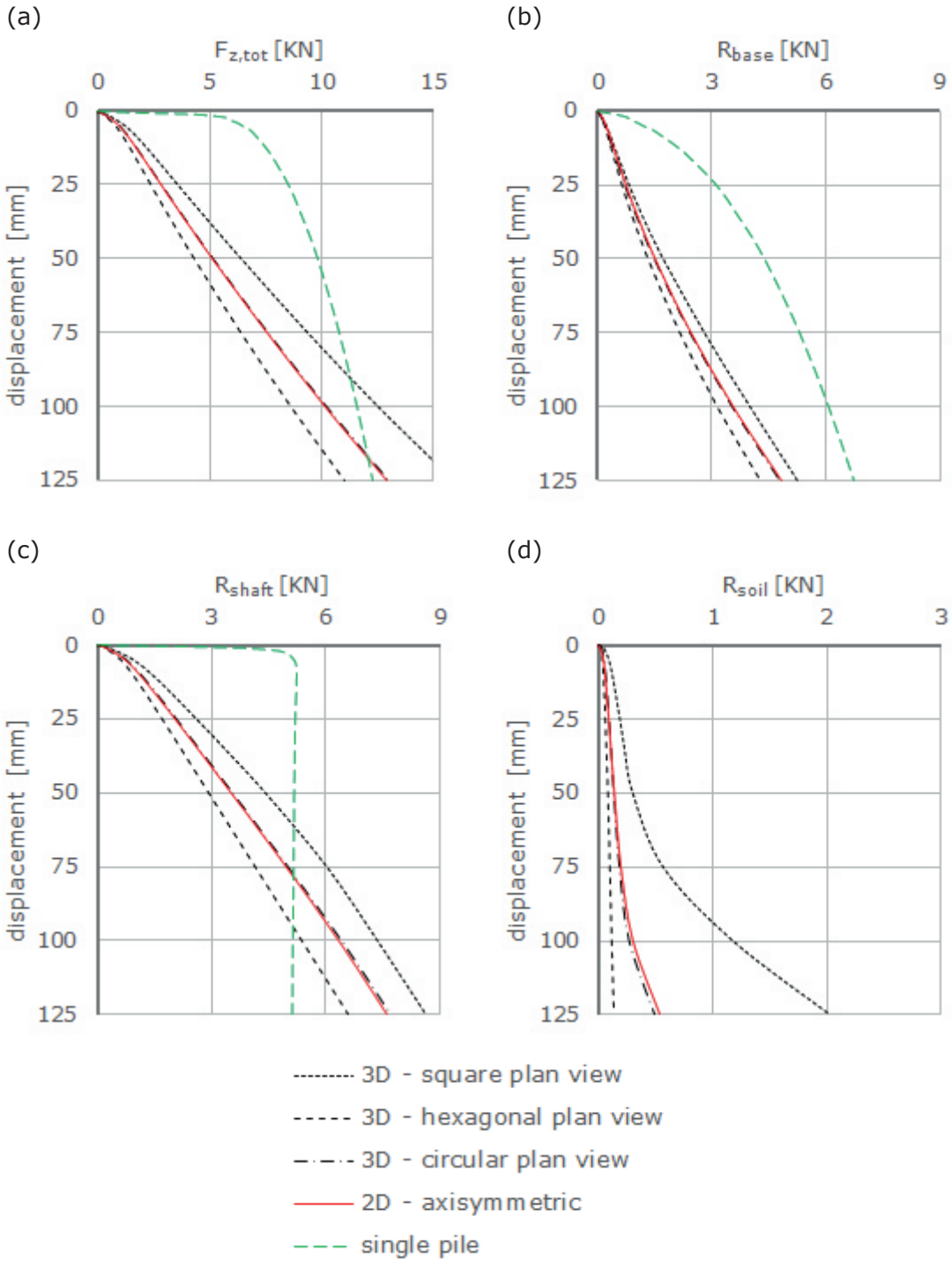

Figure 8.9: *Validation of different plan views:*
(a) total applied load, (b) base resistance,
(c) shaft resistance, (d) load transferred directly to the soil
D: 12.5 cm | L: 2.5 m | Sp: 0.5 m

8.2.3 Validation of different load distributing layers - entire pile group

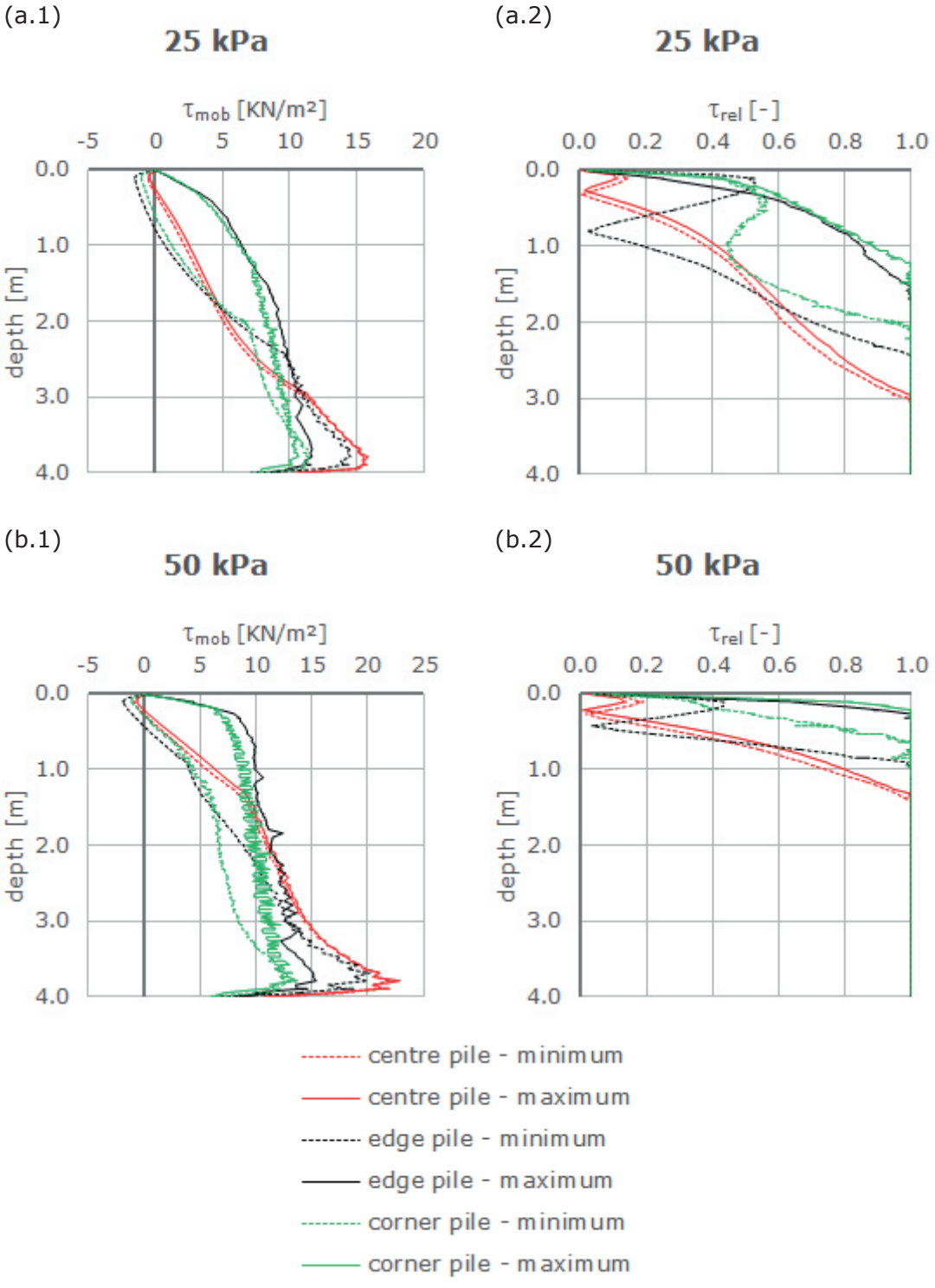

Figure 8.10: *Detailed interpretation of the shaft:*
(a) load step 25 kPa, (b) load step 50 kPa
D: 25 cm | L: 4.0 m | Sp: 1.0 m | gravel

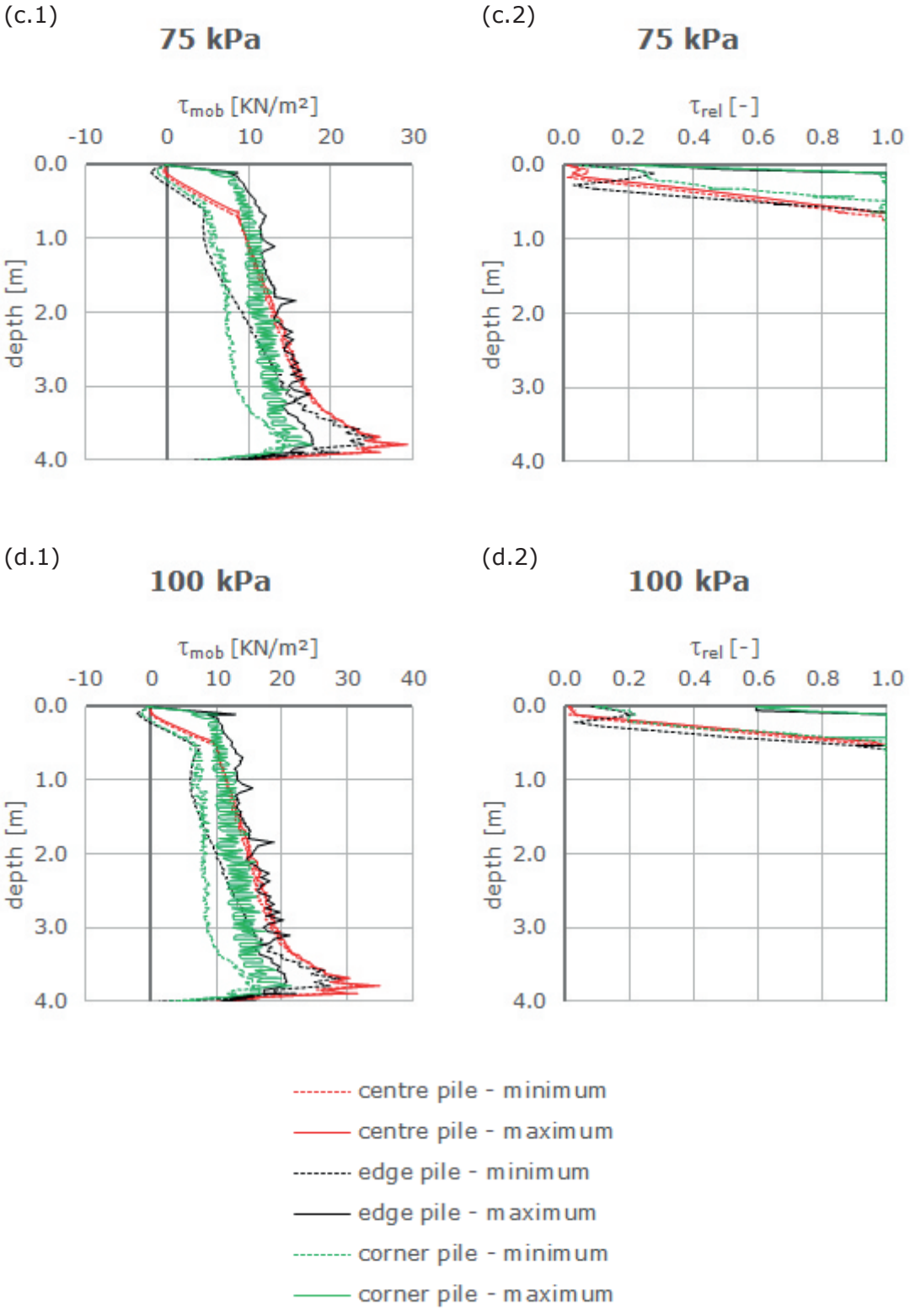

Figure 8.11: *Continuation of figure 8.10: (c) load step 75 kPa, (d) load step 100 kPa D: 25 cm | L: 4.0 m | Sp: 1.0 m | gravel*

8.2.4 Validation of different pile group configurations - entire pile group

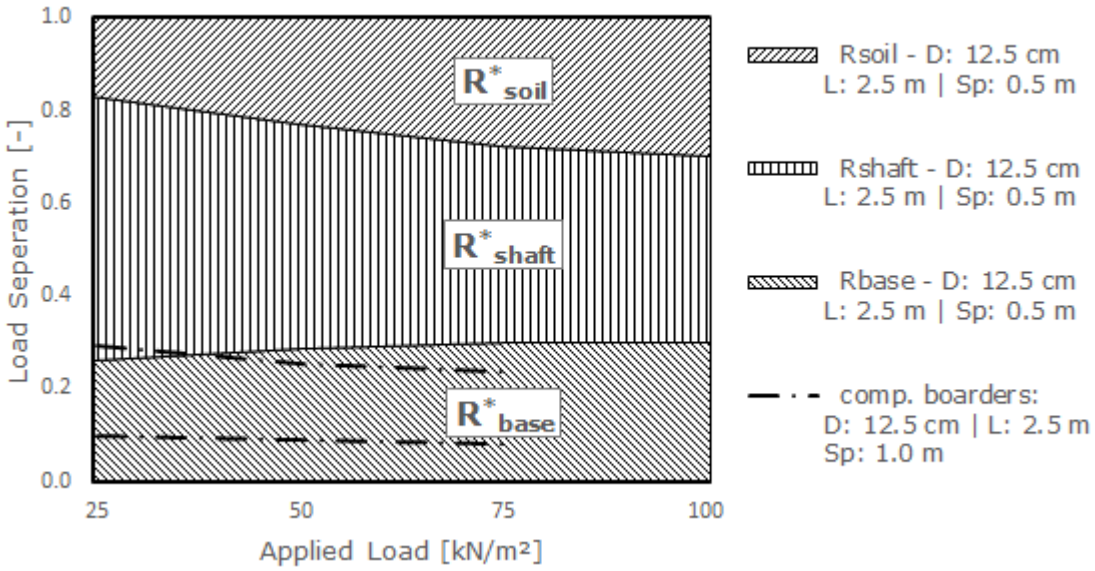

Figure 8.12: *Load separation*
D: 12.5 cm | L: 2.5 m | Sp: 0.5 m
D: 12.5 cm | L: 2.5 m | Sp: 1.0 m

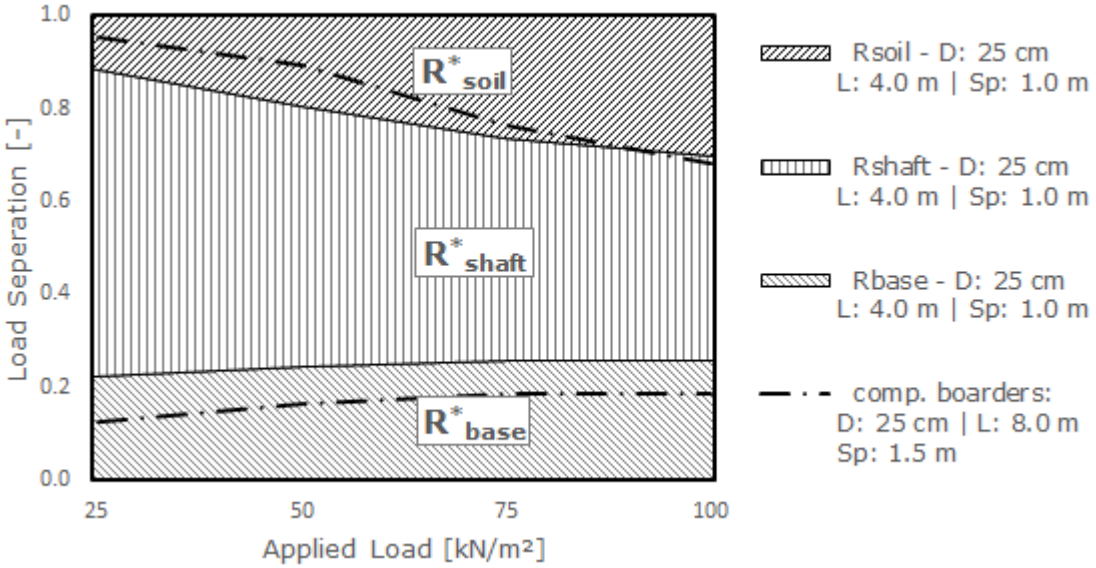

Figure 8.13: *Load separation*
D: 25 cm | L: 4.0 m | Sp: 1.0 m
D: 25 cm | L: 8.0 m | Sp: 1.5 m

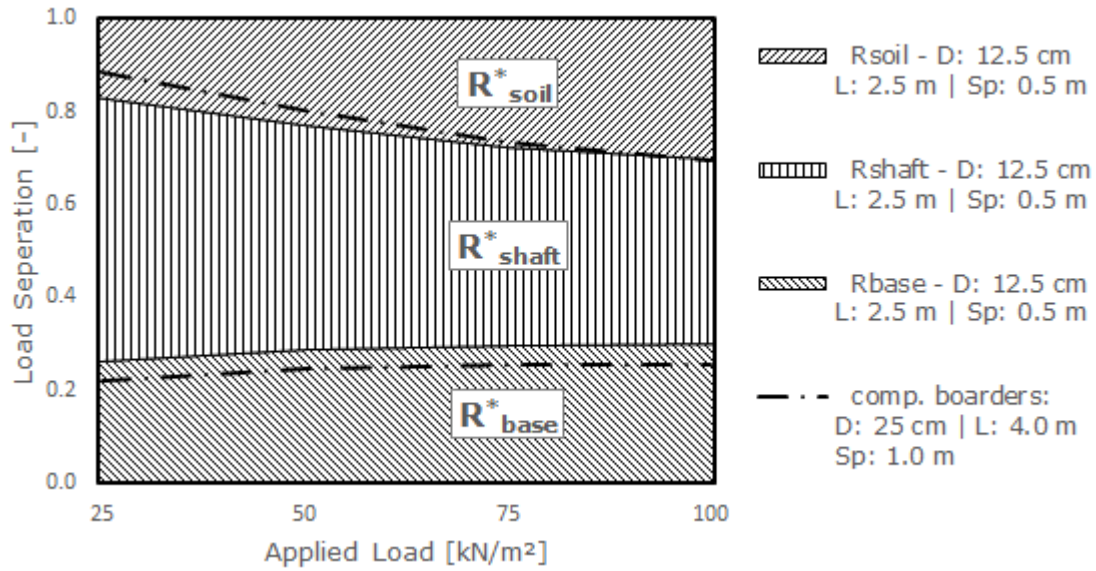

Figure 8.14: *Load separation*
D: 12.5 cm | L: 2.5 m | Sp: 0.5 m
D: 25 cm | L: 4.0 m | Sp: 1.0 m

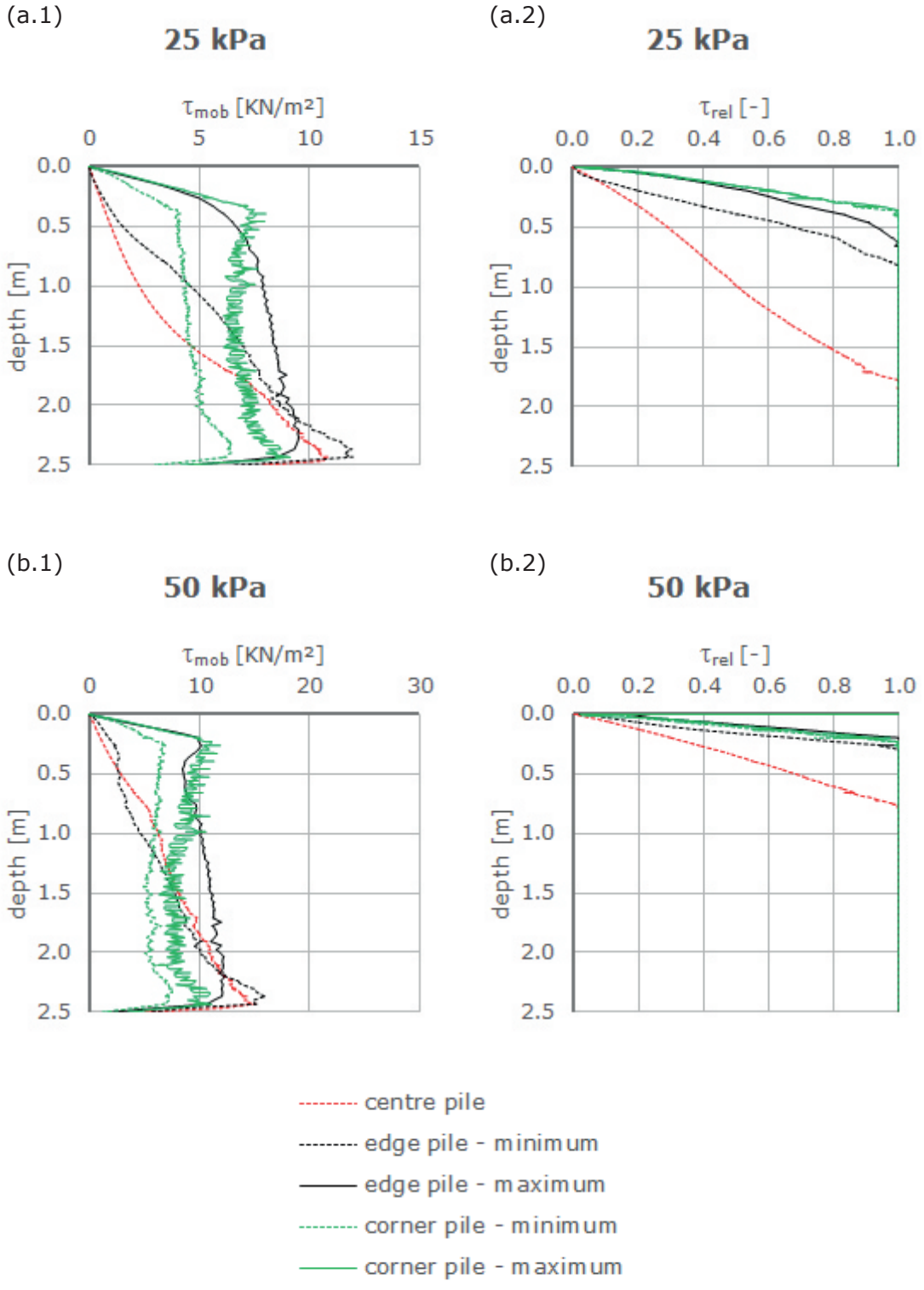

Figure 8.15: *Detailed interpretation of the shaft:*
(a) load step 25 kPa, (b) load step 50 kPa
D: 12.5 cm | L: 2.5 m | Sp: 0.5 m

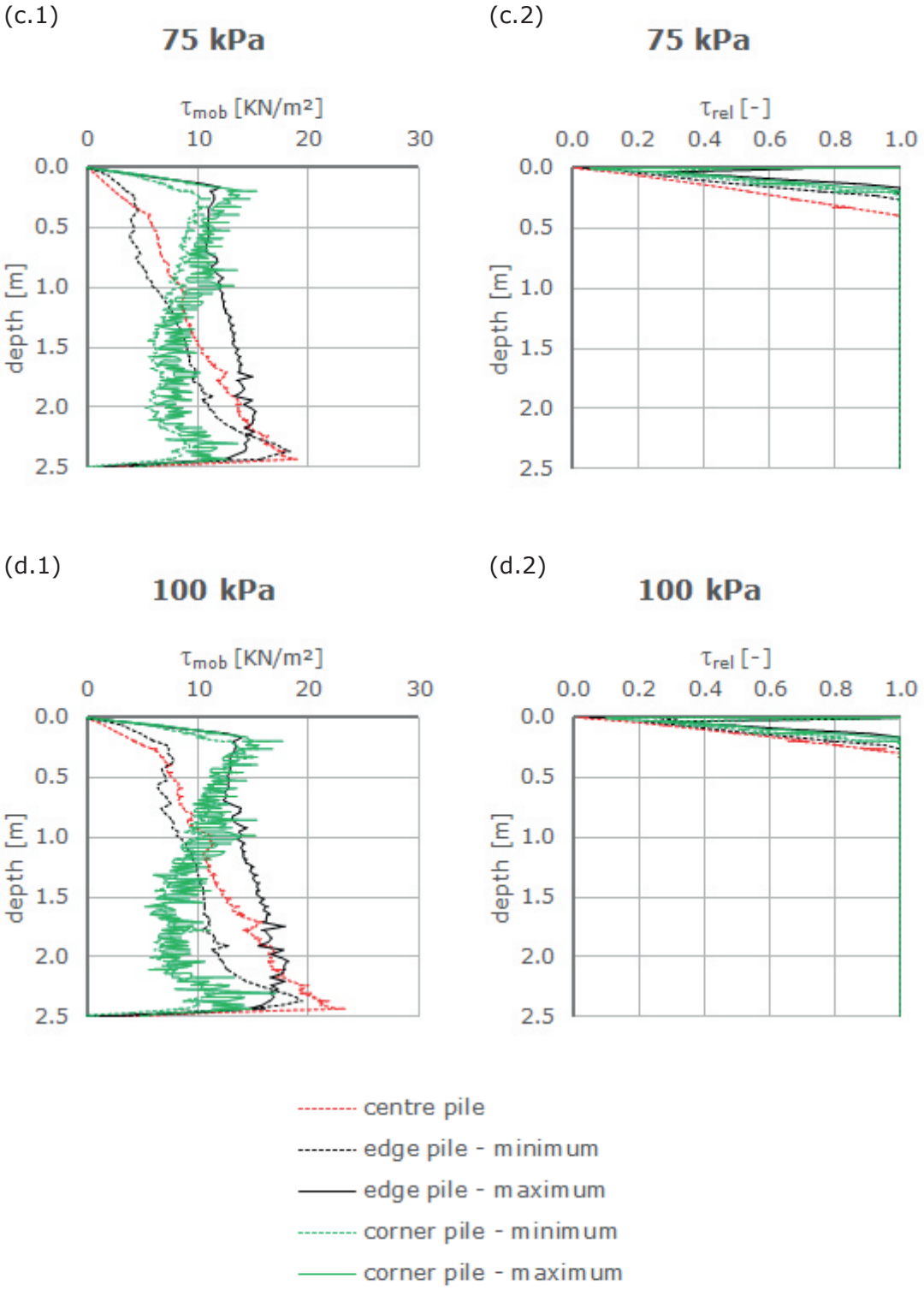

Figure 8.16: *Continuation of figure 8.15:*
(c) load step 75 kPa, (d) load step 100 kPa
D: 12.5 cm | L: 2.5 m | Sp: 0.5 m

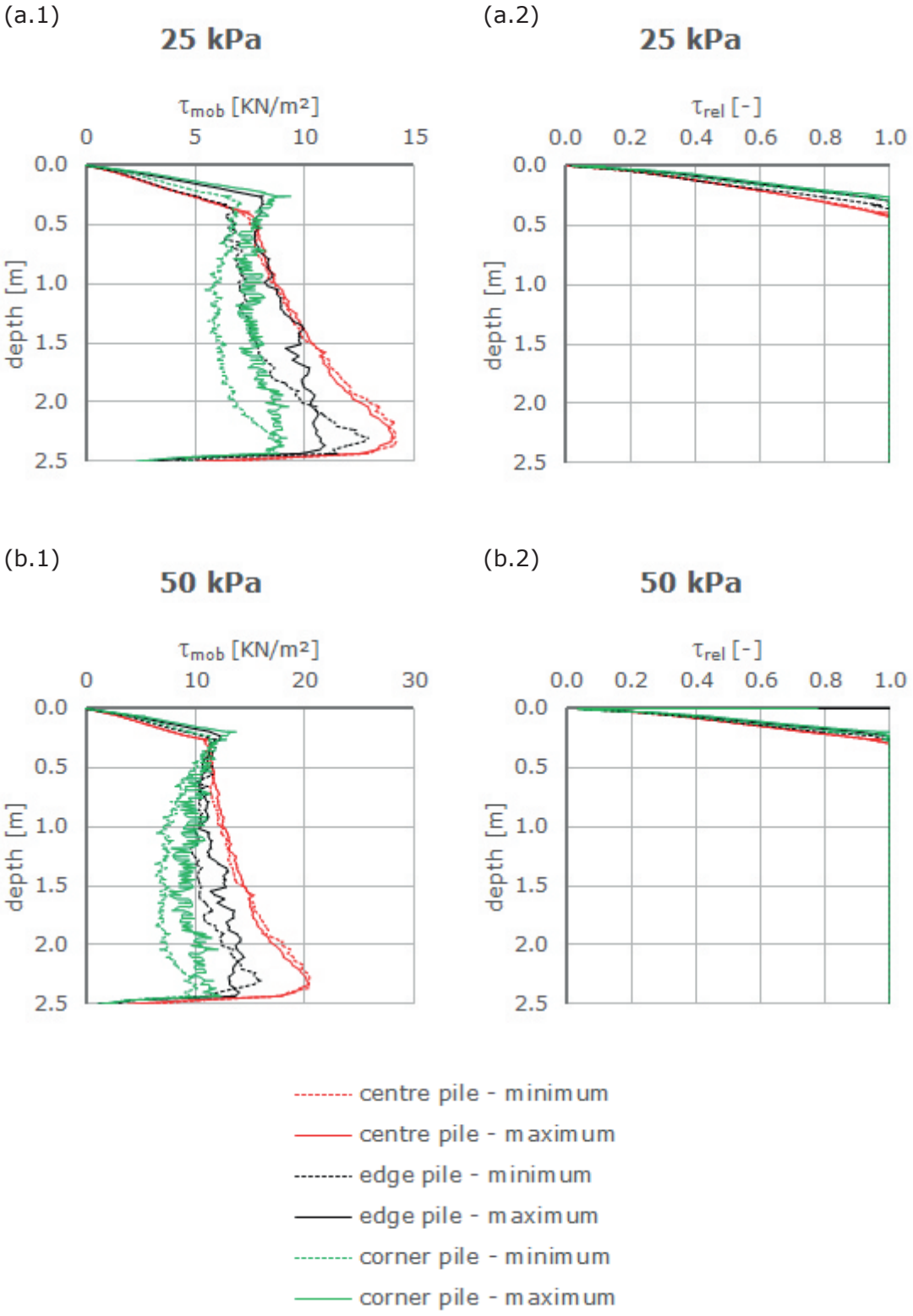

Figure 8.17: *Detailed interpretation of the shaft:*
(a) load step 25 kPa, (b) load step 50 kPa
D: 12.5 cm | L: 2.5 m | Sp: 1.0 m

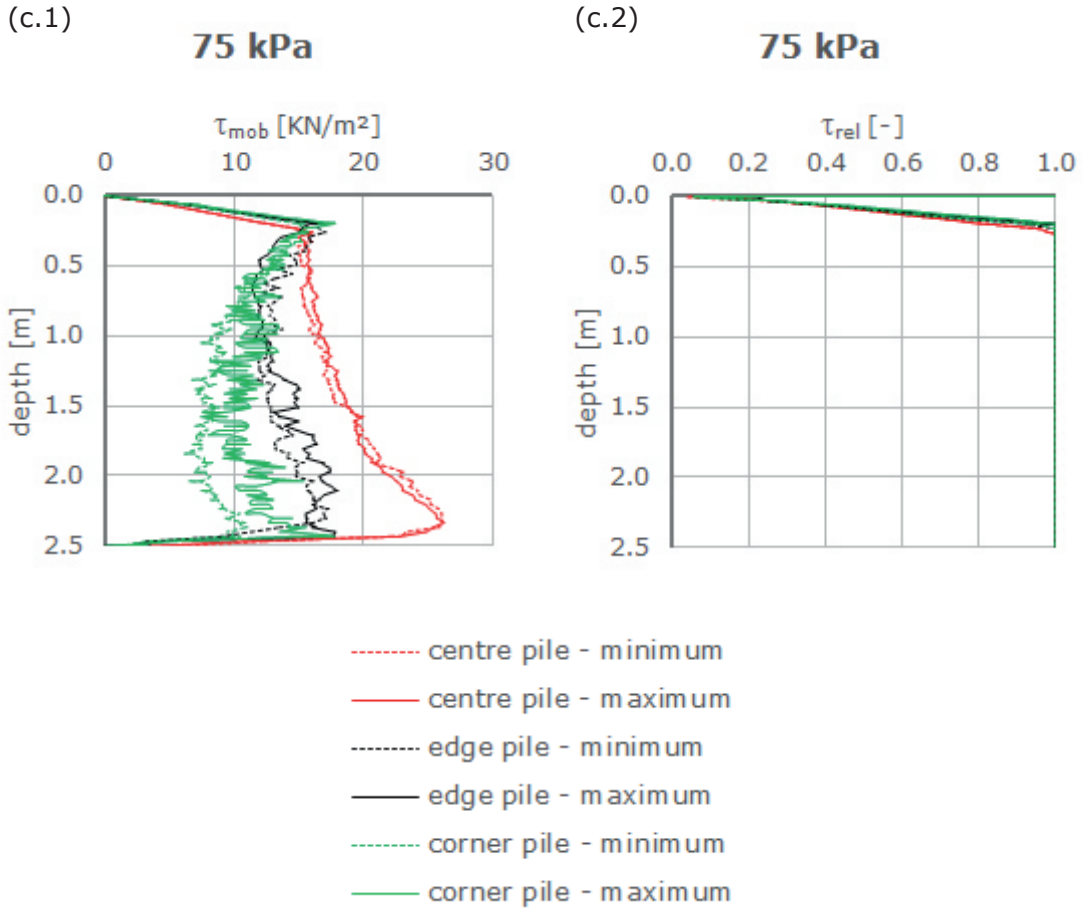

Figure 8.18: *Continuation of figure 8.17:*
(c) load step 75 kPa
D: 12.5 cm | L: 2.5 m | Sp: 1.0 m

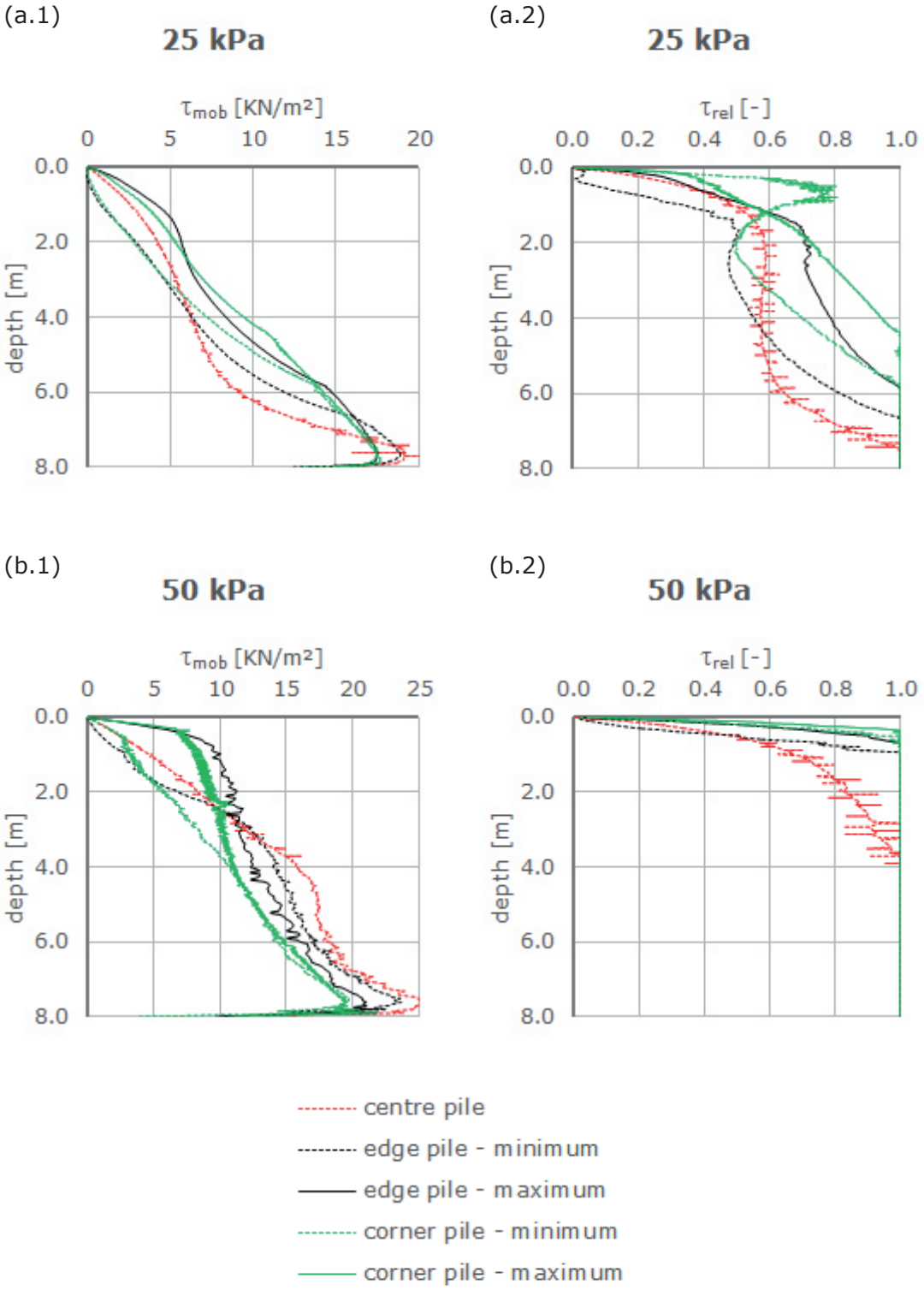

Figure 8.19: *Detailed interpretation of the shaft:*
(a) load step 25 kPa, (b) load step 50 kPa
D: 25 cm | L: 8.0 m | Sp: 1.5 m

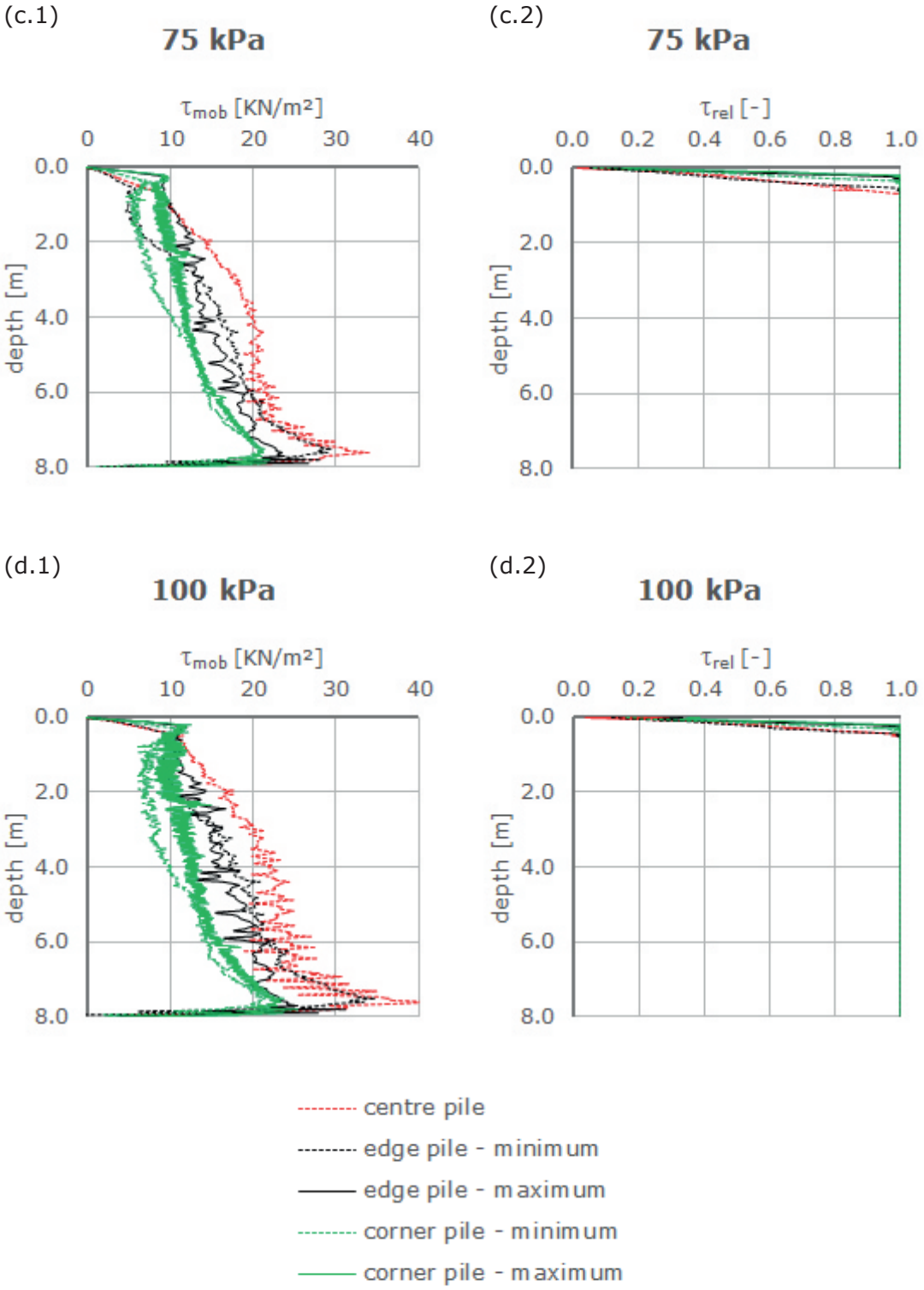

Figure 8.20: *Continuation of figure 8.19:*
(c) load step 75 kPa, (d) load step 100 kPa
D: 25 cm | L: 8.0 m | Sp: 1.5 m

8.3 Model catalogue - 2D

Nr.	Designation	D [cm]	L [m]	Sp [m]	Comment
single pile models					
1	ST__00	12.5	2.5	-	single pile
2	ST__01	25	4.0	-	single pile
3	ST__10	12.5	4.0	-	single pile
4	ST__11	25	8.0	-	single pile
5	ST__00_T30	12.5	2.5	-	conical tip - α = 30°
6	ST__00_T45	12.5	2.5	-	conical tip - α = 45°
7	ST__00_T60	12.5	2.5	-	conical tip - α = 60°
8	ST__11_30	25	8.0	-	conical tip - α = 30°
9	ST__11_45	25	8.0	-	conical tip - α = 45°
10	ST__11_60	25	8.0	-	conical tip - α = 60°
11	ST__11_TS0_5	25	8.0	-	tapered shape - ROT = 0.5 cm/m
12	ST__11_TS1_0	25	8.0	-	tapered shape - ROT = 1.0 cm/m
13	ST__11_TS1_5	25	8.0	-	tapered shape - ROT = 1.5 cm/m
14	ST__11_TS1_5_L	31	8.0	-	tapered shape - ROT = 1.5 cm/m
infinite pile group					
15	ST0100	12.5	2.5	1.0	gravel layer
16	ST0111	25	8.0	1.5	gravel layer
17	ST1000	12.5	2.5	0.5	concrete slab
18	ST1001	25	4.0	1.0	concrete slab
19	ST1010	12.5	4.0	0.5	concrete slab
20	ST1011	25	8.0	1.0	concrete slab
21	ST1100	12.5	2.5	1.0	concrete slab
22	ST1101	25	4.0	1.5	concrete slab
23	ST1110	12.5	4.0	1.0	concrete slab
24	ST1111	25	8.0	1.5	concrete slab

8.4 Model catalogue - 3D

Nr.	Designation	D [cm]	L [m]	Sp [m]	Comment
single pile models					
1	ST__00	12.5	2.5	-	single pile
2	ST__11	25	8.0	-	single pile
infinite pile group					
3	ST1000_CIR	12.5	2.5	0.5	circular plan view
4	ST1000_SQU	12.5	2.5	0.5	square plan view
5	ST1000_HEX	12.5	2.5	0.5	hexagonal plan view
6	ST1111_CIR	25	8.0	1.5	circular plan view
7	ST1111_SQU	25	8.0	1.5	square plan view
8	ST1111_HEX	25	8.0	1.5	hexagonal plan view
monolithic block | shallow foundation					
9	shallow foundation	-	-	-	
10	E2e6_4.0	-	4.0	-	
11	E4.3e5_4.0	-	4.0	-	
12	E1e5_4.0	-	4.0	-	
13	E2.5e4_4.0	-	4.0	-	
14	E1e4_4.0	-	4.0	-	
15	E4.3e5_2.5	-	2.5	-	
16	E4.3e5_8.0	-	8.0	-	
entire pile group					
17	ST0001	25	4.0	1.0	gravel layer
18	ST1000	12.5	2.5	0.5	slice of cake model
19	ST1001	25	4.0	1.0	
20	ST1100	12.5	2.5	1.0	
21	ST1111	25	8.0	1.5	
22	ST1001_cake	25	4.0	1.0	slice of cake - coarse mesh
23	ST1001_cake_FM	25	4.0	1.0	slice of cake - verry fine mesh
24	ST1001_TS	25	4.0	1.0	tapered pile shape ROT = 1.5 cm/m

8.5 Modelling hints for PLAXIS 3D

The following bullet list provides some tricks to overcome problems which might occur while modelling. Furthermore some hints for an easier post processing procedure are given.

- **modelling an arbitrary plan view**
  An arbitrary plan view of a model can be achieved by using a prescribed displacement as boundary. A prescribed displacement can be created out of each surface. The boundary conditions in respect of displacements have to be assigned as $Fixed$ in x and y direction and $Free$ in z direction. Beyond the prescribed displacement boundary, volumes have to be deleted.

- **producing a proper mesh**
  An arbitrary clicking on the local mesh refinement button is in my point of view not a elegant way to obtain a proper gradation from a very fine to coarse mesh. Before meshing one should think about the approximate desired element size for different regions. In a further step soil clusters with an individual adequate size have to be modelled. Finally for the mesh generation the $expert\ settings$ should used and the $element\ dimension$ should be set to $\sim 1\ m$. Since the $coarseness\ factor$ for soil clusters is a percentage value of the $element\ dimension$ it is possible to assign each soil cluster the approximate desired element size. If the model consists out of volumes with sharp angles which are not located at an essential position the $enhancedmeshrefinement$ should be turned of to avoid numerous hidden elements.

- **inaccurate snapping**
  From my experience PLAXIS can not handle locations and sizes smaller than the millimetre range. If the position of a volume is accurate to half a millimetre it probably will be moved to a full millimetre position. As a further consequence the mesh generation will be aborted due to inaccurate snapping.

- **modelling of soil volumes**
  A possibility to overcome the above mentioned problems is the way of modelling volumes. At the beginning a huge volume with the size of the entire model has to be generated. The partitioning to individual volumes is carried out by surfaces. No $intersectandrecluster$ should be applied. In the $meshgenerationwindow$ this is done automatically and for each newly created volume an individual $coarseness$ - $factor$ can be assigned. I modelled the piles by starting with a circular line in the x-y plane. Than I extruded the line in z direction to obtain a tube which I used to create an interface. In a final step I arranged them as a pile group. The tube was elongated on both sides by the desired element size. This elongation can be used as an interface extension. Do not forget to assign a proper $coarseness\ factor$ for each surface.

- **modelling of surfaces exhibiting an arbitrary position**
  Modelling a double inclined polygon with more than three vertexes frequently encounters problems since it is not possible to place all points perfectly on the plane. This problem can be solved by creating several triangles and afterwards combining them to one large surface.

- **interpretation of interfaces**
  Sometimes post processing can be quite tricky! Nodes usually are located at an arbitrary position. Nevertheless, a relatively easy way to be able to perform an accurate a fast post processing along a section is possible. Before generating the mesh a line has to be drawn along the interface where the post processing needs to be carried out. This line should have known coordinates, in best case it is a vertical or horizontal line. Now the mesh is forced to have nodes along this line. Based on the known coordinates it is possible to filter the nodes with an easy if-function in MS Excel. With the obtained values along the desired section further post processing as e.g. a numerical integration or generation of a diagram is possible.

- **auxiliary beam elements**
  A possibility of reading out structural forces of piles is to incorporate auxiliary beam elements. Input parameters are the area and the young's modulus which has to be reduced by a certain factor (e.g. 1000) during the computation. It has to be remarked that this is only possible for piles with linear elastic material behaviour. Usually stress concentrations occur at the ends of the beam element and for the interpretation a stress point with a distance of $\sim 15\ cm$ has to be chosen manually. For a faster post processing procedure a point should be modelled at the desired distance.

- **structural forces in volumes - auxiliary soil volume**
  Without exception I encountered problems with this tool. The automatically added centre lines were always slightly inclined and thus the results unusable. By checking the coordinates it could be shown that the inclined line is not a space diagonal. For models with a single pile located in the centre of the quarter model it was possible to overcome this problem by using the x_{min} and y_{min} feature. Since the calculation times for switching between calculation phases were tremendous I modelled a small auxiliary volume with a height of $10\ cm$ below the pile. This measure shortened the time of switching between phases and the data were extracted on top of the element.

- **efficient performance**
  Efficient execution of large models can only be done when the computer is utilised twenty-four-seven. A useful possibility is to run several models as a batch file . It is possible to run the PLAXIS Input and PLAXIS Output application at the same time. Furthermore the command runner can also be used for models which are prone to hang up by executing a certain command. Sometimes I used it for generating the mesh since saving the model via the command line was possible whereas a click in the program was already too much. Afterwards I had to restart PLAXIS and was finally able to continue.